İSTANBUL TECHNICAL UNIVERSITY ★ INSTITUTE OF SCIENCE AND TECHNOLOGY

PERFORMANCE EVALUATION OF PRECAST COLUMNS UNDER SEISMIC EXCITATION

M.Sc. Thesis by

Melih SÜRMELİ, Civil Engineer

Department: Civil Engineering

Program: Structural Engineering

OCTOBER 2008

İSTANBUL TECHNICAL UNIVERSITY ★ INSTITUTE OF SCIENCE AND TECHNOLOGY

PERFORMANCE EVALUATION OF PRECAST COLUMNS UNDER SEISMIC EXCITATION

M.Sc. Thesis by

Melih SÜRMELİ, Civil Engineer

(501051082)

Date of submission : 10 December 2007

Date of defence examination: 28 January 2008

Supervisor (Chairman): Assis. Prof. Dr. Ercan YÜKSEL

Members of the Examining Committee: Assoc. Prof. Dr. Konuralp GİRGİN (İ.T.U.)

Assis. Prof. Dr. Cem YALÇIN (B.U.)

OCTOBER 2008

İSTANBUL TEKNİK ÜNİVERSİTESİ ★ FEN BİLİMLERİ ENSTİTÜSÜ

PREFABRİK KOLONLARIN DEPREM PERFORMANSLARININ DEĞERLENDİRİLMESİ

YÜKSEK LİSANS TEZİ

İnş. Müh. Melih SÜRMELİ

(501051082)

Tezin enstitüye verildiği tarih: 10 Aralık 2007

Tezin savunulduğu tarih: 28 Ocak 2008

Tez Danışmanı: Yar. Doç. Dr. Ercan YÜKSEL

Diğer Jüri Üyeleri: Doç. Dr. Konuralp GİRGİN (İ.T.Ü.)

Yar. Doç. Dr. Cem YALÇIN (B.Ü.)

OCAK 2008

ACKNOWLEDGEMENT

I would like to express my gratitude to Asistant Professor Ercan Yüksel for his invaluable support and attention in completing this study. Professor Faruk Karadoğan and Research Assistant Serkan Z.Yüce are also gratefully acknowledged, for supplying the experimental data used in this study.

December, 2007 Melih Sürmeli

TABLE OF CONTENTS

ABBREVIATONS

PHM	: Polygonal Hysteretic Model
SHM	: Smooth Hysteretic Model
PGA	: Peak Ground Acceleration
PGV	: Peak Ground Velocity
NF	: Near Fault
FF	: Far Fault
DI	: Damage Index

LIST OF TABLES

LIST OF FIGURES

LIST OF SYMBOLS

f_c'	: 28 day concrete cylindrical compressive strength
f_{cc}'	: Confined concrete strength
f_c	: Concrete stress
f_{ck}	: Characteristic concrete strength
f_{cd}	: Design concrete strength
f_{cp}	: Unconfined concrete post spalling strength
f_{cu}	: Stres at ε_{cu}
f_s	: Steel stress
f_y	: Steel yield stress
f_{ywk}	: Transverse reinforcement chracteristic yield strength
f_u	: Steel fracture stress
ε_c	: Concrete strain
ε_t	: Concrete tension strain capacity
ε_{cc}	: Concrete strain at peak stress
ε_{cu}	: Ultimate concrete strain
ε_{sp}	: Spalling strain
ε_y	: Yield strain
ε_{max}	: Maximum strain experienced in time history
$(\varepsilon_c)_{max}$	: Maximum strain of confined concrete experienced in time history
ε_{cun}	: Strain of concrete fiber outer side of section
ε_{cg}	: Strain of concrete fiber outer side of confined zone
ε_s	: Longitudinal reinforcement strain
$(\varepsilon_s)_{max}$	: Maximum strain of longitudinal reinforcement experienced in time history
ε_{sh}	: Strain at strain hardening
ε_{su}	: Failure strain of steel
ρ_{sm}	: Volumetric transverse reinforcement ratio required in Turkish Seismic Code
ρ_s	: Volumetric transverse reinforcement ratio present in the section
A_c	: Gross sectional area of column
A_{ck}	: Area of confined concrete
E_c	: Elastic modulus of concrete
E_{sec}	: Secant modulus of concrete
I	: Moment of Inertia
EI	: Initial flexural rigidity
EA	: Axial stiffness
EI3P	: Post yield flexural stiffness
M_{cr}	: Cracking moment
M_y	: Yield moment
M_u	: Ultimate moment
χ_y	: Yield curvature

χ_u	: Ultimate curvature
α	: Stiffness degrading parameter
β_1	: Ductilitiy based strength degrading parameter
β_2	: Energy based strength degrading parameter
R_s	: Slip length parameter
σ	: Slip sharpness parameter
λ	: Parameter for mean momet level of slip
η	: Parameter for shape of unloading
N	: Smoothness parameter for elastic-yield transition
δ_m	: Maximum experienced deformation
δ_u	: Ultimate deformation of element determined from a lateral pushover analysis
P_y	: Yield strength of the element
$\int dE_h$	: Hysteretic energy absorbed by the element during the response history
θ_m	: Maximum rotation attained during the loading history
θ_u	: Ultimate rotation capacity of the section
θ_r	: Recoverable rotation when unloading
E_h	: Dissipated energy in the section

PREFABRİK KOLONLARIN DEPREM PERFORMANSLARININ DEĞERLENDİRİLMESİ

ÖZET

Ülkemizde, prefabrik betonarme taşıyıcı sistemler ekonomik ve inşaat süresinin kısa olmasından dolayı sıklıkla endüstriyel yapılarda kullanılmaktadır. Taşıyıcı sistem genelde soket biçimindeki temellere oturtulmuş, konsol olarak çalışan kare kesitli kolonlar ile bu kolonlara mafsallı olarak bağlanmış kirişlerden oluşmaktadır. Bu tip sistemlerin deprem etkisinde her iki deprem doğrultusunda da aynı davranışı gerçekleştirmesi beklenmektedir.

17 Ağustos 1999 Kocaeli depremi sonucunda, çok sayıda endüstri tipi prefabrik betonarme bina göçmüş ya da ağır hasara uğramıştır. Yerinde yapılan incelemeler sonucunda binaların başlıca göçme nedenlerinin kolon taban kesitindeki mafsallaşmalar ve kolon kiriş birleşimlerinin yeterli dönme kapasitesine sahip olamayışı olarak belirlenmiştir. Plastik mafsal oluşmasının ana nedeni yetersiz yanal rijitlik, dayanım ve süneklilktir. Deprem yönetmeliğinde verilen elastik spektrum ve taşıyıcı sistem davranış katsayılarının prefabrik yapının deprem etkisindeki davranışını iyi ifade edemediği düşünülmektedir. Güncel çalışmalar yapının konumunun (fay hattına yakınlığının) deprem durumunda yapı davranışı üzerinde etkili olduğunu ortaya koymaktadır. Fay hattına yakın depremlerin (yakın deprem) karakteristikleri özelikle de maksimum yer hızı değerinin yüksek olması, bu depremleri uzak depremlere göre çok daha yıkıcı yapmaktadır.

Prefabrik betonarme kolon elamanlarının deprem anındaki davranışını anlayabilmek için 30x30 cm, 35x35 cm, 40x40 cm, 45x45 cm, 50x50 cm, 60x60 cm boyutlarında ve her bir kesit boyutu için %1, %2, %3 boyuna donatı oranlarını içeren 18 adet kolonun zaman tanım alanında lineer olmayan analizi gerçekleştirilmiştir. Yapılan analizler ile prefabrik betonarme kolonların performansının artan kesit boyutu ve artan donatı oranına bağlı olarak değerlendirilmesi amaçlanmaktadır. Tüm kolonlar, prefabrik çatı kirişinin mesnet reaksiyonu olarak 200 kN' luk basınç kuvvetine maruz bırakılmıştır. Bu normal kuvvet düzeyini karşılayan kesit, deprem yönetmeliğinde belirtilen 1. derece deprem bölgesi ve Z2 zemin sınıfı kriterlerine göre hesaplamış olup, 30x30cm ebatlarındaki kolon için %1.68 lik donatı oranına karşılık gelmektedir. Dünyanın çeşitli bölgelerinde meydana gelmiş kuvvetli yer hareketlerinden elde edilmiş 80 adet ivme kaydı doğrusal olmayan dinamik hesapta kullanılmıştır. İvme kayıtları seçilirken maksimum yer ivmesi (PGA), maksimum yer hızı (PGV) ve fay hattına uzaklık gibi özellikler dikkate alınmıştır.

Farklı kesit özelliklerine sahip 3 adet prefabrik kolon numunesi (S30_18, S35_18 ve S40_20), İTÜ Yapı ve Deprem Mühendisliği Laboratuarında, depremi benzeştiren deplasman çevrimleri kullanılarak incelenmiştir. Deney sonuçları ile uyumlu kuvvet-deplasman ilişkileri elde edebilmek için IDARC2D Ver6.01 adlı programdan yararlanılmıştır. IDARC2D statik ve dinamik karakterli yükler için yapı sistemlerinin lineer ve lineer olmayan analizini ve hasar değerlendirmesini yapabilen bir bilgisayar programıdır. Deneyde uygulanan yerdeğiştirme çevrimleri kullanılarak çevrimsel

analiz her üç kolon için gerçekleştirilmiştir. IDARC2D ile yapılan analizlerde, parabolik çevrimsel davranış modeli (SHM) tercih edilmiştir. SHM modeli betonarme kesitin davranışını ifade eden rijitlik azalması, dayanım azalması ve kayma oyulması parametrelerini içermektedir. Her üç numune için bu parametreler belirlenmiştir.

Bu çalışmada moment-eğrilik ve normal kuvvet-moment karşılıklı etki diyagramlarının oluşturulması için XTRACT programından yararlanılmıştır.

Çevrimsel davranış ve kesit özellikleri belirlendikten sonra, zaman tanım alanında lineer olmayan toplam 1440 analiz gerçekleştirilmiş ve prefabrik betonarme kolonların performansları Park&Ang hasar modeline göre değerlendirilmiştir. Bu hasar modeli maksimum elastik olmayan deplasmanları ve deplasman geçmişini dikkate alabilmektedir. Park&Ang hasar indeksi 3 adet performans seviyesi içermektedir. Hasar indeksinin 1 den büyük olması göçme durumunu, 0.4 ile 1 arasında aldığı değerler ağır hasar durumunu, 0.4 den küçük olması ise tamir edilebilir hasar durumunu ifade etmektedir.

Gerçekleştirilen doğrusal olmayan dinamik analiz hesap sonuçlarına dayanarak her kolon için bir hasar indeksi havuzu oluşturulmuş ve kolonların performans seviyeleri belirlenmiştir. Şiddetli yer hareketi karakteristiklerinin kolon performansı üzerindeki etkisini gözlemlemek amacıyla hasar indeksiyle PGA ve PGV arasında ilişkiler oluşturulmuştur. Hasar indeksiyle PGA ve PGV arasındaki ilişkiler sabit kesit boyutu için boyuna donatı oranı etkisini ve sabit boyuna donatı oranı için kesit boyutu etkisini de göstermektedir

Diğer etkili performans parametreleri olan zaman tanım alanında hesapta gerçekleşmiş en büyük boyuna donatı birim şekil değiştirmesi $(\varepsilon_s)_{max}$ ve en büyük sargılı beton birim şekil değiştirmesi $(\varepsilon_c)_{max}$ değerleri hesaplanmış olup deprem yönetmeliğinde tanımlanmış sınır durumlara (minimum hasar (MN), güvenlik (GV) ve göçme (GC)) göre hasar değerlendirimesi yapılmıştır. Bu sınır değerler gerilme-şekildeğiştirme diagramını dört bölgeye ayırmaktadır: minimum hasar bölgesi $(\varepsilon_{max}<\varepsilon_{MN})$, belirgin hasar bölgesi $(\varepsilon_{MN}<\varepsilon_{max}<\varepsilon_{GV})$, ileri hasar bölgesi $(\varepsilon_{GV}<\varepsilon_{max}<\varepsilon_{GC})$ ve göçme bölgesi $(\varepsilon_{max}>\varepsilon_{GC})$. Ayrıca PGV ile performans göstergeleri $(\varepsilon_s)_{max}$, $(\varepsilon_c)_{max}$ ile ilişkiler oluşturulmuştur.

Bu çalışmanın sonuçları tüm kolonlara 200 kN'luk sabit deprem yükü uygulandığı dikkate alınarak ifade edilirse:

Aynı boyuna donatı oranına sahip prefabrik kolonların performansı üç ayrı hasar kriterine(hasar indeksi, çelikte ve sargılı betonda zaman tanım alanında oluşmuş maksimum şekil değiştirme miktarı) göre değerlendirildiğinde, kesit boyutunun arttırılmasının kolonda oluşacak hasar miktarının azalmasına neden olduğu açıkça görülebilmektedir. Yakın depremler uzak depremlere göre çok daha yıkıcı olabilmektedir. PGV değerinin arttırılması hasar indeksi ve sargılı beton birim şekil değiştirmesinde artışa neden olmaktadır. Gerçekleşmesi muhtemel depremin PGV değeri, PGA değerinden, oluşacak hasarın tahmin edilmesi açısından çok daha etkin bir parametredir. Tüm kesit boyutları dikkate alınarak hasar indeksine göre yapılan değerlendirmede, boyuna donatı oranı % 2 ve % 3 olan prefabrik kolonlarda hemen hemen aynı davranış gözlenmektedir; ancak donatı oranı % 1 olan kolonların hasar indeksi değerleri daha büyüktür. Eğer yapının tasarım aşamasında orta hasar (tamir edilebilir) görmesi hedefleniyorsa 60x60cm ebatlarında donatı oranı % 2 den büyük kolonların kullanılması önerilmektedir. Ağır hasar ve göçme olasılığı en çok, boyuna donatıda zaman tanım alanında meydana gelmiş en büyük şekil değiştirme değerine göre yapılan değerlendirmede gözlenmiştir. Hasar indeksi bunu izlemektedir. Ancak neredeyse tüm yer hareketleri sargılı betonda zaman tanım alanında meydana gelmiş en büyük şekil değiştirme değerlerinin Deprem Yönetmeliği'nde verilen güvenlik sınırının altında yer almasına neden olmaktadır. Her kesit boyutu için hasar indeksi değerinin 0.4 olma durumuna karşılık gelen PGV değeri hesaplanmış olup, bu değerler 30x30 cm ve 60x60 cm ebatlarındaki kolonlar için sırasıyla 60 cm/s ve 160 cm/sn olarak belirlenmiştir.

PERFORMANCE EVALUATION OF PRECAST COLUMNS UNDER SEISMIC EXCITATION

SUMMARY

In Turkey, precast concrete structural systems are commonly used in industrial facilities because of their economy and construction speed. In general, the structural configuration consists of square-shaped cantilever columns founded in socket type foundations and with simply supported beams. This type of framing is expected to behave similar in two main earthquake directions.

During the M_w 7.4 earthquake that struck northwestern Turkey on August 17, 1999 many precast industrial buildings collapsed or were extensively damaged. Based on site investigations, main reasons of the building collapse were defined as plastic hinging at the base of columns and pounding of the precast elements at the roof level. The main reason of plastic hinging is insufficient lateral rigidity, strength and ductility. It is thought that the elastic spectra and structural behavior factors (R) given in Turkish Seismic Code does not describe well enough the behavior of precast building under seismic excitation. Recent investigations have shown that the response of structures exposed to earthquake loading is affected by location of structure closeness to fault line. The primary characteristics of near-fault ground motions, especially high peak ground velocity (PGV), make near-fault earthquakes more destructive compared to far fault ground motions.

To define "exact" behavior of prefabricated column elements under seismic excitation, nonlinear time history analysis were performed using various sectional dimensions (30x30 cm, 35x35 cm, 40x40 cm, 45x45 cm, 50x50 cm, 60x60 cm) and for each cross sectional dimension, three longitudinal reinforcement ratio (%1, %2, %3) were studied. The main purpose of the current study is to investigate the performance of precast columns due to increasing sectional dimensions and longitudional reinforcement ratio. A simulated lateral seismic load of 200 kN, which correspons to the support reaction of simply supported precast roof beam for one storey industrial type building, is applied to the columns. Assuming that the building located on firm soil, in Seismic Zone I of Turkey and the building was designed according to Turkish Seismic Code. To carry the seismic weight of 200 kN, the columns were proportioned as 30x30 cm with 1.68 % longitudinal reinforcement ratio. Totally 80 earthquake records selected from various locations of the world were subjected to the column models in the nonlinear dynamic analyses. While selecting earthquake records, different characteristics were considered such as peak ground acceleration (PGA), peak ground velocity (PGV), closeness to fault line, etc.

Three precast columns (S30_18, S35_18 and S40_20) which have different sectional properties were tested in Structural and Earthquake Engineering Laboratory of ITU using earthquake simulated loads. An analytical work was performed to simulate the experimental results. This was done by using IDARC2D Ver.6.01 which is a computer program for the elastic and inelastic analysis and damage evaluation of buildings and their components under combined dynamic, static and quasi-static

loading. Quasi-static cyclic analysis was performed for each specimen by applying piecewise linear cyclic displacement history which is same with the used in the experimental study. It is preferred to use smooth hysteretic model (SHM) in IDARC2D. The (SHM) consists of stiffness, strength degradation and pinching parameters that represent realistic response of reinforced concrete section. For the tested columns, mean values of the degradation parameters of SHM were determined by comparing the experimental and the analytical results.

A cross-sectional analysis program XTRACT which comprises moment-curvature and axial force-mment interaction is used to obtain the envelop curves.

After determining hysteretic behavior and section properties, a total number of 1440 nonlinear time history analysis were performed and the performance of precast columns were evaluated by damage model proposed by Park & Ang. This damage model accounts for damage due to maximum inelastic excursions, as well as damage due to history of deformations. Park & Ang damage index has three performance levels; values greater than 1, values between 0.4 and 1, and values less than 0.4, which describes collapse, severe damage and moderate damage conditions, respectively.

Based on the performed nonlinear time history analyses, a damage index tool was created for every column and the column performance levels were determined. To determine the effect of strong ground motion properties on precast column performance, relationships were set up between damage indexes (DI) and the ground motion characteristics of PGA and PGV. The relationships between damage indexes (DI) and PGA, PGV also demonstrate the effect of longitudinal reinforcement ratio for same sectional dimensions and the effect of sectional dimensions for the same longitudinal reinforcement ratio on precast column performance.

The other significant performance indicators, which are maximum strain of longitudinal reinforcement $(\varepsilon_s)_{max}$ and maximum strain of confined concrete $(\varepsilon_c)_{max}$ experienced in time history analyses, were calculated and damage evaluation was performed via the performance limits defined in Turkish Seismic Code which are minimum damage (MN), safety (GV) and collapse (GC). These limits divide stress-strain curve into four regions which are minimum damage ($\varepsilon_{max}<\varepsilon_{MN}$), moderate damage ($\varepsilon_{MN}<\varepsilon_{max}< \varepsilon_{GV}$), severe damage ($\varepsilon_{GV}<\varepsilon_{max}<\varepsilon_{GC}$) and collapse ($\varepsilon_{max}>\varepsilon_{GC}$). The relationships between PGV and indicators $(\varepsilon_s)_{max}$, $(\varepsilon_c)_{max}$ were also set up.

Based on the results of this investigation, the following conclusions can be drawn taking into account for a constant seismic weight of 200 kN for all section types:

Increasing section dimensions decrease observed damage of precast columns for same longitudinal reinforcement ratio if performance evaluation is done due to three different damage indicators; damage index, confined concrete strain and longitudinal steel strain experienced in time history. Near fault earthquakes caused more damage compared to the far fault earthquakes. Increasing PGV values results as increasing damage index and confined concrete strain experienced in time history. The PGV of the potential earthquake is more is more effective than PGA to estimate damage observed on the structure. For the same sectional dimensions, the behavior of the columns having longitudinal reinforcement ratio of 2 % and 3 % are similar if DI values are taken into consideration, whereas columns having longitudinal reinforcement ratio of 1 % have larger index values. It is recommended to use 60x60 cm sectional dimensions, if minor damage is intended in design. The probability of severe damage and collapse condition were mostly observed according to longitudinal steel strain, damage index follows it, whereas almost all of the ground motions caused damage under safety limit for confined concrete strain.The threshold values of PGV of each cross sectional dimension which match a damage index of 0.4 were obtained; corresponding values are 60 cm/sn and 160 cm/sn for sectional dimensions of 30x30 cm and 60x60 cm, respectively.

1. INTRODUCTION

Precast frame buildings are widely used in the construction of industrial facilities and commercial malls. Single story warehouses represent the most common structural configuration, which consists of cantilever columns connected by simply supported precast and prestressed beams. Connection of the non-moment resisting beams to the columns is achieved on site. The general structural configuration and front view are shown in Fig. 1.1, Fig. 1.2, respectively.

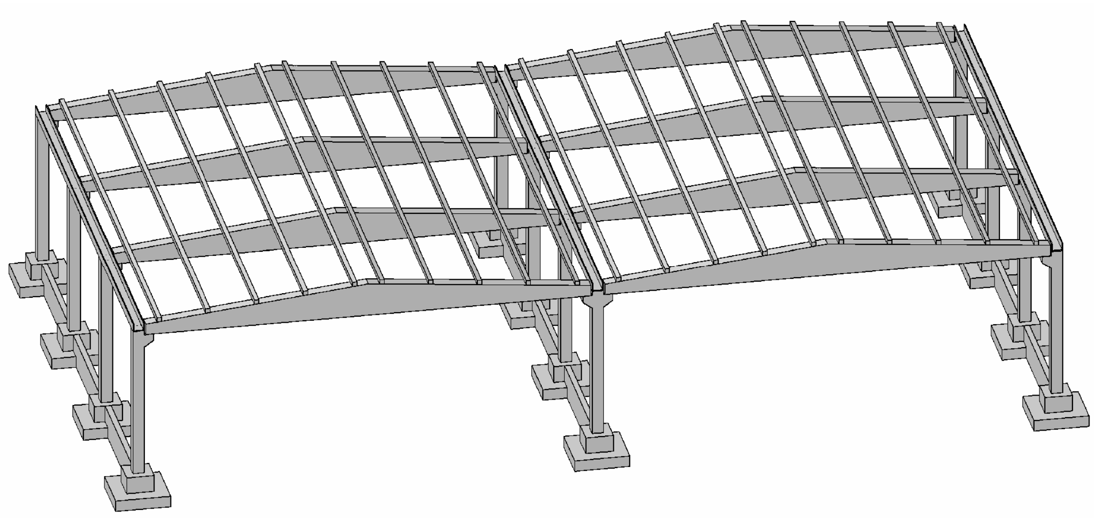

Figure 1.1: The structural configuration of precast buildings in Turkey

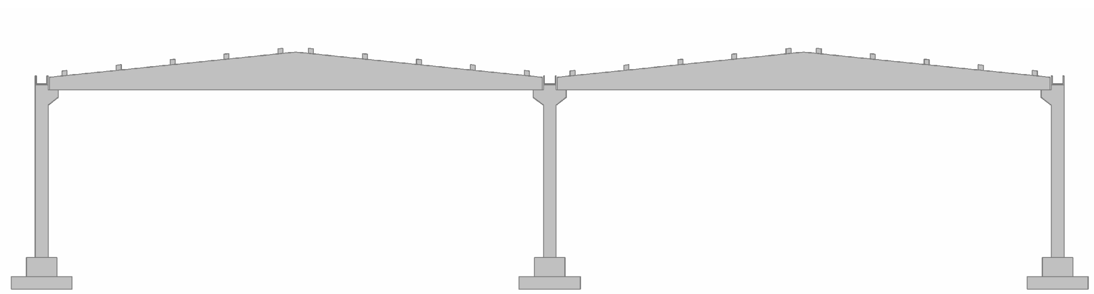

Figure 1.2: Front view of the structural configuration of precast buildings

In general, the structural configuration depends entirely on the cantilevered columns for lateral strength and stiffness. Many industrial buildings collapsed in Turkey during the last devastating earthquakes of Ceyhan (1998) and Marmara-Kocaeli (1999), which led to major disruptions in the manufacturing industry. Based on site investigations, structural damage and collapse of precast buildings was widely reported throughout the epicentral regions of the August 1999 Kocaeli and November 1999 Duzce earthquakes in Turkey [1-5]. Types of structural damage were frequently observed in the one-story industrial buildings: flexural hinges at the base of the columns, (Fig.1.3); and axial movement of the roof girders which led to pounding against the supporting columns or unseating of the roof girders [6]. It has been concluded that the reason for damage and collapse of single-storey industrial buildings was due to inadequate behavior of diaphram caused large relative lateral displacements of frames, poor detailing of columns and inadequate element connections [1].

Figure 1.3: Plastic Hinges at Column Base [1]

As a single degree of freedom (SDOF) system, precast columns are designed simply by using elastic spectrum depending on site conditions given in seismic codes.

However, it has been presented that assessment of peak demands due to inelastic shaking is carried out only by methods used for far fault shaking. Present US documents such as ATC40 [20], FEMA273 [21], the Uniform Building Code [22] and FEMA302 [23] use a basis for seismic design generally consider near fault shaking effects in the development of elastic response spectra, they do not currently consider the increased inelastic demands that may occur during near fault shaking [7]. Rupture directivity effects of near fault ground motions cause a large long period velocity pulse that occurs on the horizontal component perpendicular to the strike of the fault. This impulsive character results large displacement response caused severe damage on buildings [8,9].

The effect of peak ground velocity on maximum inelastic deformations of non-degrading elastoplastic SDOF is investigated by using non-impulsive ground motion records (PGV<60) and it was found that high PGV values increase the maximum inelastic deformations which can be used as a damage indicator [10]. As a more recent study [11] strengthen the conclusion that PGV is a proper intensity measure candidate for deformation demands on SDOF systems compared with other intensity measures, such as PGA and PGV/PGA.

In this study, performance of precast columns have been investigated by performing nonlinear time history analyses by using 40 far fault and 40 near fault records for six different cross sectional dimensions and three different longitudinal steel reinforcement ratios.

Evaluation of performance of precast columns was done using damage index proposed by Park and Ang [12] which accounts for the combination of maximum deformation response and hysteretic energy dissipation. This index has been calibrated against numerous experimental results and fault observations. Park, Ang and Wen have assigned to damage index two limits: a reparability limit of 0.4 and a collapse limit of 1 [13]. However, Bozorgnia, Y., and V.V. Bertero indicated two drawbacks of Park and Ang damage index [14]. First, for elastic response, when the damage index supposed to be zero, it will be greater than zero. The second disadvantage is the value of damage index is grater than 1 when the system achieves the deformation capacity under monotonic loading, although the maximum value must be 1. Despite its drawbacks, Park and Ang damage index has been extensively used for different applications due to its simplicity and its expensive calibration against experimentally observed seismic structural analysis.

The other significant performance indicators, which are maximum strain of longitudinal reinforcement $(\varepsilon_s)_{max}$ and maximum strain of confined concrete $(\varepsilon_c)_{max}$ experienced in time history, were calculated and performance evaluation was also done due to performance levels defined in Turkish Seismic Code [18] which are minimum damage (MN), safety (GV) and collapse (GC).

2. EXPERIMENTAL BACKGROUND

13 full scale precast columns, which had different sectional dimensions and reinforcement ratios, were tested in Structural and Earthquake Engineering Laboratory of ITU [19]. All the specimens were subjected to constant vertical loads with cyclic displacement reversals. The used testing set-up is shown in Fig. 2.1.

The name of columns used in the analytical work are listed in Table 2.1. The first number of specimen name stands for section dimensions and the second, rebar diameter.

Table 2.1: Column properties

Sample	Section dimensions	Longitudinal reinforcement	Steel ratio
S30_18	30x30 cm	8 Φ18	0.023
S35_18	35x35 cm	8 Φ18	0.017
S40_20	40x40 cm	8 Φ20	0.016

The columns have a height of 4 m from top of the socket foundations. The concrete and rebar quality are C45 and S420, respectively. Transverse reinforcements are located as Φ8/10 in the confinement zone and as Φ8/15 in the remaining part.

Dimensions and cross sections of specimens are shown in Fig. 2.2 and Fig. 2.3, respectively.

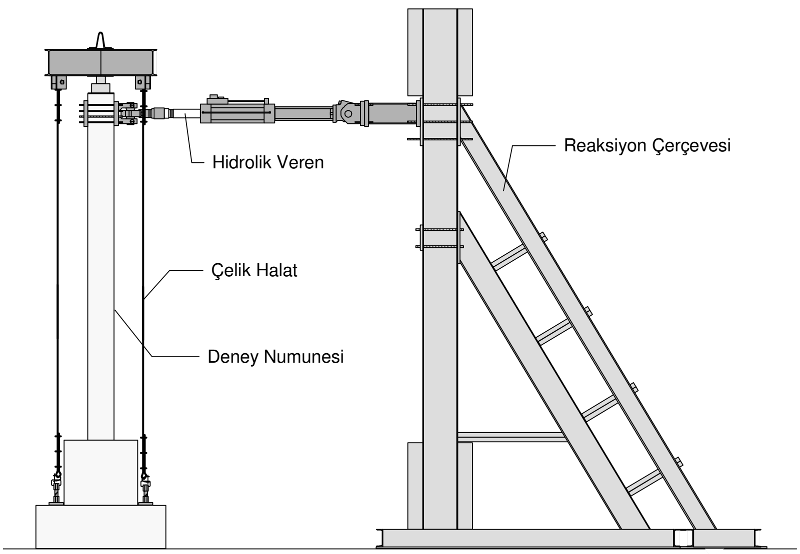

Figure 2.1: Experimental set-up

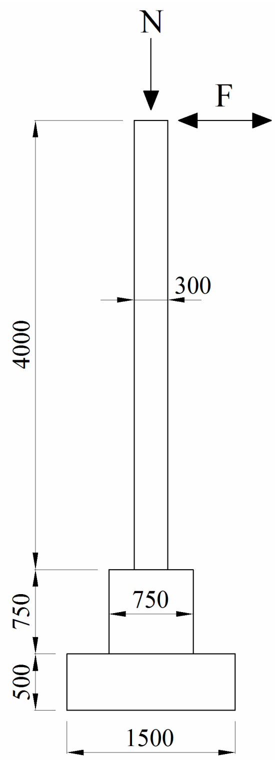

Figure 2.2: Dimensions of specimen

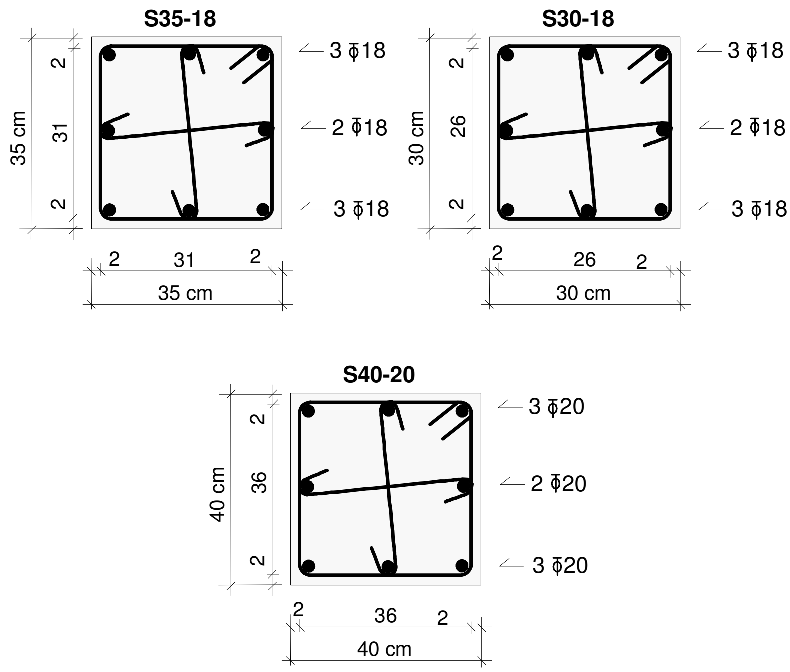

Figure 2.3: S30_18, S35_18 and S40_20 columns cross sections

During the production of the precast columns, 15x30 cm cylindrical specimens were taken to perform compression tests in the Material Laboratory of ITU. Adequate amount of transverse and longitudinal reinforcements were also tested. The results of the concrete compression tests are shown in Table 2.2

Table 2.2: Concrete compressive strength (150x300 mm cylinders)

Column	Sample 1 f_{c1} [MPa]	Sample 2 f_{c2} [MPa]	Sample 3 f_{c3} [MPa]	Mean f_{cm} [MPa]	Std. dev. σ [MPa]
S30_18, S35_18	51.6	40.1	45.6	45.8	5.8
S40_20	43.5	46.1	48.2	45.9	2.4

Test results for the transverse and longitudinal reinforcement are listed in Table 2.3 and Table 2.4, respectively.

Table 2.3: Rebar yield stresses

Rebar	Sample 1 f_{y1} [MPa]	Sample 2 f_{y2} [MPa]	Sample 3 f_{y3} [MPa]	Sample 4 f_{y4} [MPa]	Mean f_{ym} [MPa]	Std. dev. σ [MPa]
Φ8	482.8	455.4	491.8	475.4	476.3	15.5
Φ18	444.7	425.1	452.3	487.5	452.4	26.1
Φ20	539.7	539.9	541.1	540.7	540.4	0.7

Table 2.4: Rebar ultimate stresses

Rebar	Sample 1 f_{u1} [MPa]	Sample 2 f_{u2} [MPa]	Sample 3 f_{u3} [MPa]	Sample 4 f_{u4} [MPa]	Mean f_{um} [MPa]	Std. dev. σ [MPa]
Φ8	603.5	600.3	602.2	599.4	601.3	1.8
Φ18	555.9	533.3	557.6	647.4	573.5	50.5
Φ20	660.0	654.3	655.6	664.3	658.5	4.5

All of the specimens were exposed to cyclic displacements under constant axial force, until reaching severe damage which are crashing of concrete at the base of column, buckling of the longitudinal reinforcement and breaking of some longitudinal reinforcement. Photographs taken at different level of damages for each specimen are shown in Fig. 2.4.

Figure 2.4: The damages at the base of columns for different specimens

The constant axial force for specimens S30_18, S35_18 and S40_20 are 210 kN, 280 kN and 365 kN, repectively which correspond to %5 of axial force level that can be carried by specimens’ cross sections, individually. The cyclic displacement protocol used in the experimental works starts from small displacements and each displacement threshold are repeated three times. The displacement cycles are shown in Fig. 2.5.

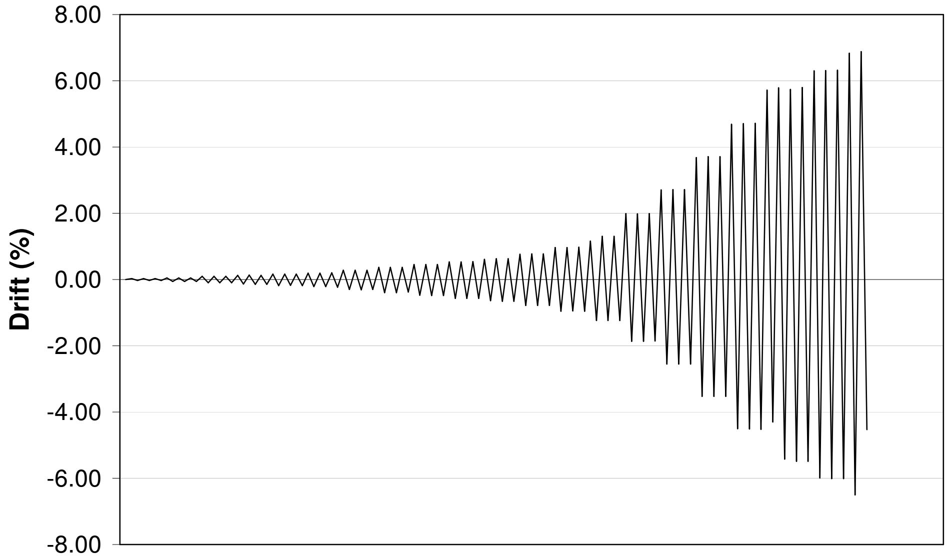

Figure 2.5: Repeated symmetric cycles

3. THEORETICAL STUDY

3.1 The Nonlinear Analysis Program of IDARC2D

In an effort to understand the behavior of building structures during earthquake motions, significant researches have been carried out. Due to the inherent complexities that buildings have, often, researches have focused on understanding element behavior through component testing.

Cyclic behavior of structures can be modeled by improved nonlinear computer analysis program named IDARC2D [15] which links experimental researches and analytical developments. IDARC2D includes the following analysis types: quasi-static cyclic analysis, inelastic dynamic analysis, monotonic and adaptive pushover analysis.

As describing the earthquake motion behavior, hysteresis has a very significant role in the analysis. Two hysteretic models exist in IDARC2D which are polygonal hysteretic model (PHM) and smooth hysteretic model (SHM).

The used hysteretic model in this study to represent the precast column behavior is smooth hysteretic model (SHM) which consists of hysteretic characteristics such as stiffness degradation, strength deterioration and pinching.

Non-degrading SHM is modeled by two parallel springs: post-yielding spring and hysteretic spring. An additional spring called slip-lock is introduced to consider pinching effect. These three springs are shown in Fig. 3.1. Post-yielding spring is a linear elastic spring whose coefficient is calculated by multiplication of initial stiffness by a constant parameter. The stiffness and strength degrading and non-degrading cyclic behavior are taken into consideration by the hysteretic spring. Slip-lock spring is tied as serious to hysteretic spring.

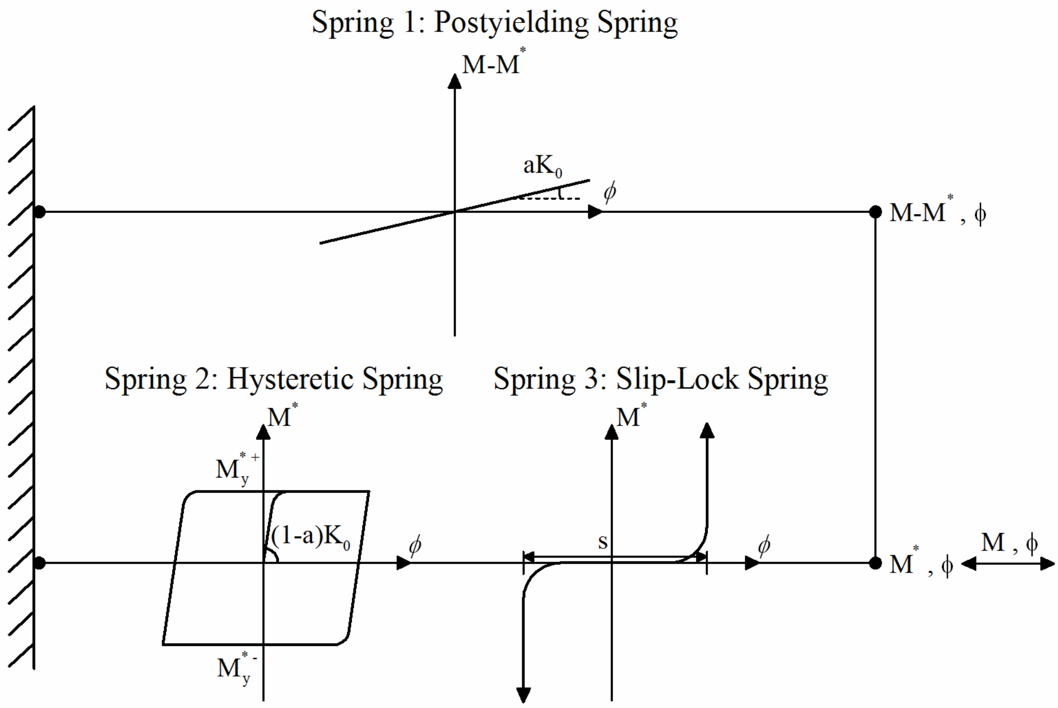

Figure 3.1: Multiple spring representation of smooth hysteretic model (SHM)

All these effects are defined in references [15,17] in details. Stiffness degradation expresses decrease of the load-reversal slope due to increasing ductility. A corresponding stiffness degrading parameter in SHM (α) is defined having a range of 2 to 200. Strength degradation includes an envelope degradation, which occurs when the maximum deformation attained in the past is exceeded, and continues energy based degradation. Corresponding parameters for strength degradation are ductility based (β_1) and energy based (β_2) strength degradation parameters. These parameters vary from 0.01 to 0.60 (no degrading to severe degrading). The stiffness and strength degradation are shown in Fig. 3.2. Pinching hysteretic loops usually are as a result of crack closure. These effects are defined by three parameters: slip length parameter (R_s), slip sharpness parameter (σ) and parameter of mean moment level of slip (λ). Also, to define characteristics of non-degrading smooth hysteretic model, smoothness parameter for elastic yield transition (N) and parameter for shape of unloading (η) are introduced. When N gets close to 10 the model reduces to bilinear system and when η has a value of 0.5 the unloading curve transform to linear.

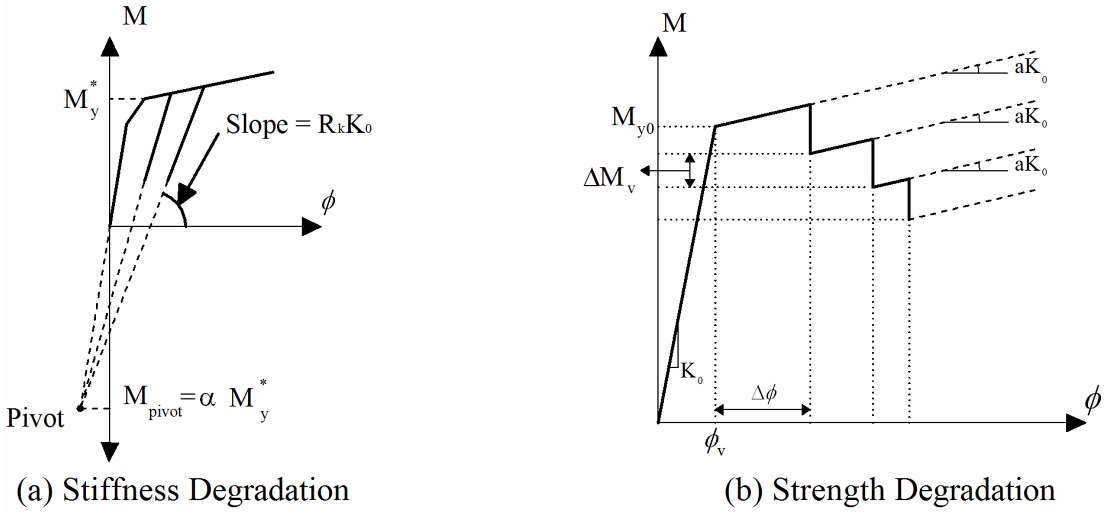

Figure 3.2: Stiffness and strength degradation

3.2 Simulation Study

A simulation study was performed by using IDARC2D. Quasi-static cyclic analysis was performed by applying piecewise linear cyclic displacement history which is the same with prescribed in the test. For tested 3 columns, (S30_18, S35-18, S40_20) mean values of the degradation parameters of SHM were determined by comparing experimental and analytical results.

IDARC2D has two alternatives to define section properties. Tri-linear moment curvature envelops have been used for reinforced concrete sections. A cross-sectional analysis program XTRACT [16] which includes moment-curvature, axial force-moment interaction and capacity orbit analysis, was used for creating moment curvature data.

Although any material model is available in XTRACT, default models which are Mander unconfined and confined concrete models and bilinear with strain hardening steel model, are used for moment-curvature computation.

The default strain values of XTRACT were used for unconfined concrete model; the strain at peak stress is taken as 0.002; and the crashing and spalling strains are taken as 0.004 and 0.006, respectively. The unconfined model formulation is described in the following equations and general stress-strain diagram is given in Fig. 3.3.

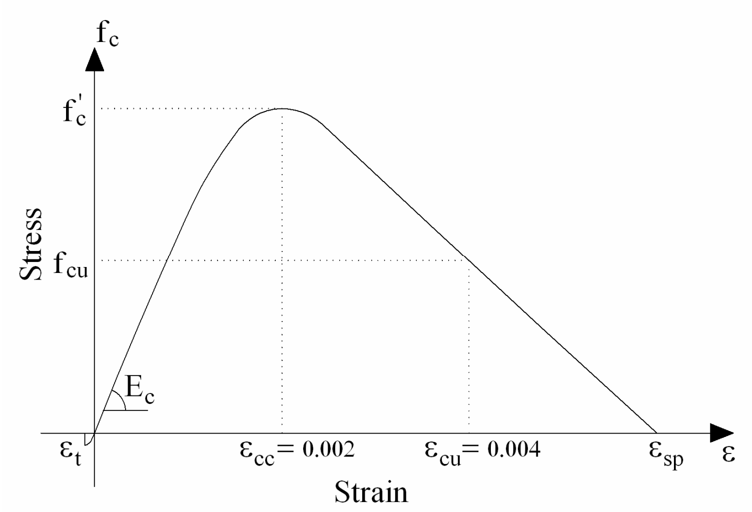

Figure 3.3: Stress-strain diagram for the Mander unconfined concrete model

For strain - $\varepsilon < 2 \cdot \varepsilon_t$ $\quad f_c = 0$ **(3.1)**

For strain - $\varepsilon < 0$ $\quad f_c = \varepsilon \cdot E_c$ **(3.2)**

For strain - $\varepsilon < \varepsilon_{cu}$ $\quad f_c = \dfrac{f_c^{'} \cdot x \cdot r}{r - 1 + x^r}$ **(3.3)**

For strain - $\varepsilon < \varepsilon_{sp}$ $\quad f_c = f_{cu} + \left(f_{cp} - f_{cu}\right) \cdot \dfrac{\varepsilon - \varepsilon_{cu}}{\varepsilon_{sp} - \varepsilon_{cu}}$ **(3.4)**

$$x = \frac{\varepsilon}{\varepsilon_{cc}} \quad \textbf{(3.5)}$$

$$r = \frac{E_c}{E_c - E_{\sec}} \quad \textbf{(3.6)}$$

$$E_{\sec} = \frac{f_c^{'}}{\varepsilon_{cc}} \quad \textbf{(3.7)}$$

Where ε is concrete strain, f_c is concrete stress, E_c is elastic modulus, E_{sec} is secant modulus, ε_t is tension strain capacity, ε_{cu} is ultimate concrete strain (0.004), ε_{cc} is strain at peak stress (0.002), ε_{sp} is spalling strain (0.006), $f_c^{'}$ is 28 day compressive strength, f_{cu} is stress at ε_{cu} and f_{cp} is post spalling stress.

The unconfined stress-strain diagram for specimen S40_20 is depicted in Fig. 3.4.

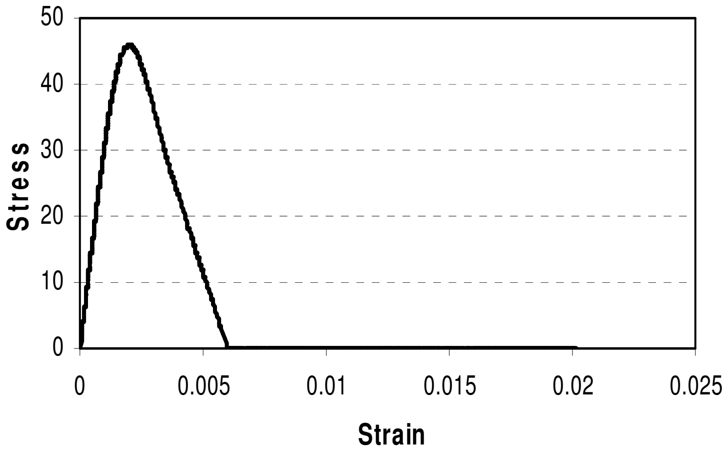

Figure 3.4: The Mander unconfined concrete model for specimen S40_20

The equations of confined concrete model are similar with unconfined concrete's. The formulation of confined concrete model is described in following equations and general stress-strain diagram is given in Fig. 3.5.

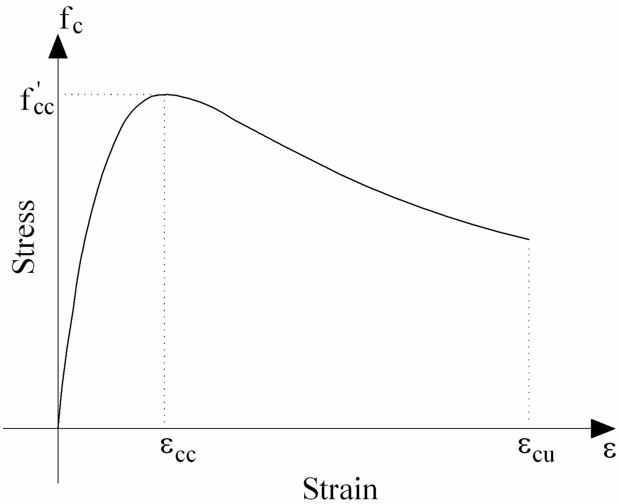

Figure 3.5: Stress-strain diagram for the Mander confined concrete model

For strain - $\varepsilon < 2 \cdot \varepsilon_t$ $\quad f_c = 0$ $\quad$ (eq. 3.1)

For strain - $\varepsilon < 0$ $\quad f_c = \varepsilon \cdot E_c$ $\quad$ (eq.3.2)

For strain - $\varepsilon < \varepsilon_{cu}$ $\quad f_c = \dfrac{f'_{cc} \cdot x \cdot r}{r - 1 + x^r}$ $\quad$ **(3.8)**

$x = \dfrac{\varepsilon}{\varepsilon_{cc}}$ $\quad$ (eq.3.5)

$$\varepsilon_{cc} = 0.002 \cdot \left[1 + 5\left(\frac{f_{cc}^{'}}{f_c^{'}} - 1\right)\right] \qquad \textbf{(3.9)}$$

$$r = \frac{E_c}{E_c - E_{\sec}} \qquad \text{(eq.3.6)}$$

$$E_{\sec} = \frac{f_{cc}^{'}}{\varepsilon_{cc}} \qquad \textbf{(3.10)}$$

Where $f_{cc}^{'}$ is confined concrete strength.

The confined stress-strain diagram for specimen S40_20 is depicted in Fig. 3.6.

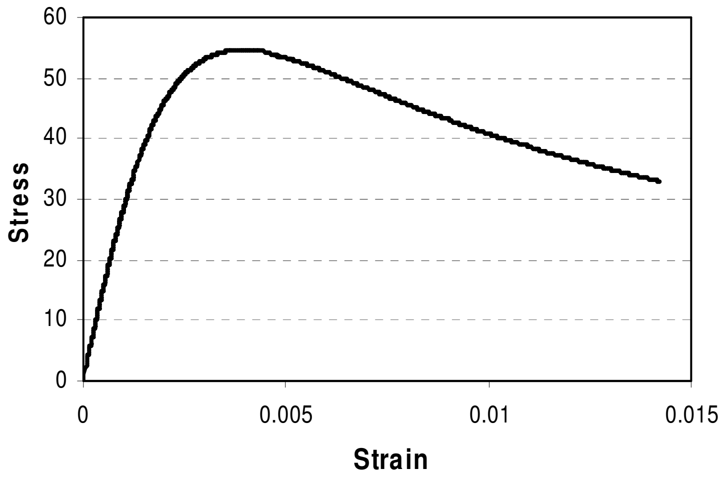

Figure 3.6: The Mander confined concrete model for specimen S40_20

The formulation of bilinear with parabolic strain hardening steel model is described in following equations and general stress-strain diagram is given in Fig. 3.7.

For strain - $\varepsilon < 2 \cdot \varepsilon_y$ $\quad f_s = E \cdot \varepsilon$ **(3.11)**

For strain - $\varepsilon < \varepsilon_{sh}$ $\quad f_c = f_y$ **(3.12)**

For strain - $\varepsilon < \varepsilon_{su}$ $\quad f_s = f_u - (f_u - f_y) \cdot \left(\frac{\varepsilon_{su} - \varepsilon}{\varepsilon_{su} - \varepsilon_{sh}}\right)^2$ **(3.13)**

Where ε is steel strain, f_s is steel stress, f_y is yield stress, f_u is rapture stress, ε_y is yield strain, ε_{sh} is strain at strain hardening, ε_{su} is failure strain E is elastic modulus.

For all specimens, strain at strain hardening is taken as 0.02 and failure strain is taken as 0.10. The stress-strain relationship of steel model for specimen S40_20 is depicted in Fig. 3.8.

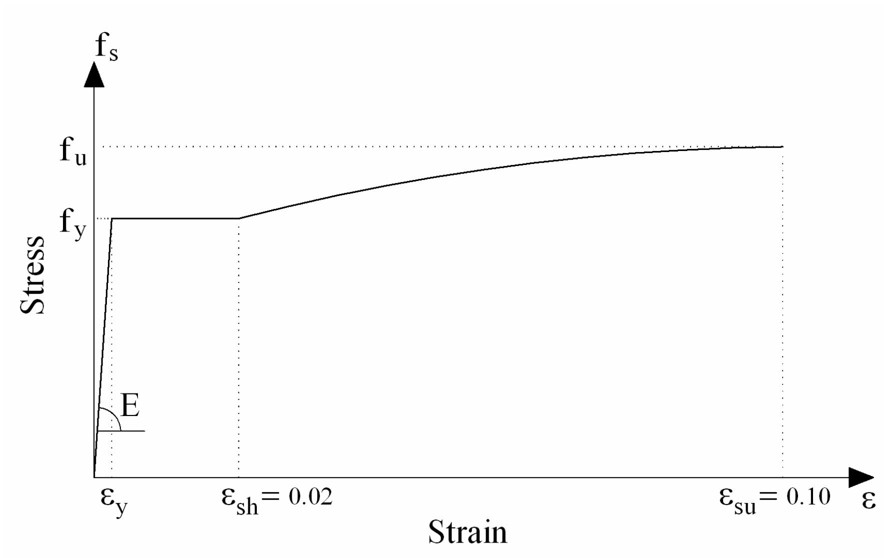

Figure 3.7: Stress-strain diagram for steel model

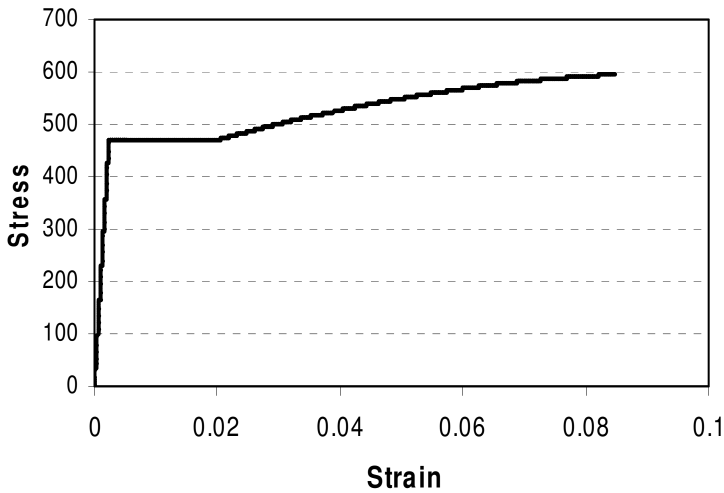

Figure 3.8: The bilinear with parabolic strain hardening steel model for specimen S40_20

The stress values for all material types are taken as approximately mean values of material experiments' results.

After defining section properties, the cross section is divided into triangle meshes having maximum mesh size of 20 mm, (Fig. 3.9).

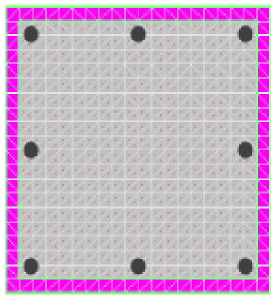

Figure 3.9: The finite element model of column cross section

After moment-curvature analysis is performed, XTRACT has the capability of bi-linearization of the polygonal moment-curvature relationship with reasonable approximation. Since SHM model in IDARC2D is formed by using the bi-linear force-displacement relationship, it is very reasonable to use XTRACT for preparing input data for IDARC2D. A typical idealized moment curvature relationship is shown in Fig. 3.10.

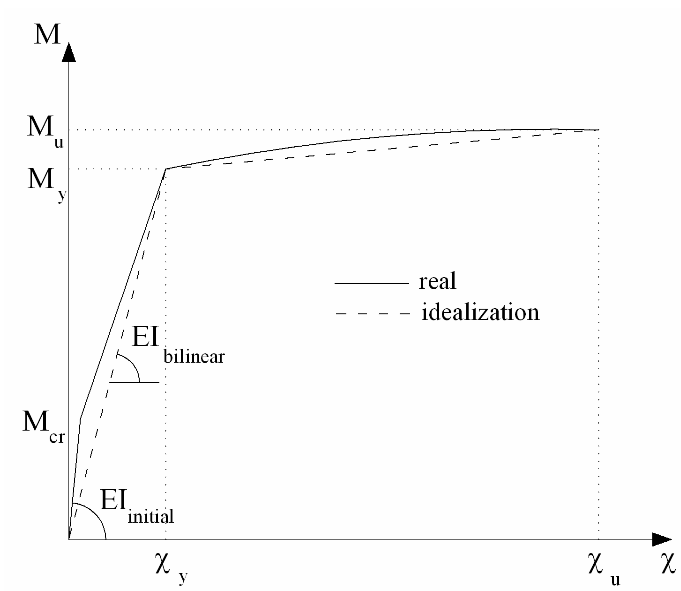

Figure 3.10: Idealized bi-linear moment curvature relationship

The moment curvature relationships obtained for S40_20 is depicted in Fig. 3.11.

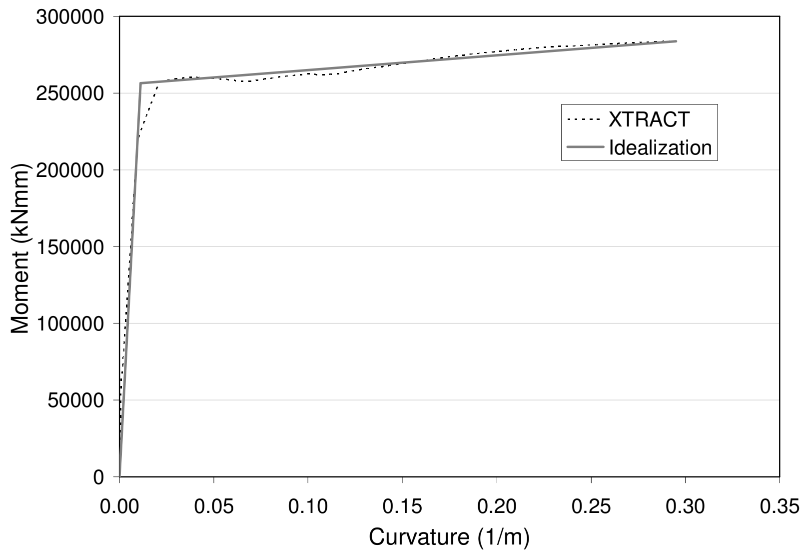

Figure 3.11: Bi-linear moment curvature graph for sample S40_20

Also, moment-axial force interaction analysis was performed by XTRACT and two axial load levels were determined; axial yield force (ANY) and axial balance force (ANB) as shown in Fig. 3.12. The axial force applied to the specimen is defined as axial normal (AN).

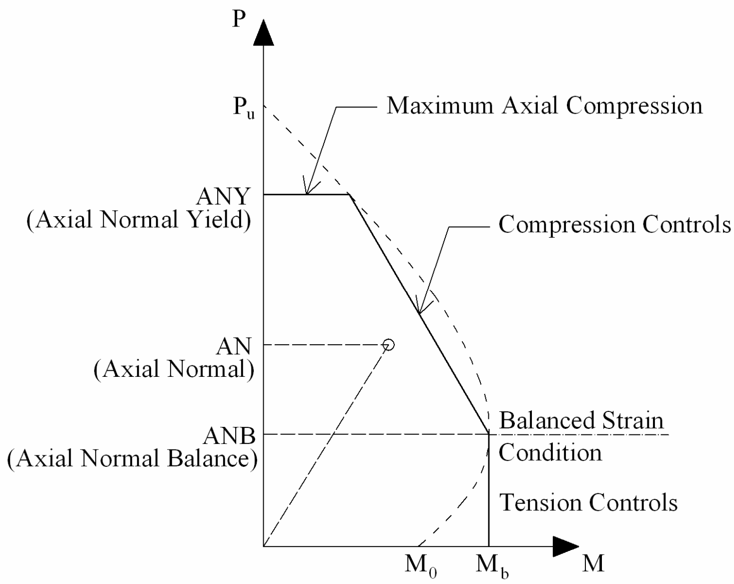

Figure 3.12: P-M interaction diagram

The idealized (bilinear) moment-curvature relations (Fig. 3.13) include following characteristics: EI (initial flexural stiffness obtained from bi-linear idealization), EI3P (post yield flexural stiffness), M_{cr} (cracking moment), M_y (yield moment), χ_y (yield curvature), χ_u (ultimate curvature), EA (axial stiffness).

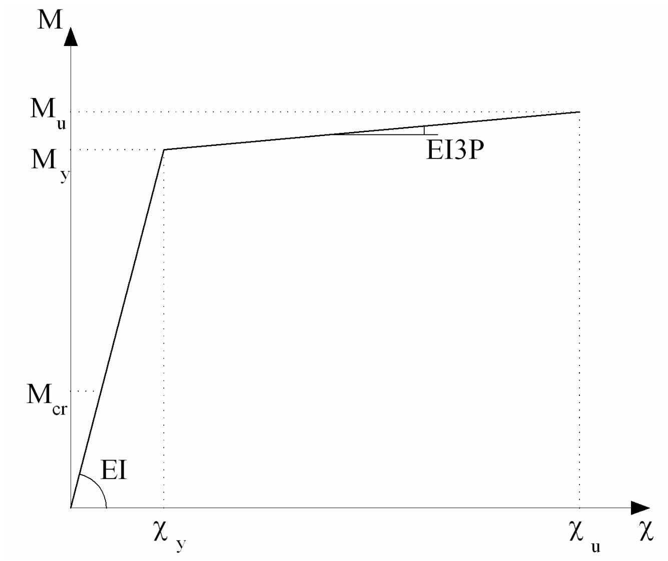

Figure 3.13: Bilinear moment-curvature relation

Table 3.1 contains the necessary information to define the envelop of moment curvature relations for the tested three specimens. The base shear versus top displacement relations of S30_18, S35_18 and S40_20 extracted from quasi-static cyclic analyses are shown in Fig. 3.14, Fig. 3.15 and Fig. 3.16 respectively.

Table 3.1: The moment curvature data for the tested specimens

Specimen	EI (kNm^2)	EI3P (%EI)	M_{cr} (kNm)	M_y (kNm)	χ_{yield} (1/m)	$\chi_{ultimate}$ (1/m)	EA (kN)
S30_18	8562	0.1975	25.9	124.5	0.014613	0.4161	2882700
S35_18	13800	0.2645	38.7	163.7	0.011940	0.3618	3923675
S40_20	22300	0.4359	57.9	256.4	0.011578	0.2951	5131200

The calibrated smooth hysteretic model parameters used for all tested columns are listed in Table 3.2. The ranges for these parameters defined in program manual are given in Table 3.3.

Table 3.2: The parameters of smooth hysteretic model (SHM)

	α	β_1	β_2	R_s	σ	λ	N	η
S30_18	4	0.10	0.10	0.08	0.02	0.60	2	0.49
S35_18	3	0.10	0.12	0.07	0.02	0.60	2	0.49
S40_20	4	0.10	0.12	0.13	0.06	0.60	2	0.49

Table 3.3: The variation of SHM parameters in IDARC2D

Parameter	*Limit (No degrading)*	*Mild*	*Moderate*	*Severe*	*Limit*
α	200	15	10	4	2
β_1	0.01	0.15	0.30	0.60	0.60
β_2	0.01	0.08	0.15	0.60	0.60
R_s	0.01	0.01	0.25	0.40	
σ	100	0.40	0.25	0.05	0.01
λ	1				0
N	10 *(bi-linear)*				1
η	0.5 *(linear)*				0

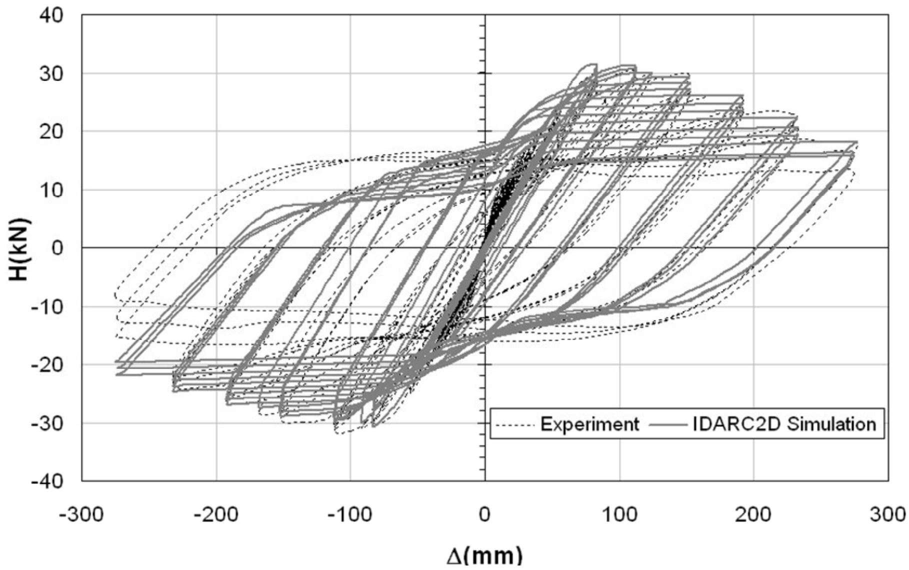

Figure 3.14: Base shear-top displacement relationship for S30_18

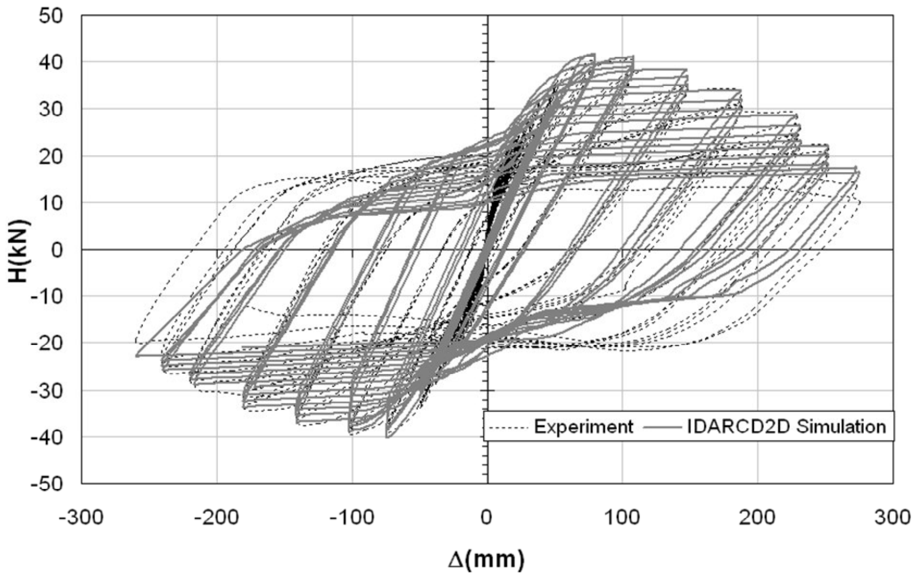

Figure 3.15: Base shear-top displacement relationship for S35_18

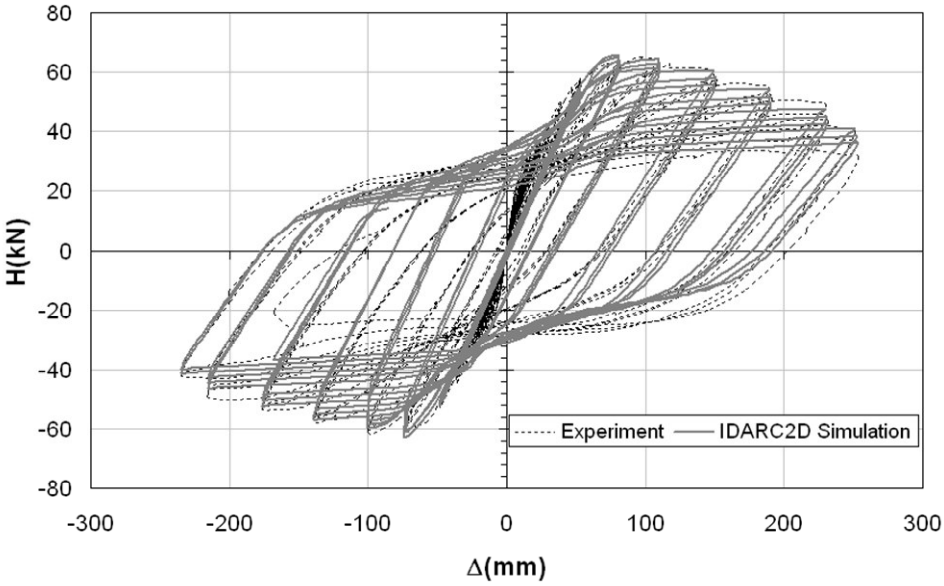

Figure 3.16: Base shear-top displacement relationship for S40_20

Envelop curves of the experimental and theoretical hysteresis are given in Fig. 3.17, Fig. 3.18 and Fig. 3.19 for all the tested specimens.

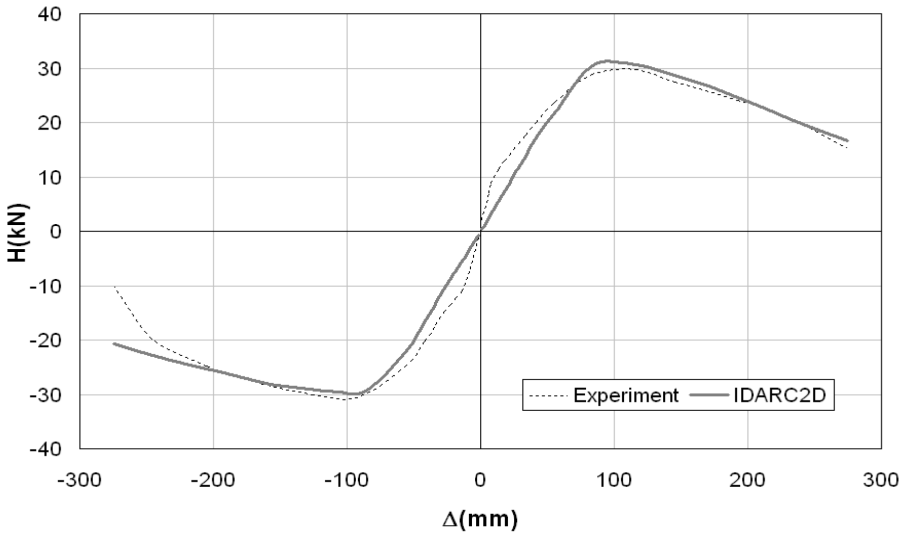

Figure 3.17: Comparison of the envelopes for S30_18

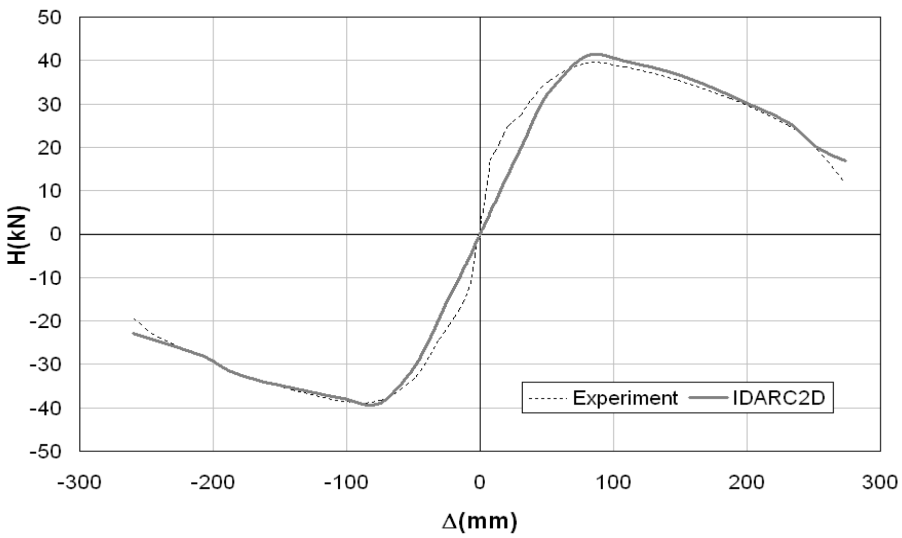

Figure 3.18: Comparison of the envelopes for S35_18

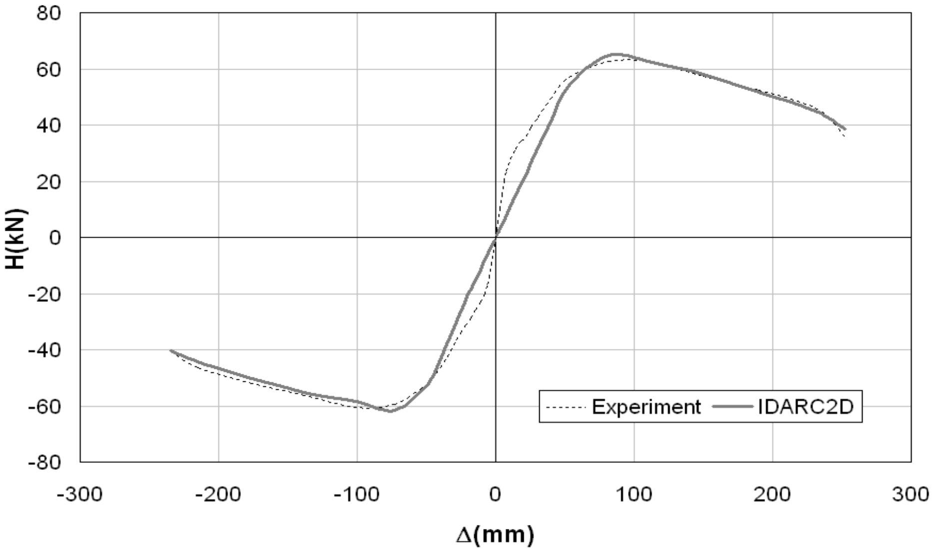

Figure 3.19: Comparison of the envelopes for S40_20

3.3 Nonlinear Time History Analyses of Precast Columns

3.3.1 Parameters of the Study

Nonlinear time history analyses of 18 precast columns were performed. The main parameters used in the study are dimensions of cross section and longitudinal reinforcement ratio. The used sectional dimensions are 30x30 cm, 35x35 cm, 40x40 cm, 45x45 cm, 50x50 cm, 60x60 cm. For each cross sectional dimension three longitudinal reinforcement ratios (1%, 2%, 3%) were used. The column samples used for nonlinear time history analysis are listed in Table 3.4.

Table 3.4: Columns used for nonlinear time history analyses

		Section dimensions					
		30x30	35x35	40x40	45x45	50x50	60x60
Steel Ratio	1%	S30_1%	S35_1%	S40_1%	S45_1%	S50_1%	S60_1%
	2%	S30_2%	S35_2%	S40_2%	S45_2%	S50_2%	S60_2%
	3%	S30_3%	S35_3%	S40_3%	S45_3%	S50_3%	S60_3%

The typical cross section of columns is given in Fig. 3.20. The section consists of 8 bars with one stirrup and two ties. Diameter of all lateral reinforcement is 8 mm and fictive diameters of bars for each column type are calculated by dividing total longitudinal reinforcement area to 8.

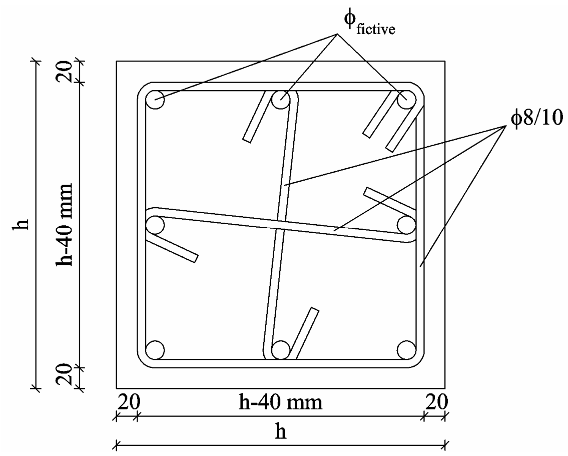

Figure 3.20: Typical cross section of columns

Default material models of XTRACT were used in the parametric study. For unconfined concrete material model, a 28 day compressive stress of 40 MPa were taken with the strain at peak stress of 0.002 and the crushing strain of 0.004. For bi-linear with parabolic strain hardening steel model, the stress-strain values were taken from Turkish Seismic Code. The corresponding values for steel model are: yield stress f_y = 420 MPa, ultimate stress f_u = 550 MPa, strain at strain hardening ε_{sh} =0.008 and ultimate strain ε_{su} =0.10.

The moment curvature relationships of columns were obtained by using XTRACT. The corresponding moment curvature data for each column are listed in Table 3.5.

The SHM model parameters used in nonlinear time history analyses are α=3, β_1=0.10, β_2=0.10, R_s= 010, σ =0.03, λ=0.60, N=2, η=0.49 which were obtained from the calibration process.

Table 3.5: The moment curvature data for columns

Column	EI (kNm^2)	EI3P (%EI)	M_{cr} (kNm)	M_y (kNm)	χ_{yield} (1/m)	$\chi_{ultimate}$ (1/m)	EA (kN)
S30_%1	5412	0.180	23.9	73.53	0.013658	0.4724	2693700
S30_%2	7709	0.317	24.2	114.6	0.014934	0.3169	2693700
S30_%3	9801	0.449	26.4	152.9	0.015678	0.3338	2693700
S35_%1	9642	0.257	33.7	110.2	0.011487	0.3847	3666425
S35_%2	14300	0.423	34.3	178.5	0.012502	0.3257	3666425
S35_%3	18400	0.527	37.4	242.2	0.013206	0.2536	3666425
S40_%1	16000	0.337	45.5	157.3	0.009864	0.3230	4778800
S40_%2	24600	0.496	48.5	263.1	0.010753	0.2943	4778800
S40_%3	31800	0.646	50.7	358.7	0.011316	0.2176	4778800
S45_%1	25100	0.391	59.3	216.9	0.008672	0.2796	6060825
S45_%2	39800	0.549	63.3	372.8	0.009407	0.2568	6060825
S45_%3	51600	0.736	69.9	508.2	0.009904	0.1880	6060825
S50_%1	37800	0.440	80.0	290.2	0.007708	0.2461	7482500
S50_%2	61000	0.594	80.0	508.1	0.008371	0.2169	7482500
S50_%3	79300	0.808	88.6	695.0	0.008805	0.1641	7482500
S60_%1	76800	0.503	133.0	483.3	0.006322	0.1993	10774800
S60_%2	125000	0.732	133.0	854.5	0.006848	0.1635	10774800
S60_%3	167000	0.908	148.0	1198.0	0.007195	0.1237	10774800

3.3.2 Strong Ground Motion Data Set

A total number of 80 ground motion records from various locations of the world were used in the analytical work. Half of the records are in far fault type and the other half are in near fault type. While selecting the records, different characteristics were considered such as peak ground acceleration (PGA), peak ground velocity (PGV), the location of earthquake record and site soil type. All of the near fault ground motions were obtained from stations that are located less than 8.9 km to the source and the corresponding PGV values range from 43.9 cm/s to 173.8 cm/s. The peak ground acceleration values (PGA) of near fault records change between 263 cm/sn^2 to 1260 cm/sn^2. 19 of the near fault ground motions (nf series) were taken from SAC steel project [24] in which the records were rearranged by changing their direction to fault normal and fault parallel components. The directions of other records were not changed. The PGA values of far fault earthquakes range from 195.2 cm/s^2 to 866.2 cm/s^2 while PGV values range from 9.2 cm/s to 58.8cm/s. The surface wave magnitude (M_s) changes between 5.7 and 7.8 for the overall strong motion data set. Far fault and near fault ground motions used in nonlinear time history analyses are listed in Table 3.6 and Table 3.7, respectively. Also, classification of the used earthquake records into several velocity and acceleration intervals are given in Fig. 3.21 and Fig. 3.22, respectively.

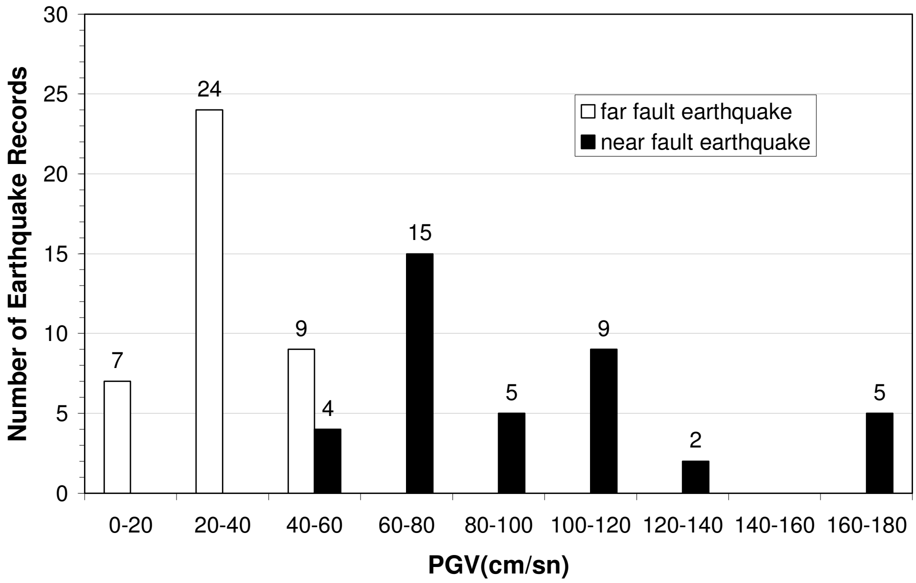

Figure 3.21: Distribution of the earthquake records into several PGV intervals

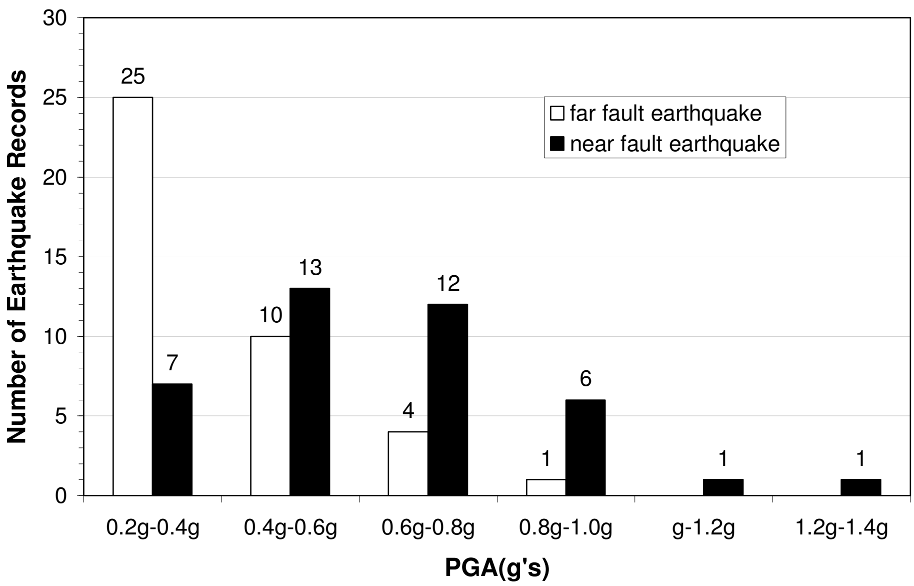

Figure 3.22: Distribution of the earthquake records into several PGA intervals

Table 3.6: Far fault earthquake records used in the analytical work

Record	M_s	d (km)	PGA (cm/s^2)	PGV (cm/s)
Kocaeli 17/08/1999 Düzce S. DZC180	7.8	12.7	306.1	58.8
Kocaeli 17/08/1999 Düzce S. DZC270	7.8	12.7	351.2	46.4
Adana-Ceyhan 27/06/1998 Ceyhan S. East	5.9*	4.0	273.7	28.1
Bingöl 01/05/2003 Bingöl S. North	6.1**	10.0	545.4	37.0
W. Washington 13/04/1949 Olympia S. Com (86)	7.1	-	274.6	17.1
S. Fernando 09/02/1971 24278 Castaic S. ORR291	6.6	24.9	262.9	25.9
Imp. Valley 15/10/1979 5053 Calexico S. CXO225	6.9	10.6	269.8	21.2
Imp. Valley 15/10/1979 5055 Holtville S. H-HVP225	6.9	7.5	248.2	48.8
Coyote Lake 06/08/1979 Gilroy Array #4 San Yasidro School Com (360)	5.7	-	246.2	32.9
Coalinga 02/05/1983 36456 Parkfield S. H-Z14000	6.5	29.9	276.6	40.9
Coalinga 02/05/1983 36456 Parkfield S. H-Z14090	6.5	29.9	268.8	28.3
Chalfant Valley 07.21.1986 54428 Zack Brothers Ranch A-ZAK270	6.0	18.7	438.5	36.9
Chalfant Valley 07.21.1986 54428 Zack Brothers Ranch A-ZAK360	6.0	18.7	392.4	44.5
Friuly 06/05/1976 8012 Tolmezzo S. TMZ000	6.5	15.8	344.3	22.0
Friuly 06/05/1976 8012 Tolmezzo S. TMZ270	6.5	15.8	309.0	30.8
Victoria 6604 09/06/1980 Cerro Prieto S. CPE045	6.4	14.4	609.2	31.6
Victoria 6604 09/06/1980 Cerro Prieto S.CPE315	6.4	14.4	575.8	19.9
Whittier Narrows 01/10/1987 24436 Tarzana, Cedar Hill S. A-TAR000	5.7	43.0	440.5	20.1
Whittier Narrows 01/10/1987 24436 Tarzana, Cedar Hill S. A-TAR090	5.7	43.0	631.8	22.9
Alkion-Greece 24/02/1981 Korinthos-OTE Building Direction (Y)	6.6#	10.0	303.6	22.6
Campano Lucano 23/11/1980 Sturno S. Dir.(Y)	6.9#	14.0	316.6	55.3
South Iceland 17/06/2000 Thjorsarbru S. Dir.(Y)	6.5#	14.0	508.3	23.8

Record	M_s	d (km)	PGA (cm/s^2)	PGV (cm/s)
Avej 22/06/2002 Avej(Bakhshdari) S. Dir.(X)	6.5#	-	437.4	22.5
Taiwan Smart 20/05/1986 29 SMART1 M07 St. 40M07NS	6.4	64.0	249.2	23.7
Superstitn Hills(B) 24/11/1987 5061 Calipatria Fire Station CAL315	6.6	28.3	242.3	14.6
Spitak 07/12/1988 12 Gukasian S. GUK000	7.0	30.0	195.2	28.6
Irpinia 23/11/1980 Sturno S. STU270	6.5*	32.0	351.2	52.7
Irpinia 23/11/1980 Sturno S. STU000	6.5*	32.0	246.2	37.0
North Palm Springs 12204 08/07/1986 San Jacinto -Soboba H08000	6.0	32.0	245.3	9.6
North Palm Springs 12204 08/07/1986 San Jacinto -Soboba H08090	6.0	32.0	234.5	9.2
Kiholo Bay, Hawai`i Island 15/10/2006 HI:Hawai`i; Honokaa, Police St. Com (90)	6.7#	-	640.0	14.8
Kiholo Bay, Hawai`i Island 15/10/2006 HI:Hawai`i; Honokaa, Police St. Com (360)	6.7#	-	639.0	24.8
El Salvador 13/01/2001 Observatorio S. Com(180)	7.8	-	419.5	38.4
El Salvador 13/01/2001 Observatorio S. Com(90)	7.8	-	372.0	26.2
Landers 28/06/1992 23 Coolwater S. CLW-LN	7.4	21.2	277.6	25.6
Landers 28/06/1992 23 Coolwater S. CLW-TR	7.4	21.2	409.1	42.3
Northridge 17/01/1994 24538 Santa Monica City Hall STM090	6.7	27.6	866.2	41.7
Northridge 17/01/1994 24538 Santa Monica City Hall STM360	6.7	27.6	363.0	25.1
Northridge 17/01/1994 224400 LA - Obregon Park OBR090	6.7	37.9	348.3	16.7
Northridge 17/01/1994 224400 LA - Obregon Park OBR360	6.7	37.9	552.4	24.5

*=MI values, **=Md values , #=Mw values

Table 3.7: Near fault earthquake records used in the analytical work

Record	M_s	d (km)	PGA (cm/s^2)	PGV (cm/s)
nf01 (Tabas) 16/09/1978 Tabas S.	7.4	1.2	882.8	110.0
nf02 (Tabas) 16/09/1978 Tabas S.	7.4	1.2	958.6	105.8
nf03 (Loma Prieta) 18/10/1989 Los Gatos S.	7.0	3.5	703.8	172.8
nf04 (Loma Prieta) 18/10/1989 Los Gatos S.	7.0	3.5	449.4	91.1
nf05 (loma Prieta) 18/10/1989 Lex Dam S.	7.0	6.3	672.9	178.6
nf06 (Loma Prieta) 18/10/1989 Lex Dam S.	7.0	6.3	363.0	68.6
nf07 (C. Mendocino) 25/04/1992 Petrolia S.	7.1	8.5	625.6	125.8
nf08 (C. Mendocino) 25/04/1992 Petrolia S.	7.1	8.5	642.3	93.0
nf09 (Erzincan) 13/03/1992	*6.7	2.0	423.9	119.2
nf10 (Erzincan) 13/03/1992	*6.7	2.0	448.3	58.1
nf12 (Landers) 28/06/1992 24 Lucerne S.	7.4	1.1	783.9	70.3
nf13 (Northridge) 17/ 01/1994 77 Rinaldi Receiving Station.	6.7	7.5	872.7	174.5
nf14 (Northridge) 17/ 01/1994 77 Rinaldi Receiving Station.	6.7	7.5	381.0	60.2
nf15 (Northridge) 17/ 01/1994 24514 Sylmar - Olive View Med FF	6.7	6.4	718.2	122.2
nf16 (Northridge) 17/ 01/1994 24514 Sylmar - Olive View Med FF	6.7	6.4	583.8	53.9
nf17 (Kobe) 16/01/1995	6.9	3.4	1067.3	160.2
nf18 (Kobe) 16/01/1995	6.9	3.4	564.0	72.3
nf19 (Kobe) 16/01/1995 Takatori S.	6.9	4.3	771.1	173.8
nf20 (Kobe) 16/01/1995 Takatori S.	6.9	4.3	416.1	63.7
Kocaeli 17/08/1999 Yarımca S. YPT060	7.8	2.6	262.9	65.7
Kocaeli 17/08/1999 Sakarya S. East	7.8	3.1	407.1	79.5
Düzce 12/11/1999 Düzce S. DZC180	7.3	8.2	341.4	60.0
Düzce 12/11/1999 Düzce S. DZC270	7.3	8.2	524.8	83.5
Chi-Chi Taiwan 20/09/1999 CHY080-West	7.6	7.0	949.6	107.5

Record	M_s	d (km)	PGA (cm/s^2)	PGV (cm/s)
Northridge 17/01/1994 0637 Sepulveda VA S. SPV360	6.7	8.9	921.2	76.6
Northridge 17/01/1994 74 Sylmar - Converter Sta SCS052	6.7	6.2	600.4	117.4
Northridge 17/01/1994 74 Sylmar - Converter Sta SCS142	6.7	6.2	880.0	102.8
Northridge 17/01/1994 24279 Newhall - Fire Sta NWH090	6.7	7.1	571.9	75.5
Northridge 17/01/1994 24279 Newhall - Fire Sta NWH360	6.7	7.1	578.8	97.2
Northridge 17/01/1994 24207 Pacoima Dam (upper left) PUL194	6.7	8.0	1260.6	103.9
Northridge 17/01/1994 Sylmar - County Hosp. Parking Lot Component (90)	6.7	6.4	592.5	76.9
Superstitn Hills(B) 24/11/1987 5051 Parachute Test Site PTS225	6.6	0.7	446.4	112.0
Superstitn Hills(B) 24/11/1987 5051 Parachute Test Site PTS315	6.6	0.7	369.8	43.9
Imp. Valley 15/10/1979 942 El Centro Array #6 H-E06140	6.9	1.0	402.2	64.9
Imp. Valley 15/10/1979 942 El Centro Array #6 H-E06230	6.9	1.0	430.7	109.8
Imp. Valley 15/10/1979 Meloland H-EMO000	6.9	0.5	308.0	71.7
Imp. Valley 15/10/1979 Meloland H-EMO270	6.9	0.5	290.4	90.5
Morgan Hill 24/04/1984 57217 Coyote Lake Dam (SW Abut) CYC195	6.1	0.1	697.5	51.6
Gazli,USSR 17/05/1976 9201 Karakyr GAZ090	7.3	5.5	704.4	71.6
Gazli,USSR 17/05/1976 9201 Karakyr GAZ000	7.3	5.5	596.4	65.4

*=MI values, **=Md values , #=Mw values

The main difference between near fault and far fault earthquake records is PGV values. The near fault earthquake records have high PGV values, whereas the far fault records have small. The following figures describe this difference. A near fault and a far fault record of Northridge Earthquake are shown in Fig. 3.23 and Fig. 3.24, respectively. In these figures, although the PGA values are in the same magnitude, PGV values of the near fault ground motion (Rinaldi station) is approximately four times bigger than the far fault ground motion, (Santa Monica Hall Station).

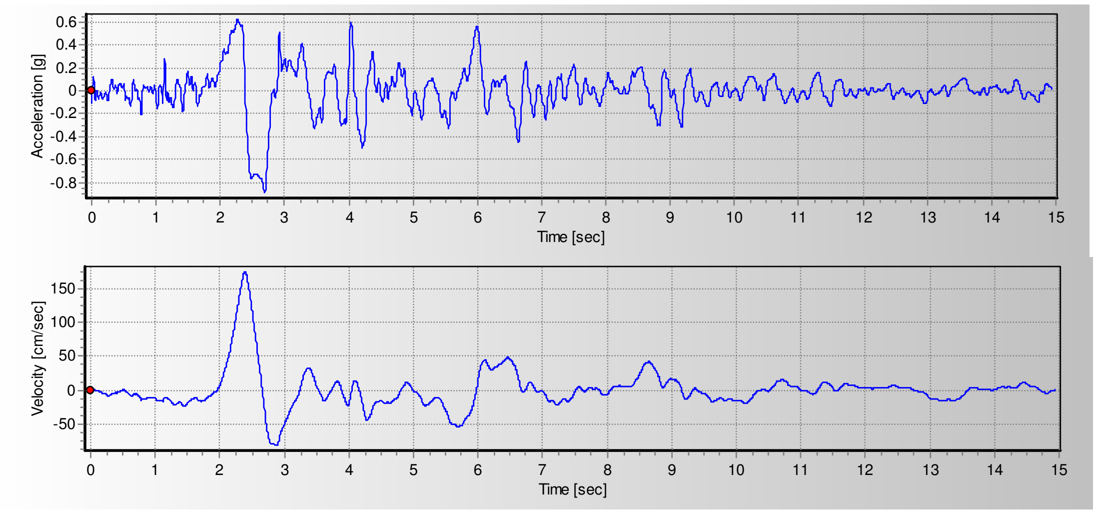

Figure 3.23: Northridge Earthquake Rinaldi Station ground motion record

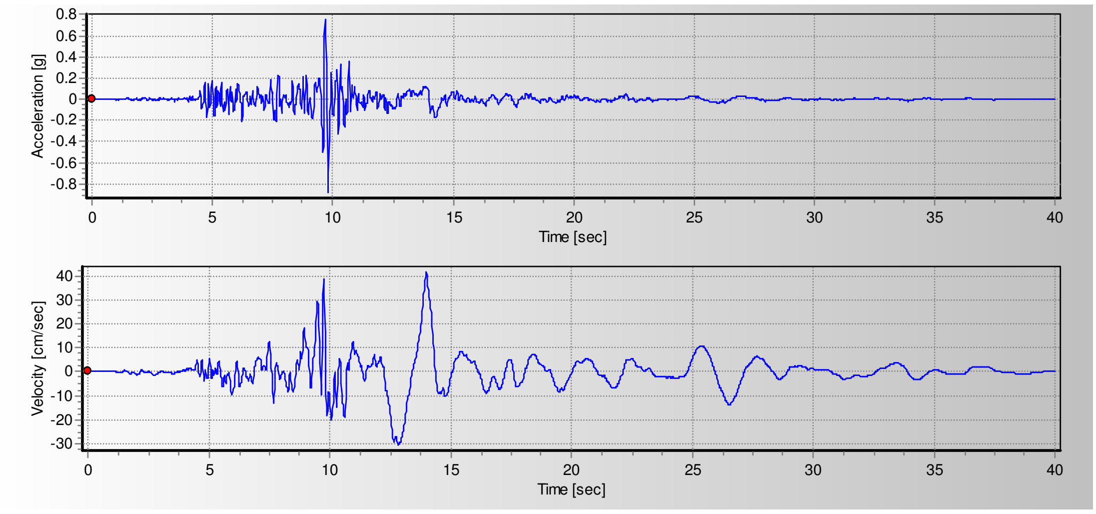

Figure 3.24: Northridge Earthquake Santa Monica Hall Station ground motion record

3.3.3 Elastic Response Spectrums

Elastic response spectrum curves for all seismic records are calculated by Seismosignal, [30]. 5% of the critical damping has been used in this calculation. Three average elastic spectra were created from 80 ground motions. The corresponding spectrums represent response of near fault, far fault and overall ground motions and these spectrums are shown in Fig. 3.25, Fig. 3.26 and Fig. 3.27, respectively. The elastic spectra given in Turkish Code is very similar to average spectra calculated from overall ground motion records (Fig. 3.27). But, if the responses for near fault and far fault ground motions are evaluated separately, it can be seen that the spectrum given in Turkish Code for firm soil have smaller acceleration values than average near fault spectra (Fig. 3.25) and have larger acceleration values than average far fault spectra (Fig. 3.26).

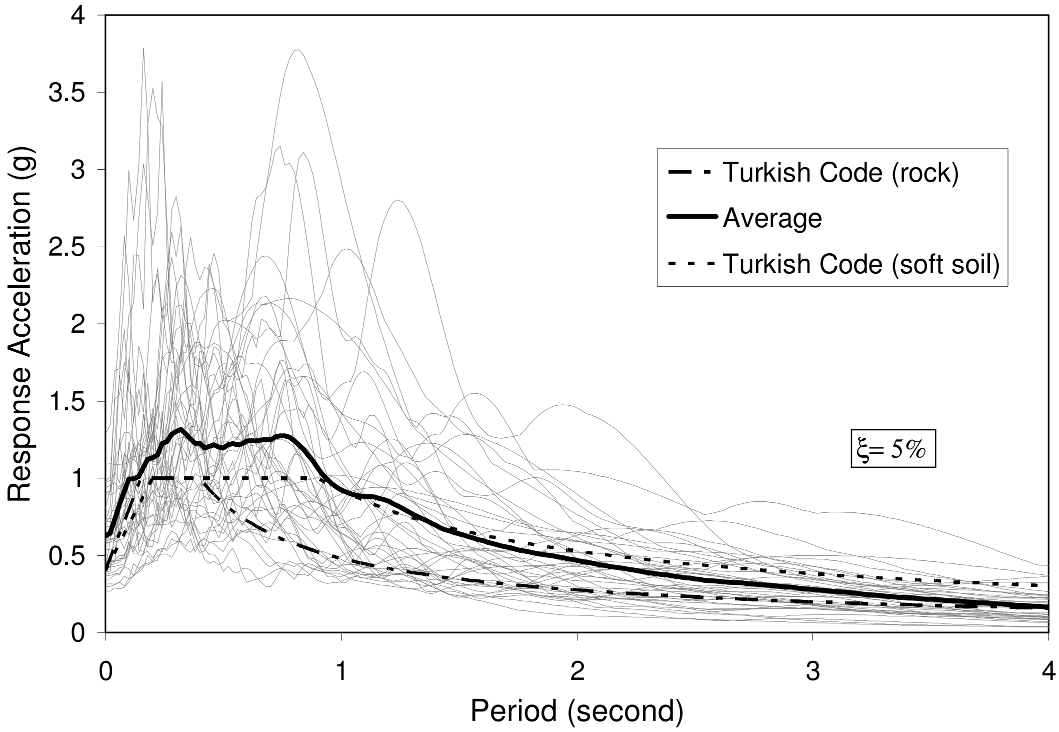

Figure 3.25: Average elastic response spectra for near fault ground motions

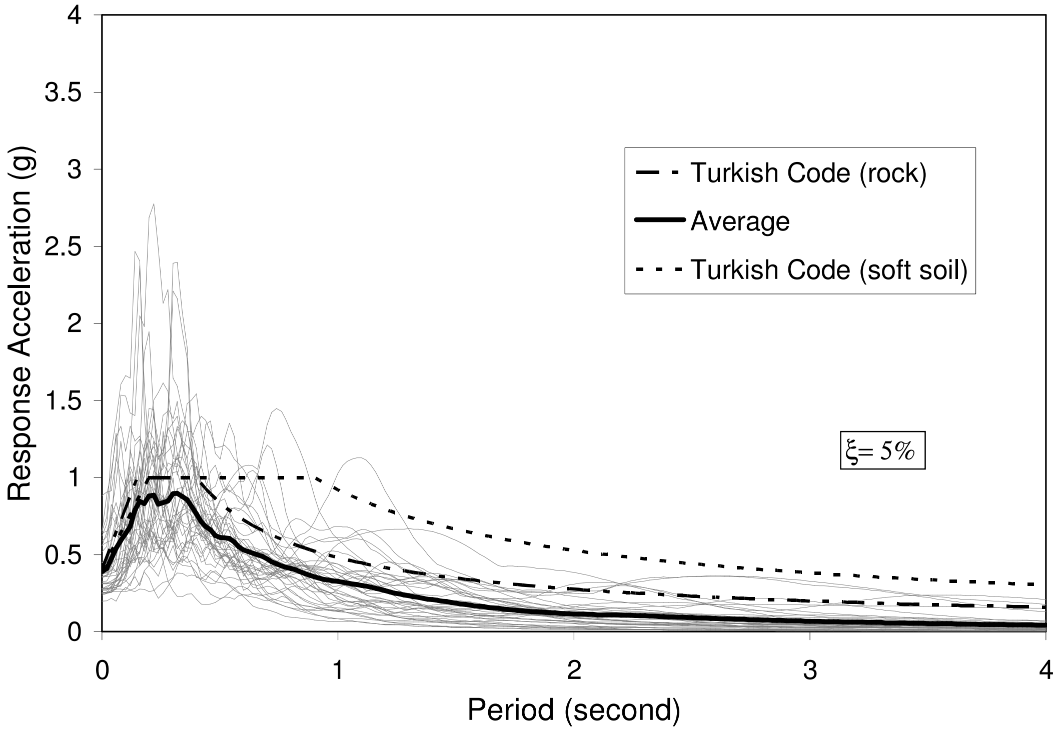

Figure 3.26: Average elastic response spectra for far fault ground motions

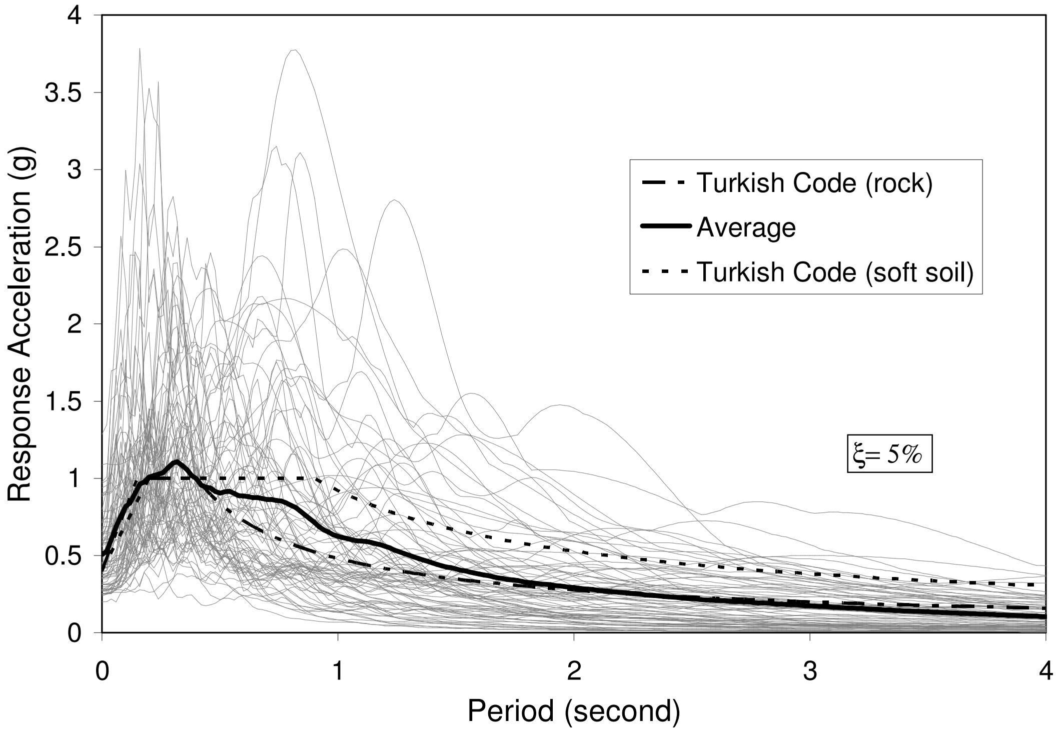

Figure 3.27: Average elastic response spectra for overall ground motions

3.3.4 Application of Nonlinear Time History Analysis by IDARC2D

3.3.4.1 Applied Mass for All Column Samples

A seismic weight of 200 kN, which corresponds to the support reaction of simply supported precast roof beam for one storey industrial type building, exposed to the columns. The column design was carried out for a ground motion with exceedance probability of 10% in 50 years and the location of the building is supposed to be in seismic zone 1 in Turkey. The corresponding effective ground motion coefficient is 0.4. Building importance factor is taken as 1.0. In Turkish Seismic Code, structural response factor (R) for the buildings in which seismic loads are fully resisted by single-storey hinged frames with fixed-in base is specified as 3.0. The elastic spectrum proposed in Turkish Seismic Code is shown in Fig. 3.28.

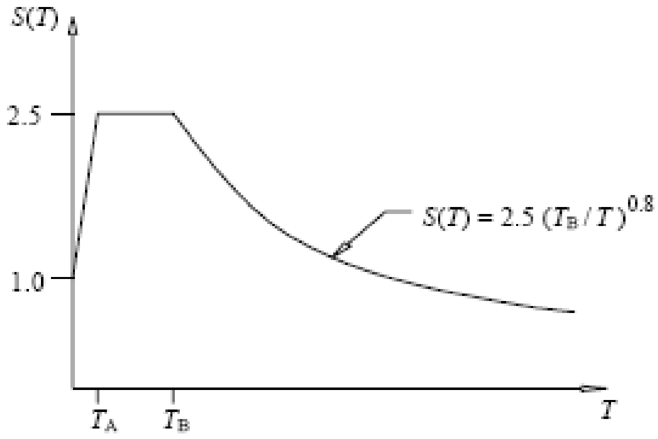

Figure 3.28: Elastic design acceleration spectra proposed in Turkish Seismic Code

Elastic design for a seismic weight of 200 kN was carried out for two types of soil: firm soil (Z2) and soft soil (Z4).

Firm Soil Case:

The selected section for the elastic design is 30x30 cm. Corresponding flexural rigidity of the column is taken as 0.4 $EI_{initial}$ [18]. Elastic modulus (E) is taken as 34450 MPa for the concrete quality of C40 and moment of inertia is calculated as follows:

$$I = \frac{b \cdot h^3}{12} = \frac{30 \cdot 30^3}{12} = 5625\,\text{cm}^3 \qquad \textbf{(3.14)}$$

The obtained vibration period (T) is 1.34 sec. According to the spectrum, the spectral acceleration coefficient then can be expressed as:

$$S(T) = 2.5 \cdot (T_B / T)^{0.8} = 2.5 \cdot (0.4 / 1.34)^{0.8} = 0.947 \qquad \textbf{(3.15)}$$

The corresponding base shear is given in Eq. 3.19.

$$V_T = \frac{A_0 \times I \times S(T)}{R} W = \frac{0.4 \times 1 \times 0.947}{3} \times 200 = 25.25 \text{ kN} \qquad \textbf{(3.16)}$$

The bending moment at fix end equals to:

$$M_T = V_T \times h = 25.25 \times 4 = 101 \text{ kNm, N = 200kN} \qquad \textbf{(3.17)}$$

The internal forces are shown in Fig. 3.29.

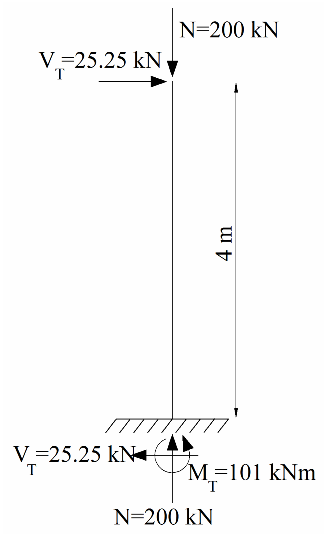

Figure 3.29: The internal forces calculated from elastic analysis

Definition of the longitudinal reinforcement:

$\lambda = 1/4 \qquad d''/h = 260/300 = 0.87 \approx 0.90$ **(3.18)**

$f_{cd} = 40/1.5 = 26.7$ MPa **(3.19)**

$$\frac{N}{b \times h \times f_{cd}} = \frac{200000}{300^2 \times 26.7} = 0.083 \qquad \textbf{(3.20)}$$

$$\frac{M}{b \times h^2 \times f_{cd}} = \frac{101 \times 10^6}{300^3 \times 26.7} = 0.14 \qquad \textbf{(3.21)}$$

$$\rho_t \cdot m = 0.23 \qquad m = \frac{f_{yd}}{f_{cd}} = \frac{365}{26.7} = 13.67 \tag{3.22}$$

Longitudinal reinforcement ratio corresponds to

$$\rho_t = \frac{0.23}{13.67} = 1.68\ \% \tag{3.23}$$

The selected reinforcement 8ϕ16 supplies the reinforcement ratio of 1.79% which is greater than 1.68%.

Soft Soil Case :

The selected section for the elastic design is 45x45 cm. The obtained vibration period (T) is 0.60 sec. The spectral acceleration coefficient is 2.5.

The corresponding base shear is:

$$V_T = \frac{A_0 \times I \times S(T)}{R} W = \frac{0.4 \times 1 \times 2.5}{3} \times 200 = 66.67\ \text{kN}$$

The bending moment at fix end equals to:

$$M_T = V_T \times h = 66.67 \times 4 = 266.7\ \text{kNm, N = 200kN}$$

Definition of the longitudinal reinforcement:

λ = 1/4 d"/h = 410/450 = 0.91 ≈ 0.90

f_{cd} = 40/1.5 = 26.7 MPa

$$\frac{N}{b \times h \times f_{cd}} = \frac{200000}{450^2 \times 26.7} = 0.037$$

$$\frac{M}{b \times h^2 \times f_{cd}} = \frac{266.7 \times 10^6}{450^3 \times 26.7} = 0.11$$

$$\rho_t \cdot m = 0.20 \qquad m = \frac{f_{yd}}{f_{cd}} = \frac{365}{26.7} = 13.67$$

Longitudinal reinforcement ratio corresponds to

$$\rho_t = \frac{0.20}{13.67} = 1.46\ \%$$

The selected reinforcement 8ϕ22 supplies the reinforcement ratio of 1.50% which is greater than 1.46%.

3.3.4.2 Input Parameters for Dynamic Analysis

Dynamic analysis was performed by Newton-Beta integration method in IDARC2D. A data file is required to read horizontal component of strong motion acceleration record. The control parameters for dynamic analysis are peak horizontal acceleration (g's), time steep for response analysis (seconds), total duration of analysis (seconds), type of structural damping (mass proportional damping is used), number of points in earthquake wave file (NPTS) and time interval of input wave (Δt). Peak horizontal acceleration values of far fault and near fault earthquake records are listed in Table 3.6 and Table 3.7, respectively. NPTS, Δt and total duration of analysis values of far fault and near fault earthquake records are listed in Table 3.8 and Table 3.9, respectively. IDARC2D allows to recieve maximum 7000 points for earthquake wave, so some of the earthquake data were reduced. All used strong motion acceleration records are provided from references [24-29].

Table 3.8: Dynamic analysis parameters for far fault earthquake records

FAR FAULT EARTHQUAKES					
NO	EARTHQUAKE NAME	DATE	Δt(s)	NPTS	DURATION(s)
1	Kocaeli	17.08.1999	0.005	5435	27.170
2	Kocaeli	17.08.1999	0.005	5435	27.170
3	Adana-Ceyhan	27.06.1998	0.005	5840	29.195
4	Bingöl	01.05.2003	0.010	6474	64.730
5	Western washington	13.04.1949	0.020	4450	88.980
6	San Fernando	09.02.1971	0.010	3000	29.990
7	Imperial valley	15.10.1979	0.005	6500	32.495
8	Imperial valley	15.10.1979	0.005	6500	32.495
9	Coyote Lake	06.08.1979	0.010	2720	27.190
10	Coalinga	02.05.1983	0.010	4000	39.990
11	Coalinga	02.05.1983	0.010	4000	39.990
12	Chalfant Valley	07.21.1986	0.005	6250	31.245
13	Chalfant Valley	07.21.1986	0.005	6250	31.245
14	Friuliy,Italy	06.05.1976	0.005	6250	31.245
15	Friuliy,Italy	06.05.1976	0.005	6250	31.245
16	Victoria,Mexico	09.06.1980	0.010	2445	24.440
17	Victoria,Mexico	09.06.1980	0.010	2445	24.440
18	Whittier Narrows	01.10.1987	0.005	6500	32.495
19	Whittier Narrows	01.10.1987	0.005	6500	32.495
20	Alkion-Greece	24.02.1981	0.010	4182	41.810
21	Campano Lucano	23.11.1980	0.010	6024	60.230
22	South Iceland	17.06.2000	0.010	6252	62.510
23	Avej	22.06.2002	0.010	5886	58.850
24	Taiwan Smart	20.05.1986	0.010	2910	29.090
25	Superstitn Hills(B)	24.11.1987	0.010	2210	22.090
26	Spitak	07.12.1988	0.010	1990	19.890
27	Irpinia	23.11.1980	0.00244	6500	15.858
28	Irpinia	23.11.1980	0.00244	6500	15.858
29	North Palm Springs	08.07.1986	0.005	5200	25.995
30	North Palm Springs	08.07.1986	0.005	5200	25.995
31	Kiholo Bay, Hawai`i Island	15.10.2006	0.005	6496	32.475
32	Kiholo Bay, Hawai`i Island	15.10.2006	0.005	6496	32.475
33	El Salvador	13.01.2001	0.005	6496	32.475
34	El Salvador	13.01.2001	0.005	6496	32.475
35	Landers	28.01.1900	0.00250	6496	16.238
36	Landers	28.01.1900	0.00250	6496	16.238
37	Northridge	17.01.1994	0.020	2000	39.980
38	Northridge	17.01.1994	0.020	2000	39.980
39	Northridge	17.01.1994	0.020	2000	39.980
40	Northridge	17.01.1994	0.020	2000	39.980

Table 3.9: Dynamic analysis parameters for near fault earthquake records

NEAR FAULT EARTHQUAKES					
NO	EARTHQUAKE NAME	DATE	Δt(s)	NPTS	DURATION(s)
1	nf01 (Tabas)	16.09.1978	0.020	2496	49.900
2	nf02 (Tabas)	17.09.1978	0.020	2496	49.900
3	nf03 (Loma Prieta)	18.10.1989	0.010	2496	24.950
4	nf04 (Loma Prieta)	19.10.1989	0.010	2496	24.950
5	nf05 (loma Prieta)	19.10.1989	0.010	3996	39.950
6	nf06 (Loma Prieta)	19.10.1989	0.010	3996	39.950
7	nf07 (C. Mendocino)	25.04.1992	0.020	3000	59.980
8	nf08 (C. Mendocino)	25.04.1992	0.020	3000	59.980
9	nf09 (Erzincan)	13.03.1992	0.005	4152	20.755
10	nf10 (Erzincan)	13.03.1992	0.005	4152	20.755
11	nf12 (Landers)	28.06.1992	0.004	6498	25.988
12	nf13 (Northridge)	17.01.1994	0.005	2988	14.935
13	nf14 (Northridge)	17.01.1994	0.005	2988	14.935
14	nf15 (Northridge)	17.01.1994	0.020	3000	59.980
15	nf16 (Northridge)	17.01.1994	0.020	3000	59.980
16	nf17 (Kobe)	16.01.1995	0.020	3000	59.980
17	nf18 (Kobe)	16.01.1995	0.020	3000	59.980
18	nf19 (Kobe)	16.01.1995	0.010	4008	40.070
19	nf20 (Kobe)	16.01.1995	0.010	4008	40.070
20	Kocaeli	17.08.1999	0.005	6250	31.245
21	Kocaeli	17.08.1999	0.010	6000	59.990
22	Düzce	12.11.1999	0.005	5175	25.870
23	Düzce	12.11.1999	0.005	5175	25.870
24	Chi-Chi taiwan	20.09.1999	0.005	6500	32.495
25	Northridge	17.01.1994	0.020	1220	24.380
26	Northridge	17.01.1994	0.005	6500	32.495
27	Northridge	17.01.1994	0.005	6500	32.495
28	Northridge	17.01.1994	0.020	2000	39.980
29	Northridge	17.01.1994	0.020	2000	39.980
31	Northridge	17.01.1994	0.020	2000	39.98
30	Northridge	17.01.1994	0.020	3000	59.980
32	Superstitn Hills(B)	24.11.1987	0.010	2235	22.340
33	Superstitn Hills(B)	24.11.1987	0.010	2230	22.290
34	Imperial valley	15.10.1979	0.005	6500	32.495
35	Imperial valley	15.10.1979	0.005	6500	32.495
36	Imperial valley	15.10.1979	0.005	6500	32.495
37	Imperial valley	15.10.1979	0.005	6500	32.495
38	Morgan Hill	24.04.1984	0.005	5990	29.945
39	Gazli,USSR	17.05.1976	0.005	3250	16.245
40	Gazli,USSR	17.05.1976	0.005	3250	16.245

3.4 Evaluation of Time History Analyses Results

3.4.1 Park & Ang Damage Model

Important research efforts have been carried out to evaluate performance of buildings. IDARC2D incorporates an approved damage index model proposed by Park & Ang to qualify the response of structures.

The Park & Ang damage model can be used to calculate different damage indices: element, story (subassembly), and overall building damage. The Park & Ang damage index for a structural element is defined as:

$$DI_{Park\&Ang} = \frac{\delta_m}{\delta_u} + \frac{\beta}{\delta_u P_y} \int dE_h \qquad \textbf{(3.24)}$$

where δ_m is the maximum experienced deformation, δ_u is the ultimate deformation of the element determined from a lateral pushover analysis, P_y is the yield strength of the element, $\int dE_h$ is the hysteretic energy absorbed by the element during the response history, and β is a model constant parameter. A value of 0.1 for the parameter β has been suggested for nominal strength deterioration. The Park & Ang damage model accounts for damage due to maximum inelastic excursions, as well as damage due to the history of deformations. Both components of damage are linearly combined.

To determine section damage of the element ends, the following modifications to the original model were used in IDARC2D since version 3.

$$DI = \frac{\theta_m - \theta_r}{\theta_u - \theta_r} + \frac{\beta}{M_y \theta_u} E_h \qquad \textbf{(3.25)}$$

where θ_m is the maximum rotation attained during the loading history, θ_u is the ultimate rotation capacity of the section, θ_r is the recoverable rotation when unloading, M_y is the yield moment and E_h is the dissipated energy in the section. The element damage is then selected as the biggest damage index of the end sections.

The Park & Ang damage model has been calibrated with observed structural damage of nine reinforced concrete buildings. Table 3.10 presents the calibrated damage index with the degree of observed damage in the structure.

Table 3.10: Interpretation of overall damage index

Degree of Damage	Partial Appearance	Damage Index	State of Building
Collapse	Partial or total collapse of building	>1.0	Loss of building
Severe	Extensive crashing of concrete; disclosure of buckled reinforcement	0.4-1.0	Beyond repair
Moderate	Extensive large cracks; spalling of concrete in columns	<0.4	Repairable
Minor	Minor cracks; partial crushing of concrete in columns		
Slight	Sporadic occurrence of cracking		

The obtained damage index values by Park&Ang Model for the tested columns and their corresponding damage photographs are given in Table 3.11.

Table 3.11: Evaluation of Park&Ang damage index

<table>
<tr><th>Column</th><th>DI</th><th>Photograph</th><th>Observations</th></tr>
<tr><td>S30_18</td><td>0.673</td><td>
</td><td>Buckling of longitudinal reinforcement crushing of confined concrete, average plastic zone length is 30 cm.</td></tr>
<tr><td>S35_18</td><td>0.874</td><td>
</td><td>Buckling of longitudinal reinforcement, crushing of confined concrete, average plastic zone length is 39 cm.</td></tr>
<tr><td>S40_20</td><td>0.895</td><td>
</td><td>Buckling of longitudinal reinforcement, crushing of confined concrete, average plastic zone length is 35 cm.</td></tr>
</table>

3.4.2 The Relationships for Determining Performance Level of Columns

The properly selected 80 earthquake ground motions were imposed to 18 different precast columns, therefore total number of 1440 nonlinear dynamic analysis were performed by IDARC2D. Depending on the analyses results, a damage index tool, in which column performance levels were demonstrated, is created. There are three performance range as listed in Table 3.10; values greater than 1, between 0.4 and 1, and less than 0.4, which describes collapse, severe damage and moderate damage conditions, respectively. Each column type was investigated based on these performance levels separately for near fault and far fault ground motions. Fig. 3.30, Fig. 3.31 and Fig. 3.32 depict number of columns that achieved DI<0.4, 0.4<DI<1 and DI>1 performance levels for far fault ground motions, respectively. Similar to this, the performance levels of columns under near fault ground motions are given in Fig. 3.33, Fig. 3.34 and Fig. 3.35.

To give an example of the difference of far fault and near fault ground motion effects on different columns, Table 3.12 and Table 3.13 is prepared for Northridge Earthquake. It is clear that damage index values obtained for near fault record is highly above than thus from far fault record.

Table 3.12: DI values of all columns subjected to Northridge NF ground motion

		Column Dimension [cm] Total DI					
		60x60	50x50	45x45	40x40	35x35	30x30
Steel ratio	1%	1.235	1.442	1.148	0.870	0.715	0.739
	2%	0.346	1.214	1.440	1.154	0.907	0.712
	3%	0.259	0.863	1.631	1.629	1.185	0.696

Table 3.13: DI values of all columns subjected to Northridge FF ground motion

		Column Dimension [cm] Total DI					
		60x60	50x50	45x45	40x40	35x35	30x30
Steel ratio	1%	0.198	0.157	0.248	0.198	0.327	0.398
	2%	0.185	0.122	0.164	0.226	0.204	0.365
	3%	0.237	0.187	0.140	0.230	0.202	0.341

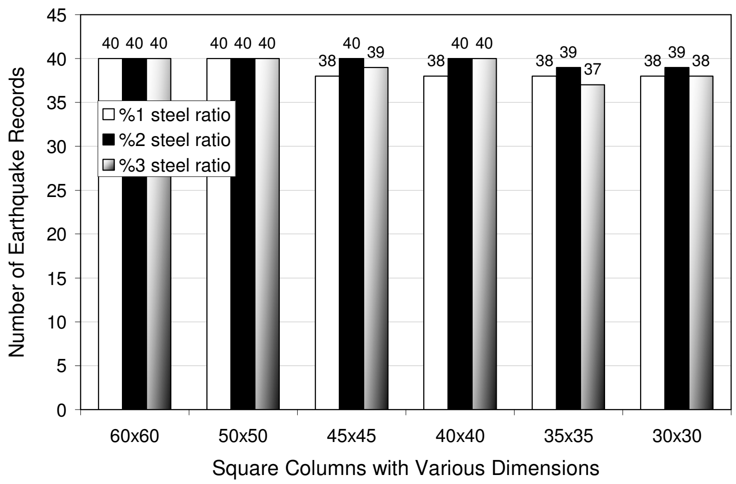

Figure 3.30: Far fault ground motions caused moderate damage (DI<0.4) on different sections

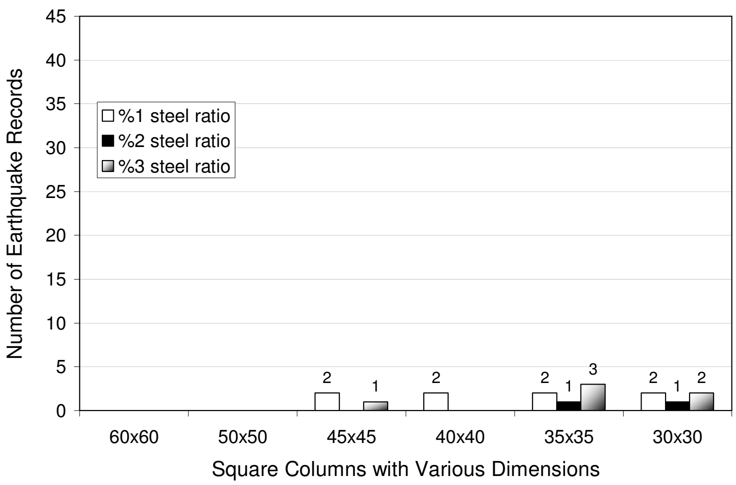

Figure 3.31: Far fault ground motions caused severe damage (0.4<DI<1.0) on different sections

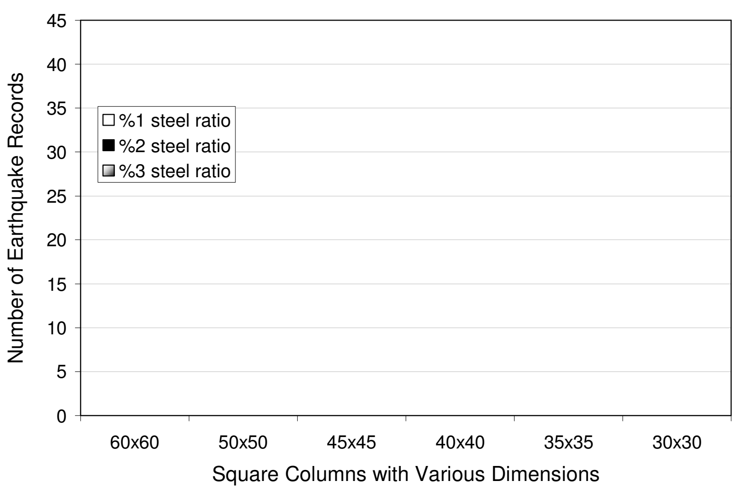

Figure 3.32: Far fault ground motions caused collapse (DI>1.0) on different sections

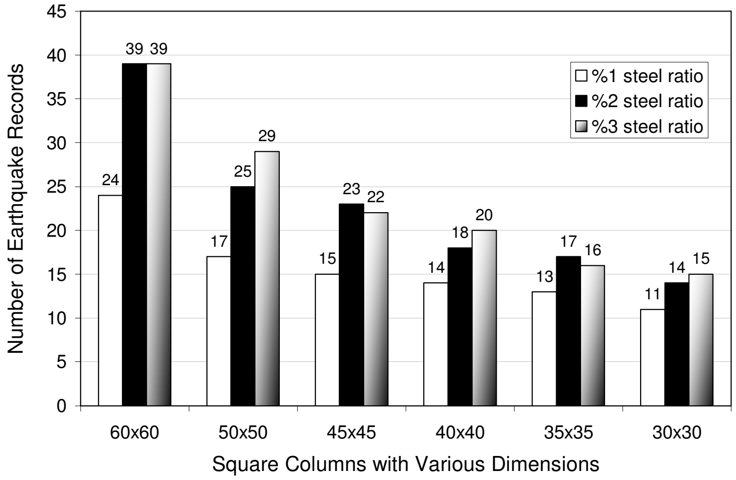

Figure 3.33: Near fault ground motions caused moderate damage (DI<0.4) on different sections

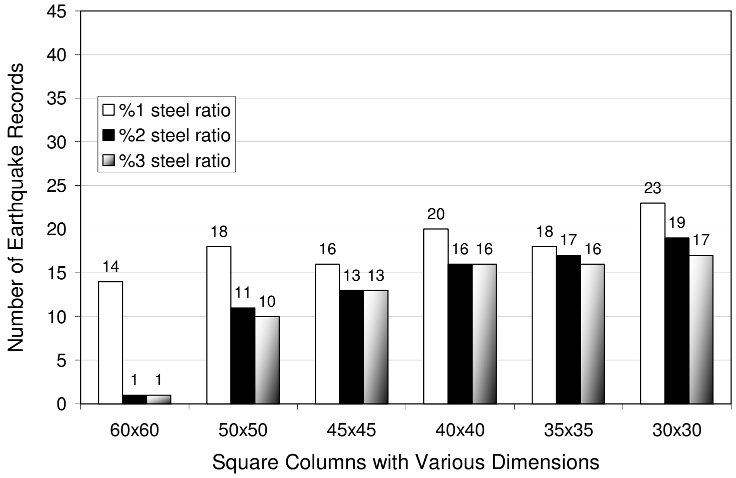

Figure 3.34: Near fault ground motions caused severe damage (0.4<DI<1.0) on different sections

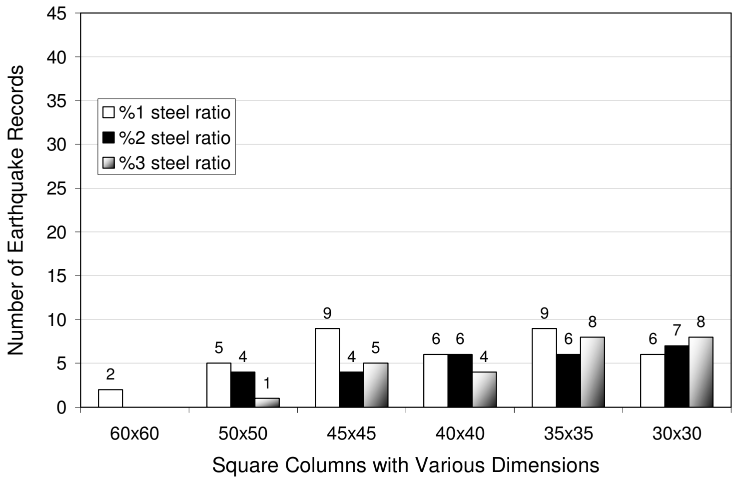

Figure 3.35: NF ground motions caused collapse (DI>1.0) on different sections

The other significant performance indicators, which are maximum strain of longitudinal reinforcement $(\varepsilon_s)_{max}$ and maximum strain of confined concrete $(\varepsilon_c)_{max}$ experienced in time history, were calculated and damage evaluation was done due to performance limits defined in Turkish Seismic Code which are minimum damage (MN), safety (GV) and collapse (GC). These limits divide stress-strain curve into four region which are minimum damage $(\varepsilon_{max}<\varepsilon_{MN})$, moderate damage $(\varepsilon_{MN}<\varepsilon_{max}<\varepsilon_{GV})$, severe damage $(\varepsilon_{GV}<\varepsilon_{max}<\varepsilon_{GC})$ and collapse $(\varepsilon_{max}>\varepsilon_{GC})$, (Fig. 3.36).

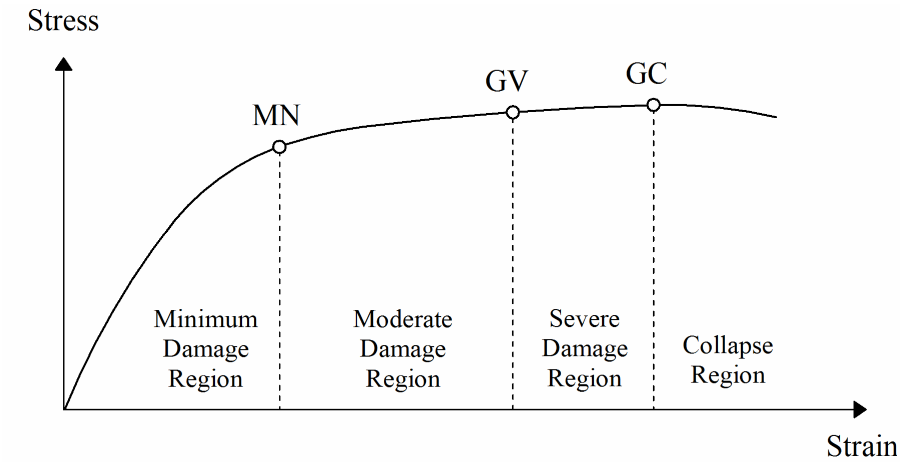

Figure 3.36: Section damage regions

The performance damage levels defined in Turkish Seismic Code follows:

a) For section minimum damage level (MN), the limits of strain of concrete fiber outer edge of section and strain of longitidunal reinforcement ratio are:

$$(\varepsilon_{cun})_{MN} = 0.0035 \quad ; \quad (\varepsilon_s)_{MN} = 0.010 \tag{3.26}$$

b) For section safety level (GV), the limits of strain of concrete fiber outer side of confined concrete and strain of longitidunal reinforcement ratio are:

$$(\varepsilon_{cg})_{GV} = 0.0035 + 0.01\,(\rho_s/\,\rho_{sm}) \leq 0.0135 \quad ; \quad (\varepsilon_s)_{GV} = 0.040 \tag{3.27}$$

c) For section collapse level (GC), the limits of strain of concrete fiber outer side confined concrete and strain of longitidunal reinforcement ratio are:

$$(\varepsilon_{cg})_{GC} = 0.004 + 0.014\,(\rho_s/\,\rho_{sm}) \leq 0.018 \quad ; \quad (\varepsilon_s)_{GC} = 0.060 \tag{3.28}$$

Where ρ_s is the volumetric transverse reinforcement ratio existing in the section, ρ_{sm} is the volumetric transverse reinforcement ratio required according to Turkish Seismic Code. Formulation of ρ_{sm} is:

$$\left.\begin{aligned} &\rho_{sm} = \frac{2}{3} \times 0.45\left[\left(A_c / A_{ck}\right) - 1\right)\right](f_{ck} / f_{ywk}) && \textbf{(3.29)} \\ &\rho_{sm} = \frac{2}{3} \times 0.12(f_{ck} / f_{ywk}) && \textbf{(3.30)} \end{aligned}\right\} \text{Larger of } \rho_{sm} \text{ is applied}$$

The concrete performance limits were calculated for different sectional dimensions and these limits are listed in Table 3.14.

Table 3.14: Concrete performance limits for different sections

Section	$(\varepsilon_{cu})_{MN}$	$(\varepsilon_{cg})_{GV}$	$(\varepsilon_{cg})_{GC}$
300	0.0035	0.0135	0.0180
350	0.0035	0.0135	0.0180
400	0.0035	0.0135	0.0180
450	0.0035	0.0132	0.0175
500	0.0035	0.0121	0.0160
600	0.0035	0.0106	0.0139

Performance of each column type were investigated due to maximum strain of longitudinal reinforcement $(\varepsilon_s)_{max}$ and maximum strain of confined concrete $(\varepsilon_c)_{max}$ experienced in time history separately for near fault and far fault ground motions.

Fig. 3.37, Fig. 3.38 and Fig. 3.39 depict number of columns that achieved $(\varepsilon_c)_{max}<(\varepsilon_{cun})_{MN}$, $(\varepsilon_{cu})_{MN}<(\varepsilon_c)_{max}<(\varepsilon_{cg})_{GV}$ and $(\varepsilon_{cg})_{GV}< (\varepsilon_c)_{max}<(\varepsilon_{cg})_{GC}$ concrete strain performance levels for far fault ground motions, respectively. Similar to this, the performance levels of columns under near fault ground motions are given in Fig. 3.40, Fig. 3.41 and Fig. 3.42.

Fig. A.1, Fig. A.2, Fig. A.3 and Fig. A.4 depict number of columns that achieved $(\varepsilon_s)_{max}<(\varepsilon_s)_{MN}$, $(\varepsilon_s)_{MN}<(\varepsilon_s)_{max}<(\varepsilon_s)_{GV}$, $(\varepsilon_s)_{GV}<(\varepsilon_s)_{max}<(\varepsilon_s)_{GC}$ and $(\varepsilon_s)_{max}>(\varepsilon_s)_{GC}$ reinforcement strain performance levels for far fault ground motions, respectively. Similar to this, the performance levels of columns under near fault ground motions are given in Fig. A.5, Fig. A.6, Fig. A.7 and Fig. A.8.

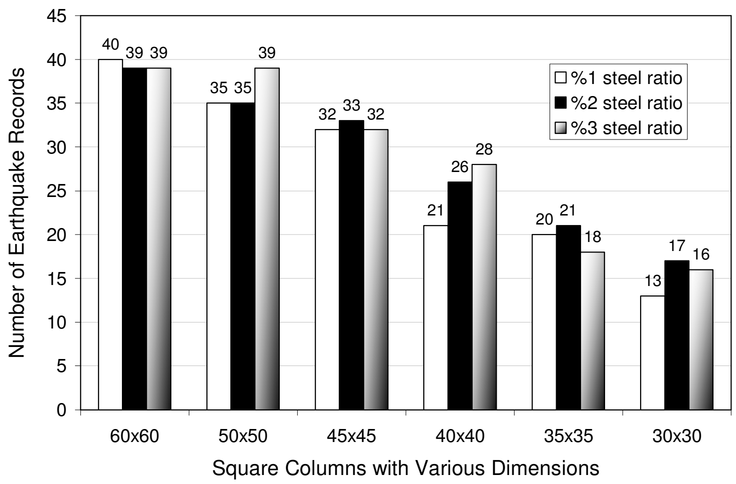

Figure 3.37: Far fault ground motions caused minimum damage $(\varepsilon_c)_{max}<(\varepsilon_{cun})_{MN}$ on different sections

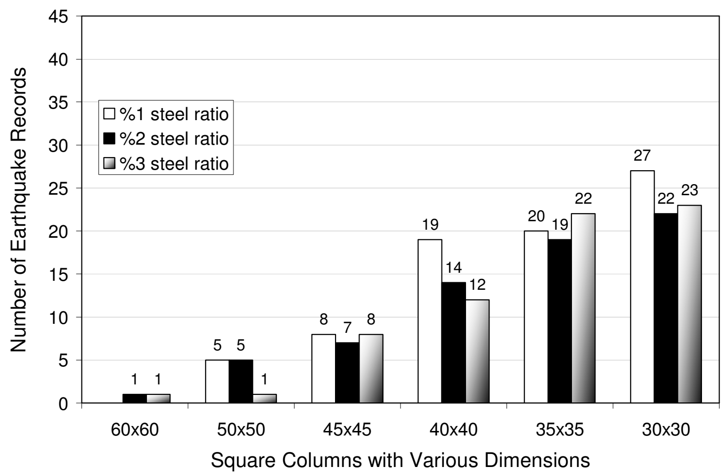

Figure 3.38: Far fault ground motions caused moderate damage $(\varepsilon_{cun})_{MN}<(\varepsilon_c)_{max}<(\varepsilon_{cg})_{GV}$ on different sections

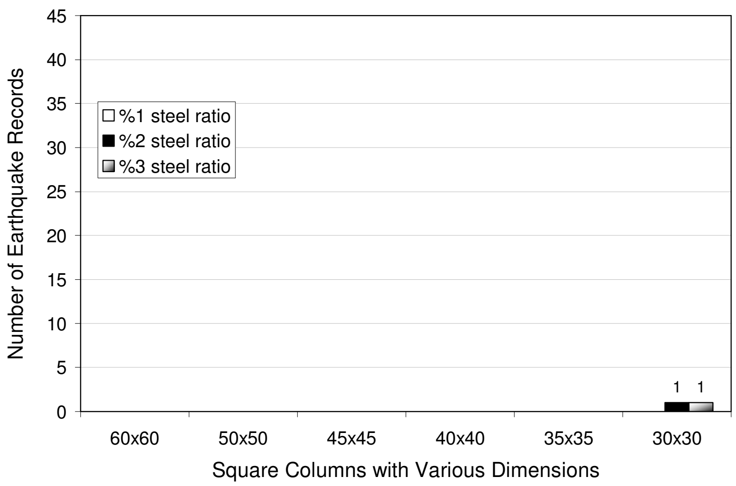

Figure 3.39: Far fault ground motions caused severe damage $(\varepsilon_{cg})_{GV}<(\varepsilon_c)_{max}<(\varepsilon_{cg})_{GC}$ on different sections

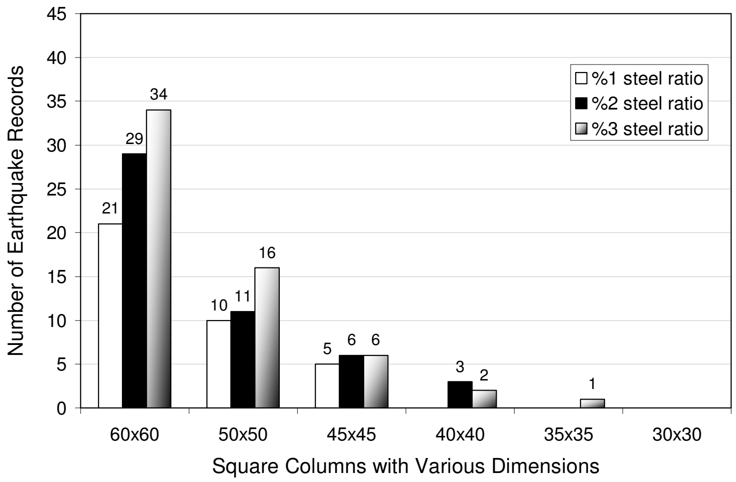

Figure 3.40: Near fault ground motions caused minimum damage $(\varepsilon_c)_{max}<(\varepsilon_{cun})_{MN}$ on different sections

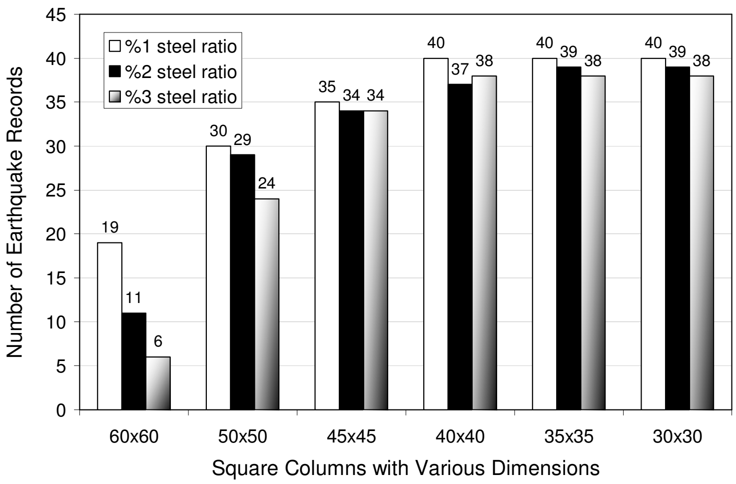

Figure 3.41: Near fault ground motions caused moderate damage $(\varepsilon_{cun})_{MN}<(\varepsilon_c)_{max}<(\varepsilon_{cg})_{GV}$ on different sections

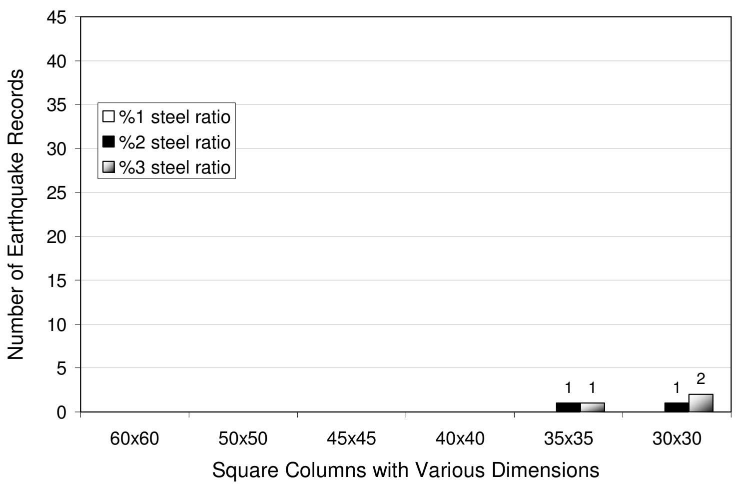

Figure 3.42: Near fault ground motions caused severe damage $(\varepsilon_{cg})_{GV}<(\varepsilon_c)_{max}<(\varepsilon_{cg})_{GC}$ on different sections

To determine the effect of strong ground motion properties on the precast column performance, relationships were set up between damage index (DI) and the main ground motion characteristics of PGA, PGV. The relationships between damage index DI and PGA, PGV also demonstrate the effect of longitudinal reinforcement ratio for the same sectional dimensions and the effect of sectional dimensions for the same longitudinal reinforcement ratio on precast column performance.

The PGV-DI relationships with increasing sectional dimensions with the same longitudinal reinforcement ratio are given in Fig. 3.43 to Fig. 3.48. The PGV-DI relationships with increasing longitudinal reinforcement ratio with the same sectional dimensions are shown in Fig. A.9 to Fig. A.11.

To take an over look at increasing sectional dimensions on column performance, three graphics, which demonstarate PGV-DI trend lines for far fault, near fault and overall ground motions, were drawn and shown in Fig. A.12, Fig. A.13 and Fig. A.14, respectively. Similar to this, PGV-DI trend lines, which demonstrate increasing longitudinal reinforcement ratio effect, were shown in Fig. A.15, Fig. A.16 and Fig. A.17, respectively.

The PGA-DI relationships investigating increasing longitudinal reinforcement ratio with same sectional dimensions are shown in Fig. A.18 to Fig. A.21. The PGA-DI relationships investigating increasing sectional dimensions with same longitudinal reinforcement ratio are shown in Fig. A.22 and Fig. A.24.

Also the relations were set up between PGV and the other significant performance indicators which are maximum strain of longitudinal reinforcement $(\varepsilon_s)_{max}$ and maximum strain of confined concrete $(\varepsilon_c)_{max}$ experienced in time history analyses. The PGV-$(\varepsilon_c)_{max}$ relationships are shown in Fig. A.25 to Fig. A.30. The PGV-$(\varepsilon_s)_{max}$ relationships are depicted in Fig. A.31 to Fig. A.36.

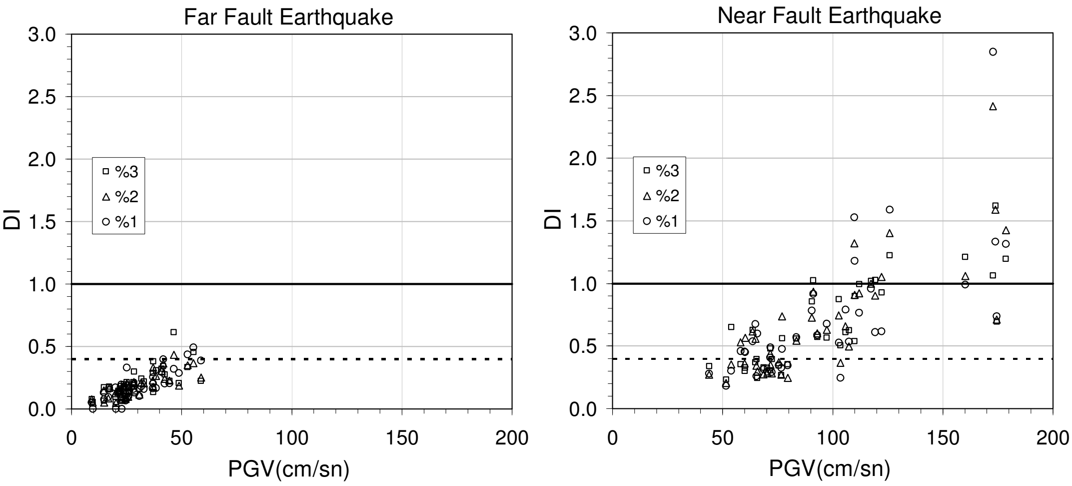

Figure 3.43: PGV-DI relationship for columns dimensions of 30x30 cm

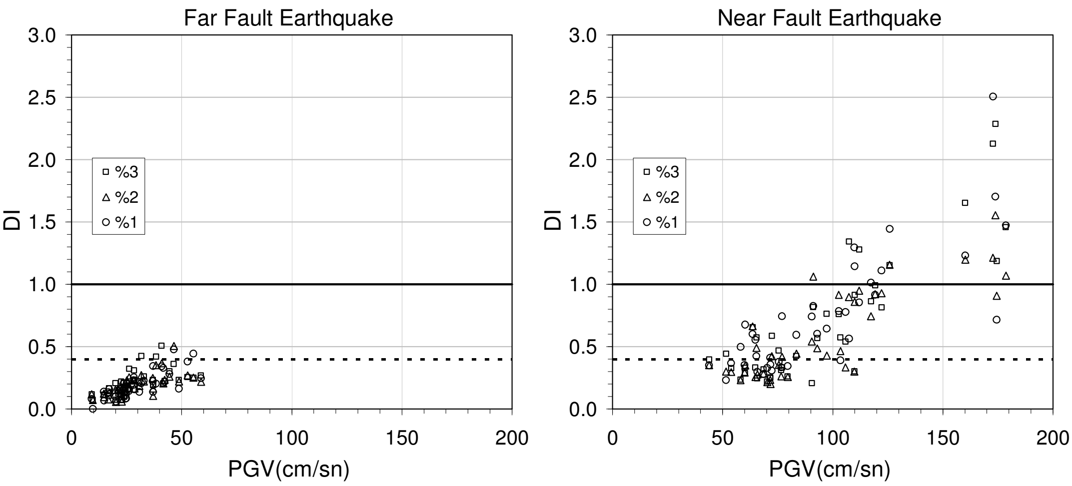

Figure 3.44: PGV-DI relationship for columns dimensions of 35x35 cm

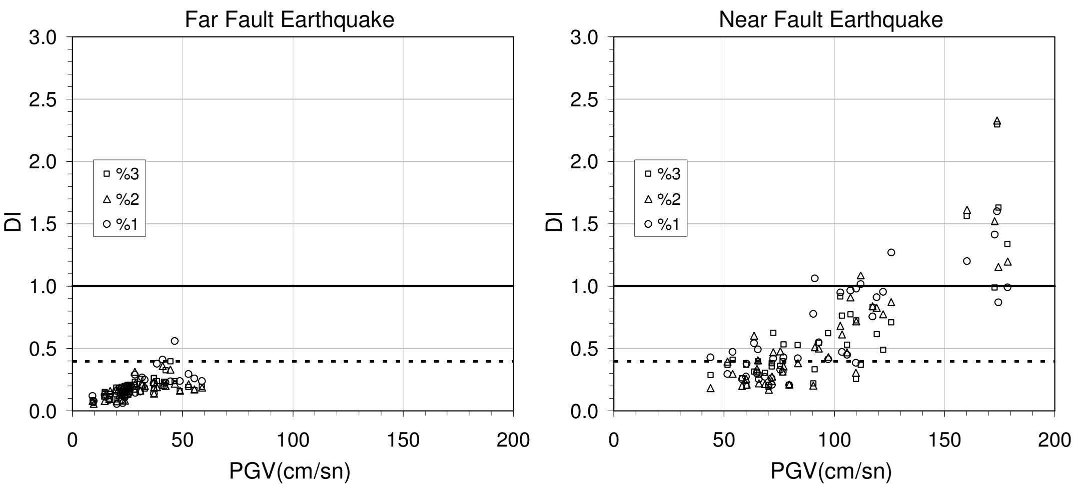

Figure 3.45: PGV-DI relationship for columns dimensions of 40x40 cm

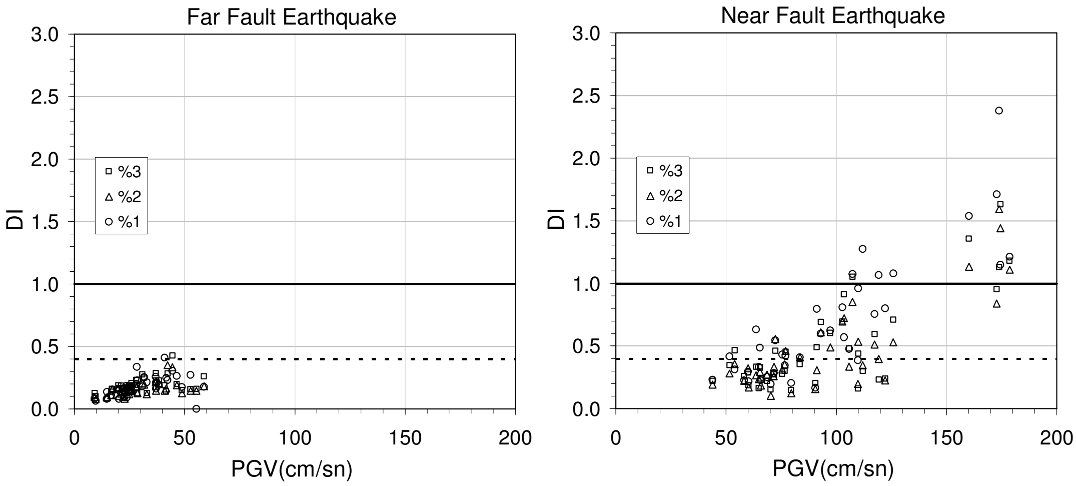

Figure 3.46: PGV-DI relationship for columns dimensions of 45x45 cm

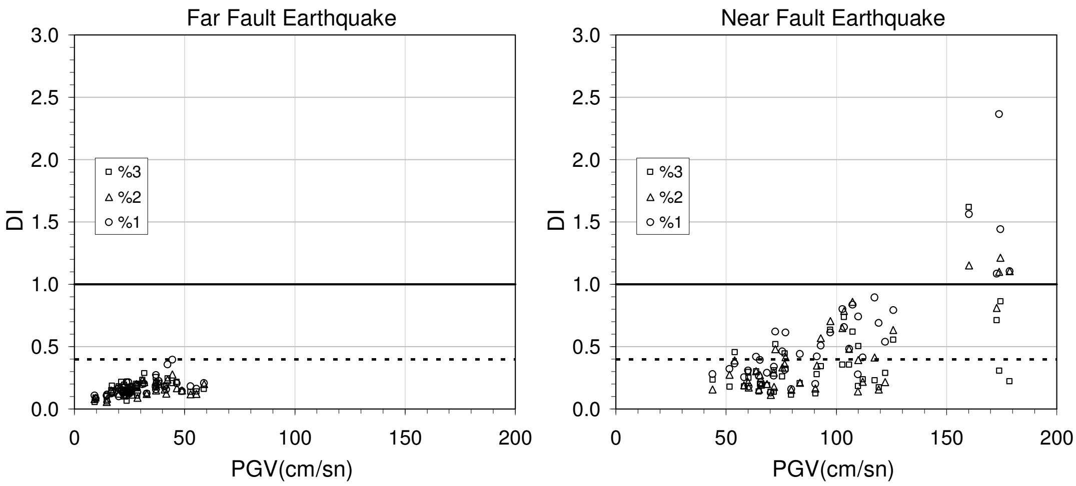

Figure 3.47: PGV-DI relationship for columns dimensions of 50x50 cm

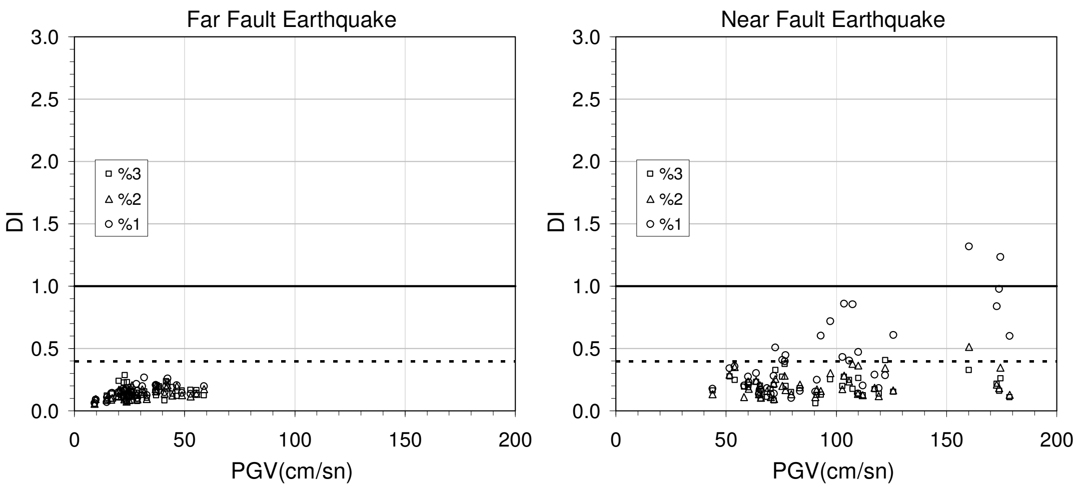

Figure 3.48: PGV-DI relationship for columns dimensions of 60x60 cm

4. CONCLUSIONS

Refering the existing experimental results for three 1/1 scale precast columns, SHM hysteretic model parameters in IDARC2D were obtained by performing quasi-static cyclic analysis. The average values of these parameters were used as input for the nonlinear dynamic analysis. The parameters are: α=3, β_1=0.10, β_2=0.10, R_s= 0.10, σ =0.03, λ=0.60, N=2, η=0.49. Also, from quasi-static cyclic analysis results, Park&Ang damage index (DI) values were calculated. Obtained DI values demonstrate that all the specimens are in severe damage zone as observed in the experiments.

To evaluate the performance of various precast columns for two different types of earthquakes namely near fault and far fault, an analytical study has been completed. The main parameters of the study are column sectional dimensions, longitudinal reinforcement ratio and earthquake type. Nonlinear time history analyses and successively performed Park & Ang damage evaluation has been carried out by computer software of IDARC2D.

To investigate the effect of strong ground motion characters on the column performance, some relations were set between DI and the ground motion characters of PGA, PGV.

Damage evaluation was also done by comparing the other significant performance indicators $(\varepsilon_s)_{max}$ and $(\varepsilon_c)_{max}$ with code specified performance limits which are minimum damage (MN), safety (GV) and collapse (GC). Some other relationships were set up between PGV and $(\varepsilon_s)_{max}$ and $(\varepsilon_c)_{max.}$

Based on the results of this investigation, the following conclusions can be drawn taking into account for a constant seismic weight of 200 kN for all column types:

1 Increasing section dimensions decrease damage index for all reinforcement ratios. When section dimensions are enlarged from 30x30 cm to 60x60 cm, the probability of severe damage and collapse condition decrease from 34.5%

to 7.5% for all earthquakes. The same probability changes from 66.7 % to 15 % for near fault earthquakes and from 4.3 % to 0 % for far fault earthquakes.

2 It is recommended to use 60x60 cm sectional dimensions having 2% longitudinal reinforcement ratio, if minor damage is intended in design.

3 Although all of the columns have moderate damage for far fault earthquakes, only 52 % of them achieved this damage level for near fault earthquakes.

4 For columns having 1% longitudinal reinforcement ratio gets a minimum damage probability of 39.2 %, whereas columns having 2% and 3% reinforcement ratio get 56.7 % and 58.8 %, respectively.

5 Enlargement of cross section dimensions is more effective than increment of the ratio of longitudinal reinforcement for the same seismic weight.

6 It is found out that increasing PGV values results as increasing damage index whether the PGA values are high or not. The PGV of the potential earthquake is more effective than PGA to estimate damages to be observed on the structure.

7 The threshold values of PGV of each cross sectional dimension which match a damage index of 0.4 were obtained; corresponding values are 60 cm/sn and 160 cm/sn for sectional dimensions of 30x30 cm and 60x60 cm, respectively.

8 It is clear that increasing section dimensions decrease maximum experienced strain of confined concrete in time history analyses for all reinforcement ratios. When section dimensions are enlarged from 30x30 cm to 60x60 cm, the probability of minimum damage condition defined in Turkish Seismic code increase from 19% to 84%.

9 For near fault ground motions, although sectional dimensions of 30x30 cm could not achieve minimum damage region given in Turkish Seismic Code for concrete strain, 70 % of sectional dimensions of 60x60 cm could do.

10 For 60x60 cm columns, the probability of being under safety limit of maximum experienced strain of longitudinal reinforcement is 84.3%, whereas this probability for 30x30 cm columns is only 31.5%. If near fault ground motions are taken into consideration, the same probability changes from 74.5% to 4% for dimensions of 60x60 cm and 30x30cm, respectively.

11 When longitudinal reinforcement ratio increases, maximum experienced strain of longitudinal steel reduces for all sectional dimensions. For the columns having longitudinal reinforcement ratio of 3%, collapse condition does not occurs, whereas the columns having longitudinal reinforcement ratio of 1% have a high probability of collapse (77.5%) for all ground motions.

12 When longitudinal reinforcement ratio increases, maximum experienced strain of confined concrete increases except for dimensions of 60x60 cm with over 2% longitudinal reinforcement ratio because the behavior of the corresponding sections are nearly elastic.

13 It is found out that increasing PGV values results as increasing maximum experienced strain of confined concrete.

14 If longitudinal reinforcement ratio increases, the effect of PGV values on the maximum experienced strain of confined concrete increases except for the dimensions of 60x60 cm having over 2% longitudinal reinforcement ratio.

REFERENCES

[1] **Saatcioglu, M., Mitchell, D., Tinawi, R., Gardner, N.J., Gillies, A.G., Ghobarah, A., Anderson, D.L., Lau, D.,** 2001. The August 17, 1999, Kocaeli (Turkey) earthquake – damage to structures, *Canadian J. Civ. Eng.*, **28**, 715-737.

[2] **Ataköy, H.,** 1999. 17 August Marmara Earthquake and the Precast Structures Built by TPCA Members, *Turkish Precast Concrete Association*, Ankara, Turkey

[3] **Sezen, H., Elwood, K.J., Whitaker, A.S., Mosalam, K.M., Wallace, J.W., Stanton, J.F.,** 2000. Structural Engineering Reconnaissance of the August 17, 1999, Kocaeli (Izmit), Turkey, Earthquake, Rep. No. 2000/09, *Pasific Engineering Research Center*, University of California, Berkeley, CA,

[4] **Bruneau, M.**, 2002. Building damage from the Marmara, Turkey earthquake of August 17, 1999, *Journal of Seismology*, **6**(3), 357-377.

[5] **Sezen, H., Whittaker, A.S.**, 2006. Seismic Performance of Industrial Facilities Affected by the 1999 Turkey Earthquake, *ASCE, J. of Performance of Constructed Facilities*, **20**(1), 28-36.

[6] **Wood, S.L.,** 2003. Seismic Rehabilitation of Low-Rise Precast Industrial buildings in Turkey, *NATO Science Series: IV: Earth and Environmental Sciences Advances in Earthquake Engineering for Urban Risk Reduction,* **66**, pp 167-177, Eds. Wasti, T., Ozcebe, G., Kluwer Academic Publishers, Nertherlands

[7] **Macrea, G.A., Morrow, D.V., Roeder, C.W.,** 2001. Near-Fault Ground Motion Effects on Simple Structures, *ASCE, Journal of Structural Engineering* **127**(9), 996-1004.

[8] **Somerville, P.G.**, 2002. Characterizing near fault ground motion for the design and evaluation of Bridges, *Proceedings of the 3th National Seismic Conference and Workshop on Bridges and Highways*, State University of New York at Buffalo, New York, pp.137-148.

[9] **Shuang, L., Li-li, X.**, 2006. Progress and trend on near –fault problems in civil engineering, *Acta Seismologica Sinica*, **20**(1), 105-114.

[10] **Akkar, S., Sucuoglu, H.**, 2003. Peak Ground Velocity Sensitive Deformation Demands and a Rapid Damage Assessment Approach, *NATO Science*

Series: IV: Earth and Environmental Sciences Seismic Assessment and Rehabilitation of Existing Buildings, **29**, pp. 77-96, Eds. Wasti, T., Ozcebe, G., Kluwer Academic Publishers, Nertherlands

[11] **Akkar, S., Ozen, O.**, 2005. Effect of peak ground velocity on deformation demands for SDOF systems. *Earthquake Engineering and Structural Dynamics*, **34**, 1551-1571.

[12] **Park, Y.J., Ang, A.H.**, 1985. Mechanistic Seismic Damage Model for Reinforced Concrete, *ASCE, Journal of Structural Engineering,* **111**(4), 722-739.

[13] **Park, Y.J., Ang, A.H., Wen, Y.K.**, 1985. Seismic Damage Analysis of Reinforced Concrete Buildings, *ASCE, Journal of Structural Engineering,* **111**(4), 740-757.

[14] **Bozorgnia, Y., and Bertero, V.V.**, 2002. Improved damage parameters for post-earthquake applications, *Proceedings, SMIP02 Seminar on Utilization of Strong-MotionData*, pp. 61-82, May 2, 2002

[15] **Reinhorn, A.M., Kunnath, S.K., Valles, R.E.**, 1994. IDARC2D V6.1 A Program for the Inelastic Damage Analysis of Buildings, *National Center for Earthquake Engineering Research*, Buffalo.

[16] **XTRACT V3.0.7**., 2006. Cross-sectional Structural Analysis of Components. Imbsen Software Systems, Sacramento, CA.

[17] **Sivaselvan, M.V., Reinhorn, A.M.,** 2000. Hysteretic Models for Deteriorating Inelastic Structures, *ASCE, Journal of Engineering Mechanics*, **126**(6), 633- 640.

[18] **Afet Bölgelerinde Yapılacak Yapılar Hakkında Yönetmelik,** 2007. Bayındırlık ve İskan Bakanlığı, Ankara.

[19] **Karadoğan, F., Yüksel, E., Yüce, S., Taşkın, K., Saruhan, H.,** 2006. Orjinal ve Güçlendirilmiş Prefabrike Betonarme Kolonlar Üzerinde Yapılan Deneysel Çalışmalar, Teknik Rapor, İstanbul.

[20] **Applied Technology Center (ATC),** 1997. Seismic Evaluation and Retrofit of Concrete Buildings, Rep. No. ATC-40, Redwood City, California.

[21] **Federal Emergency Management Agency (FEMA),** 1997. NEHRP Guidelines for the Seismic Rehabilitation of Buildings, 1996 Ed., FEMA273, Washington, D.C.

[22] **Uniform Building Code (UBC),** 1997. International Code of Building Officials (ICBO), California.

[23] **Federal Emergency Management Agency (FEMA),** 1998. NEHRP Recommended Provisions for seismic Regulations for New Buildings and Other Structures, 1997 Ed., FEMA302, Washington, D.C.

[24] **SAC Steel Project,** 1997. Impulsive Near-Field Earthquake Ground Motions, Richmond, CA 94804-4698, <http://www.sacsteel.org/>

[25] **PEER Strong Motion Database,** 2000. Pacific Earthquake Engineering Research Center, California, <http://peer.berkeley.edu/smcat/>

[26] **Türkiye Ulusal Kuvvetli Yer Hareketi Programı (TKYHP),** Afet İşleri Genel Müdürlüğü Deprem Araştırma Dairesi, <http://angora.deprem.gov.tr/>

[27] **COSMOS Virtual Data Center,** Consortium of Organizations for Strong Motion Observation Systems (COSMOS), University of California, <http://db.cosmos-eq.org/scripts/default.plx/>

[28] **Ambraseys, N., Smit, P., Sigbjornsson, R., Suhadolc, P., Margaris, B.,** 2002. Internet-Site for European Strong-Motion Data, European Commission, Research-Directorate General, Environment and Climate Programme.

[29] **United States National Strong Motion Project (NSMP),** U.S. Geological Survey (USGS), Denver, <http://agram.wr.usgs.gov/>

[30] **Seismosignal v. 3.2,** 2006, SeismoSoft, <http://www.seismosoft.com/>

APPENDIX A - Damage Indices Relationships

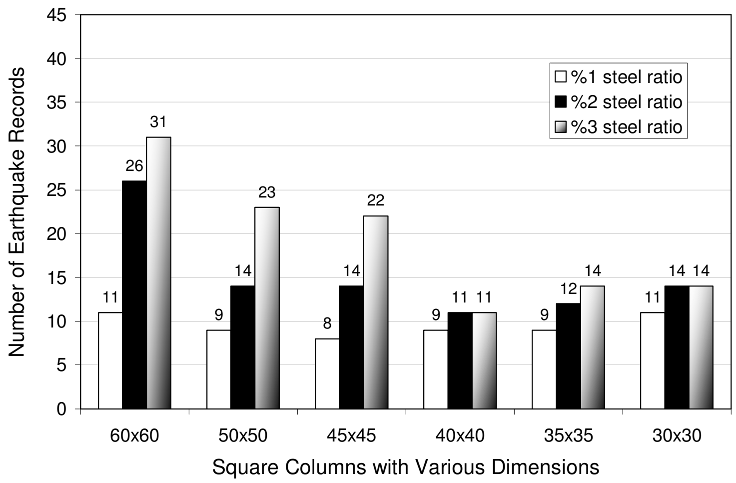

Figure A.1: Far fault ground motions caused minimum damage $(\varepsilon_s)_{max}<(\varepsilon_s)_{MN}$ on different sections

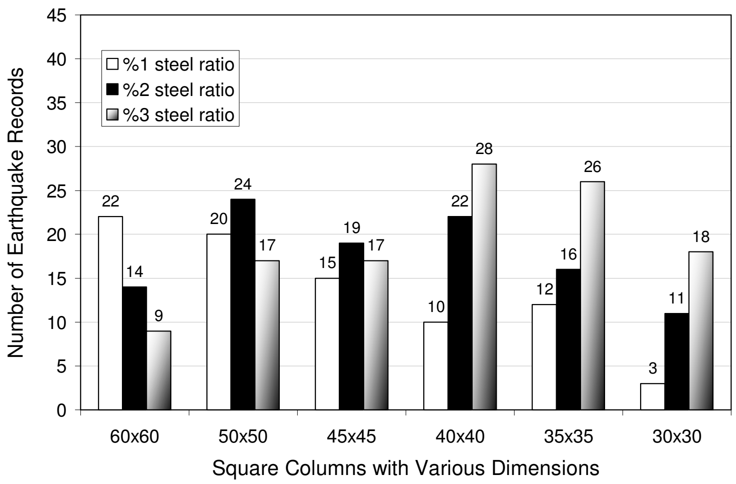

Figure A.2: Far fault ground motions caused moderate damage $(\varepsilon_s)_{MN}<(\varepsilon_s)_{max}<(\varepsilon_s)_{GV}$ on different sections

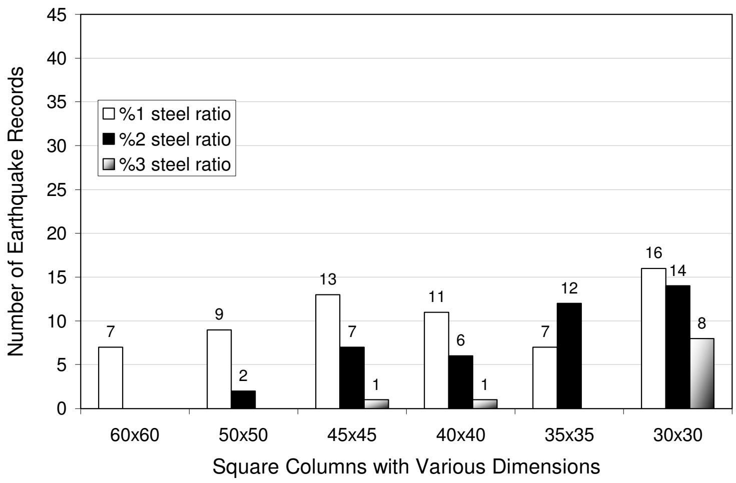

Figure A.3: Far fault ground motions caused severe damage $(\varepsilon_s)_{GV}<(\varepsilon_s)_{max}<(\varepsilon_s)_{GC}$ on different sections

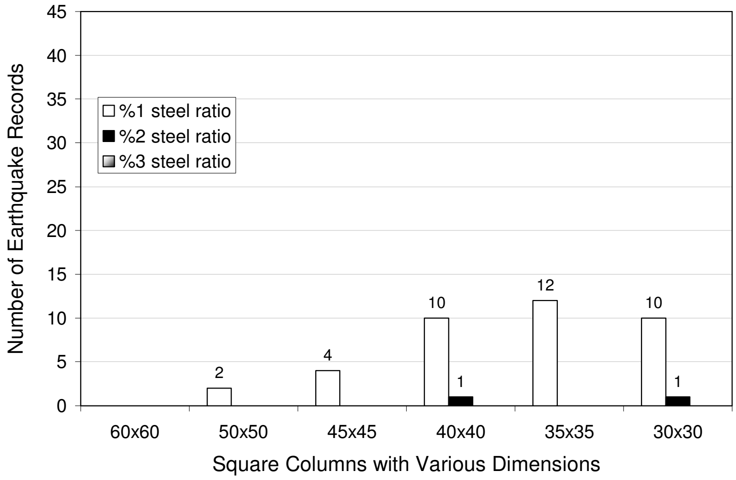

Figure A.4: Far fault ground motions caused collapse $(\varepsilon_s)_{max}>(\varepsilon_s)_{GC}$ on different sections

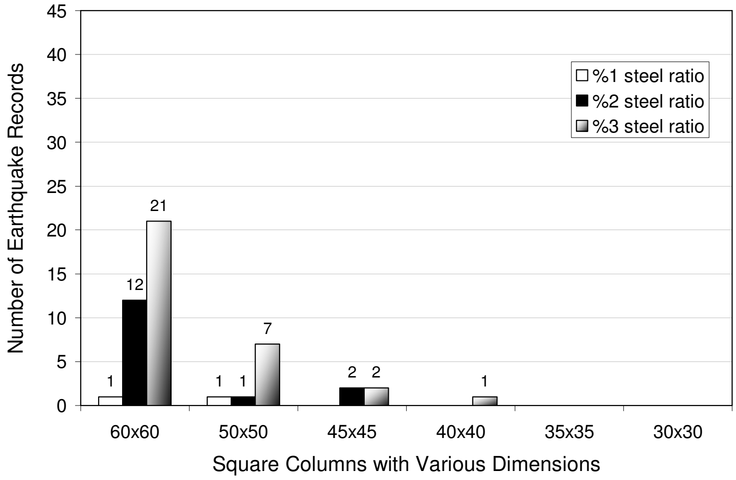

Figure A.5: Near fault ground motions caused minimum damage $(\varepsilon_s)_{max}<(\varepsilon_s)_{MN}$ on different sections

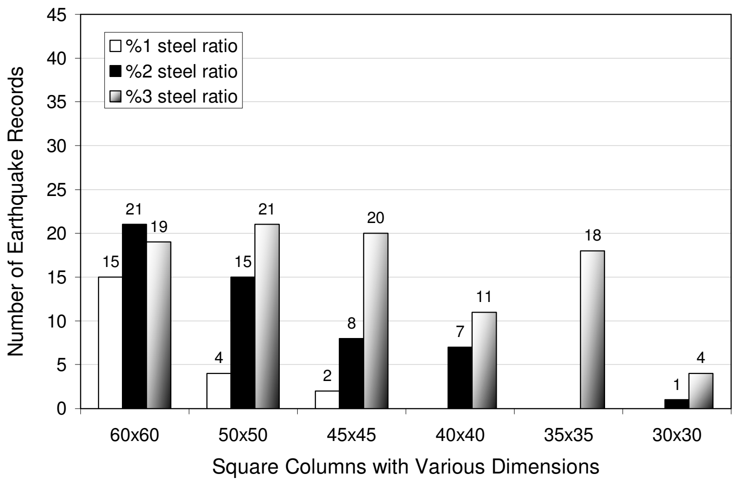

Figure A.6: Near fault ground motions caused moderate damage $(\varepsilon_s)_{MN}<(\varepsilon_s)_{max}<(\varepsilon_s)_{GV}$ on different sections

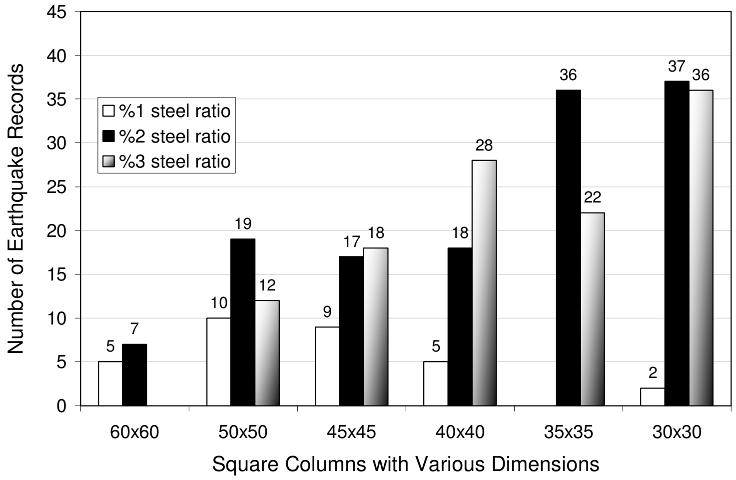

Figure A.7: Near fault ground motions caused severe damage $(\varepsilon_s)_{GV}<(\varepsilon_s)_{max}<(\varepsilon_s)_{GC}$ on different sections

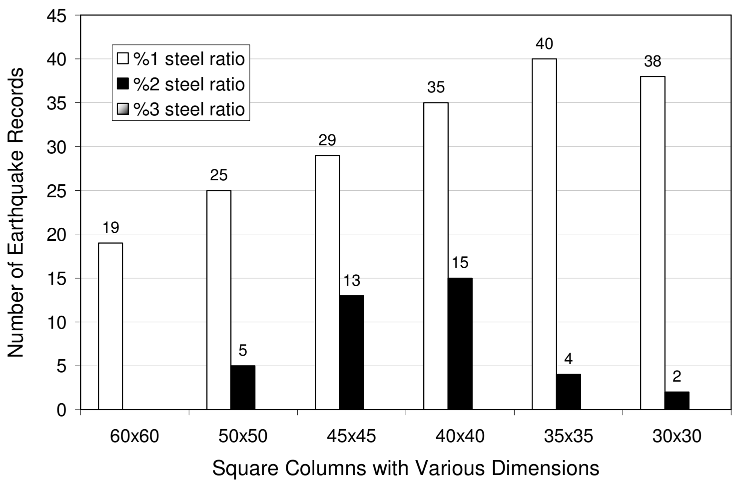

Figure A.8: Near fault ground motions caused collapse $(\varepsilon_s)_{max}>(\varepsilon_s)_{GC}$ on different sections

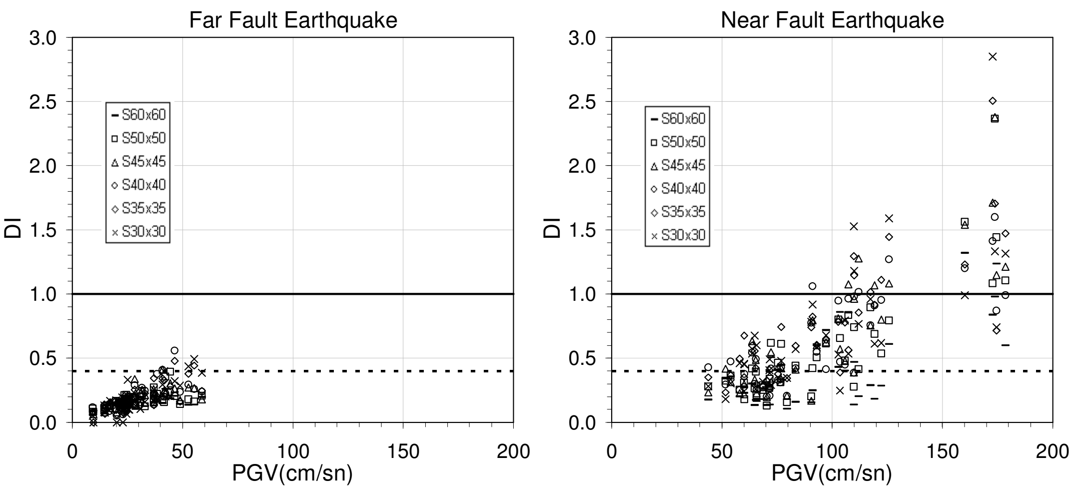

Figure A.9: PGV-DI relationship for columns longitudinal reinforcement ratio of 1 %

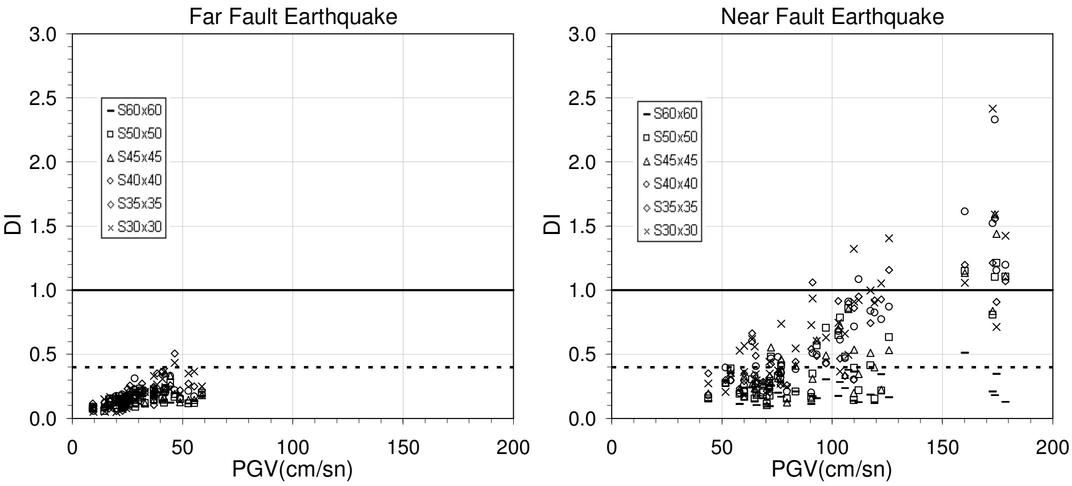

Figure A.10: PGV-DI relationship for columns longitudinal reinforcement ratio of 2 %

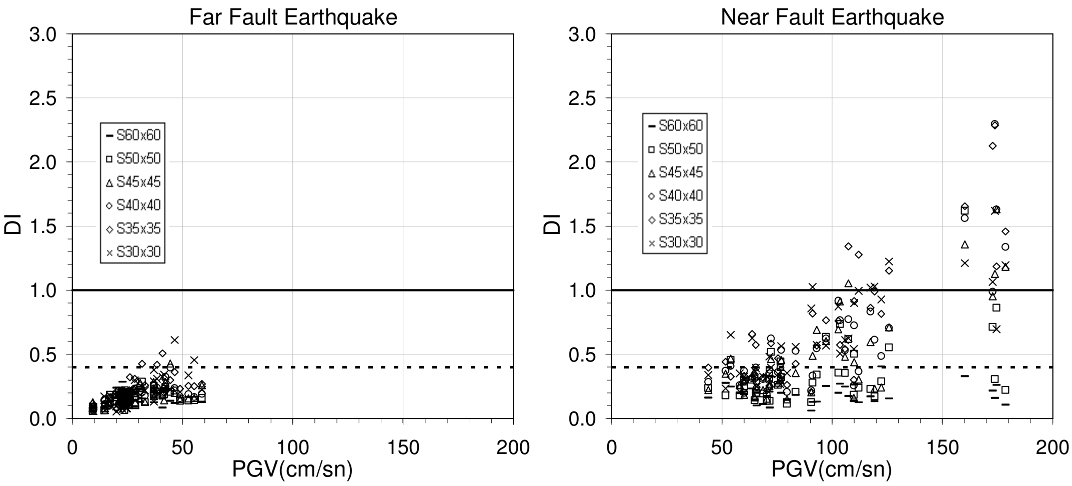

Figure A.11: PGV-DI relationship for columns longitudinal reinforcement ratio of 3 %

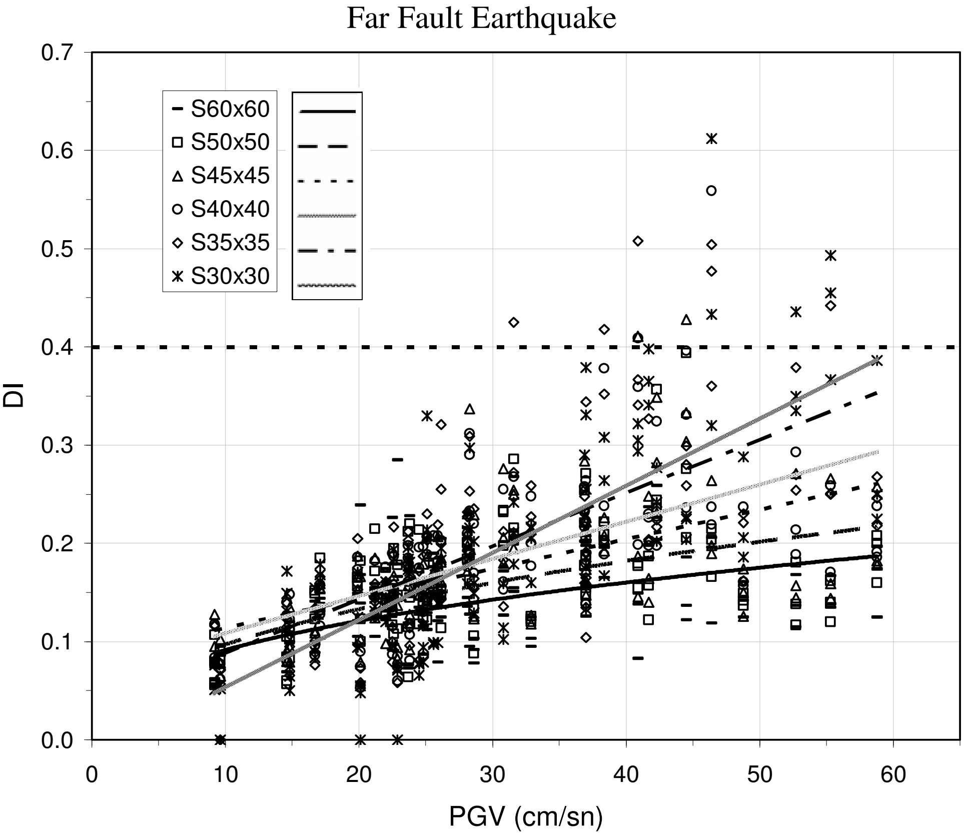

Figure A.12: PGV-DI relationship and trend lines of various sectional dimensions

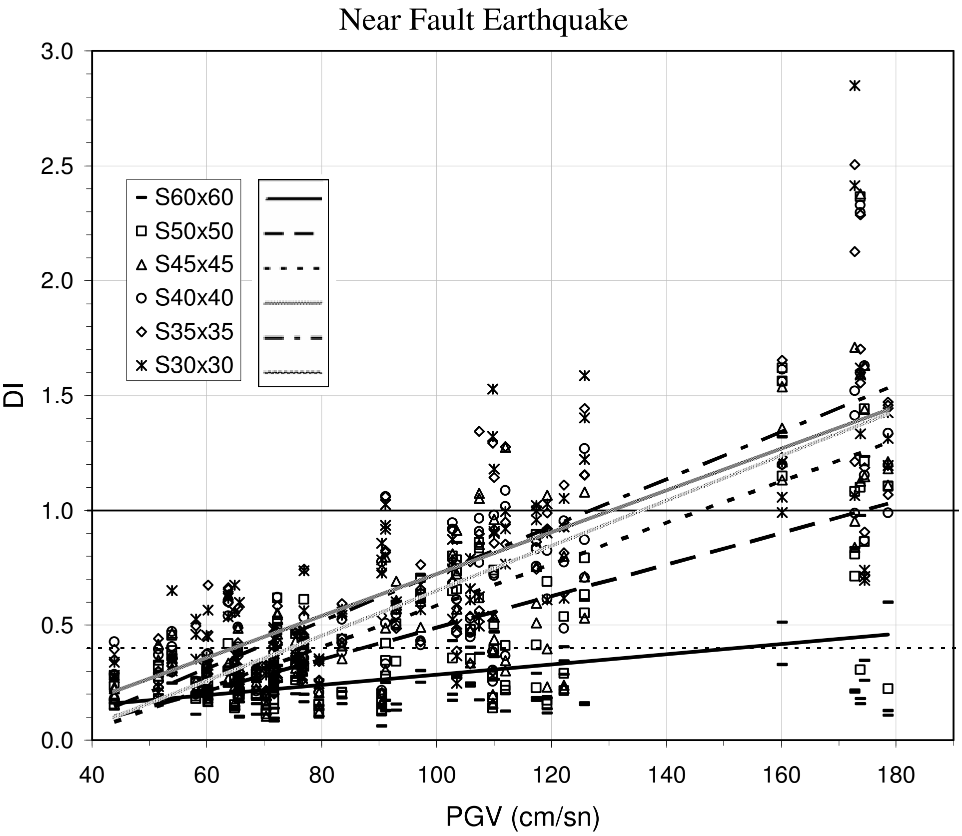

Figure A.13: PGV-DI relationship and trend lines of various sectional dimensions

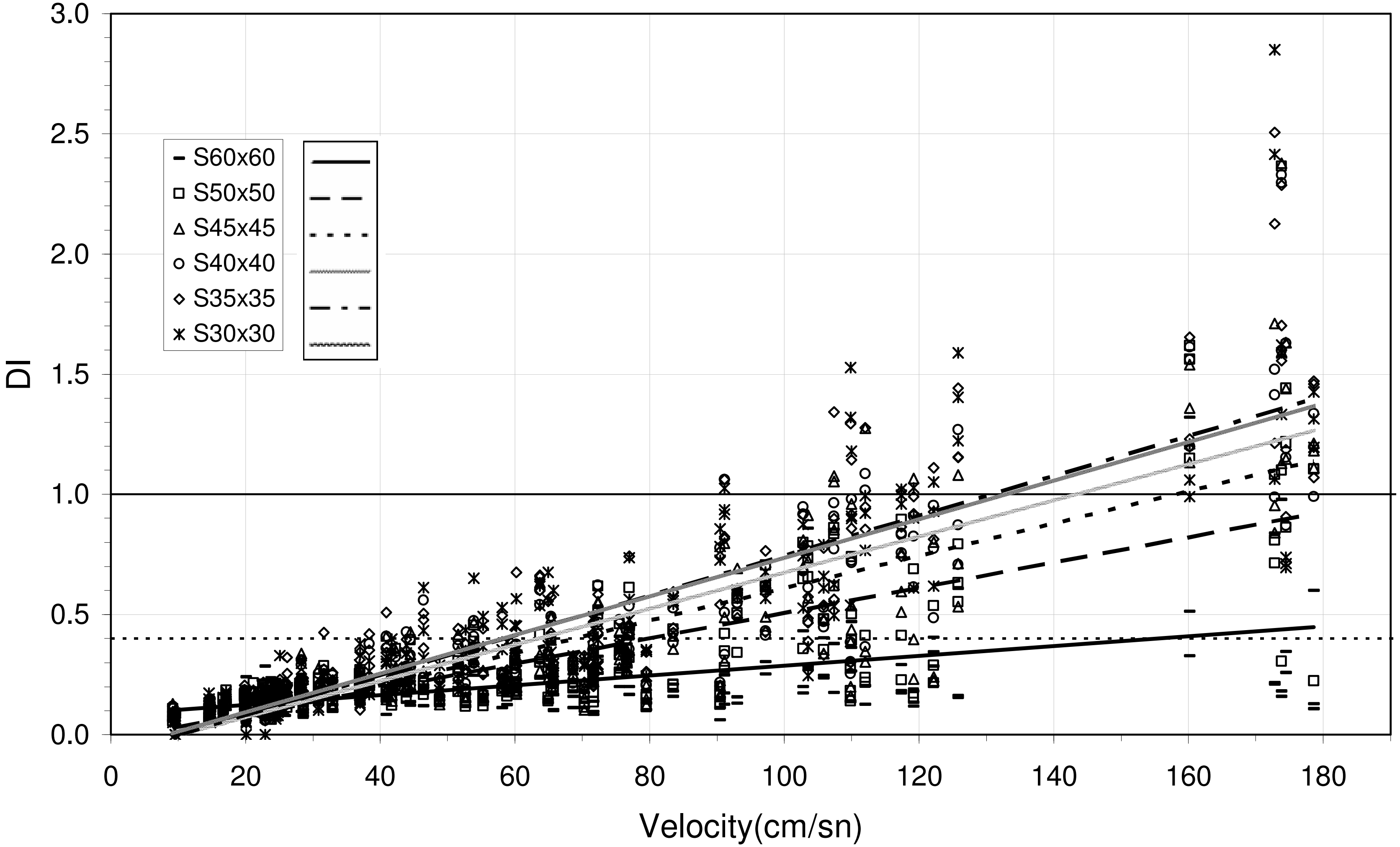

Figure A.14: PGV-DI relationship and trend lines of various column dimensions for all earthquakes

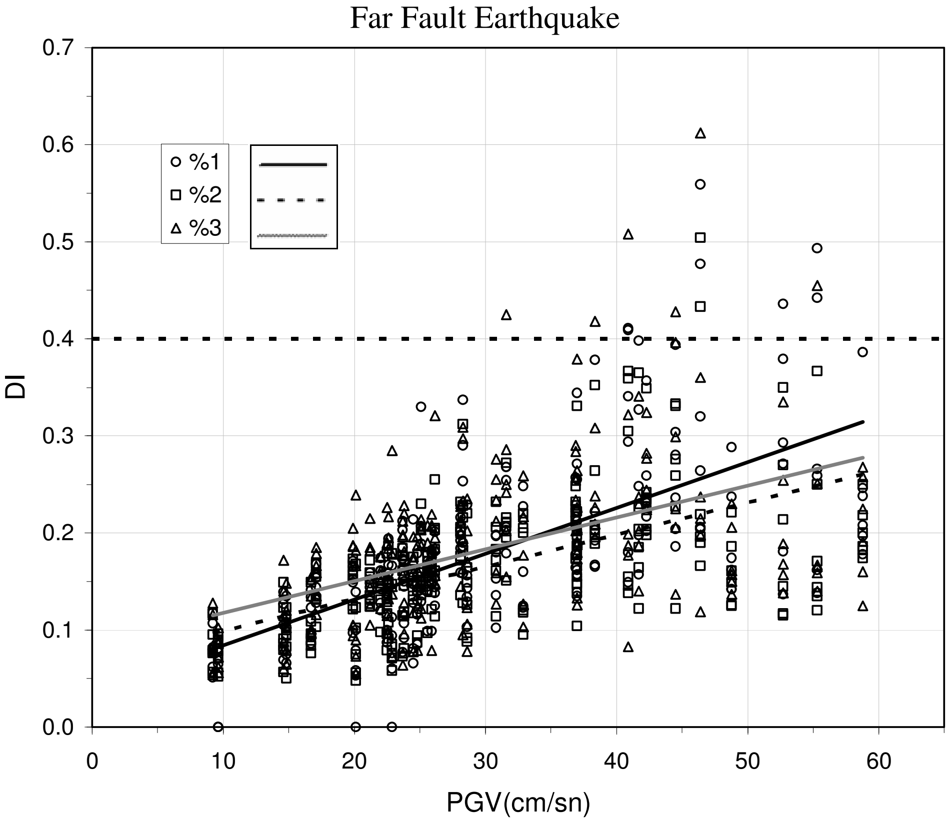

Figure A.15: PGV-DI relationship and trend lines of various longitudinal reinforcement ratios

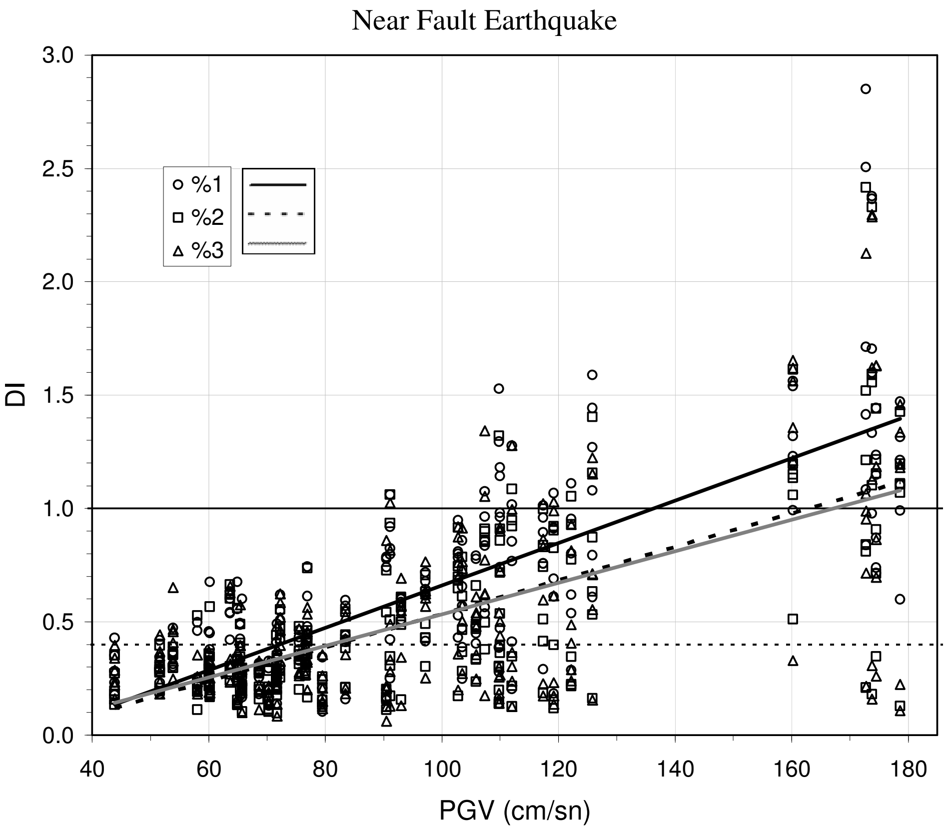

Figure A.16: PGV-DI relationship and trend lines of various longitudinal reinforcement ratios

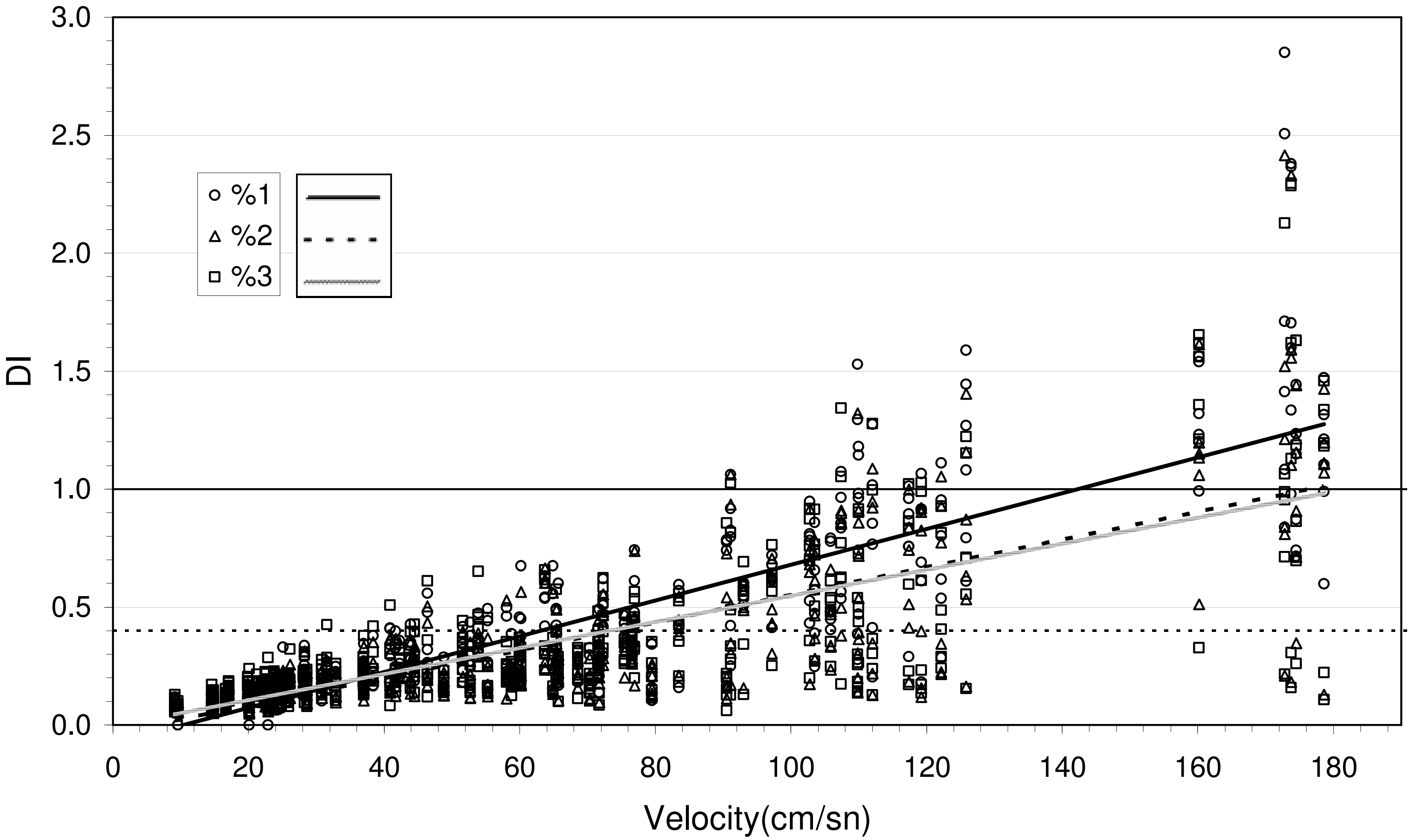

Figure A.17: PGV-DI relationship and trend lines of various longitudinal reinforcement ratios for all earthquakes

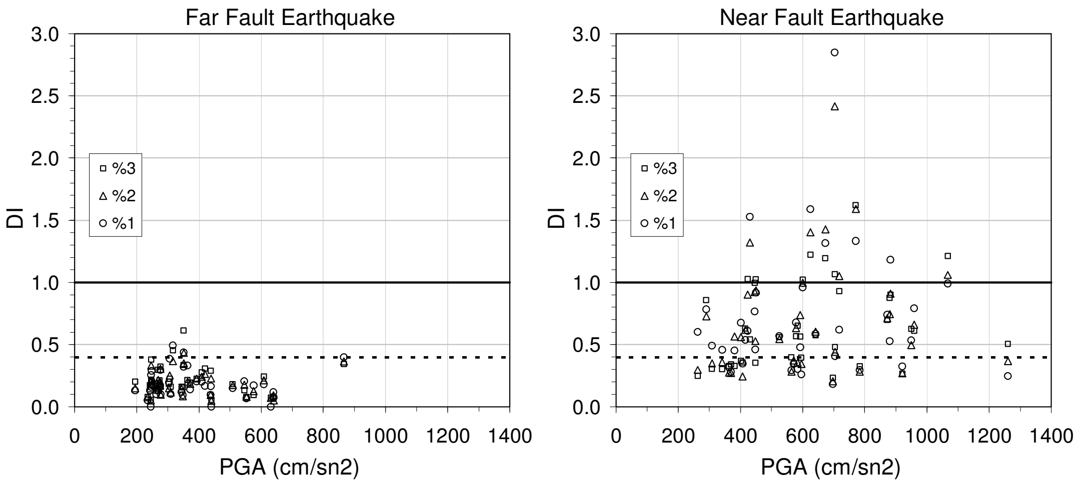

Figure A.18: PGA-DI relationship for columns dimensions of 30x30 cm

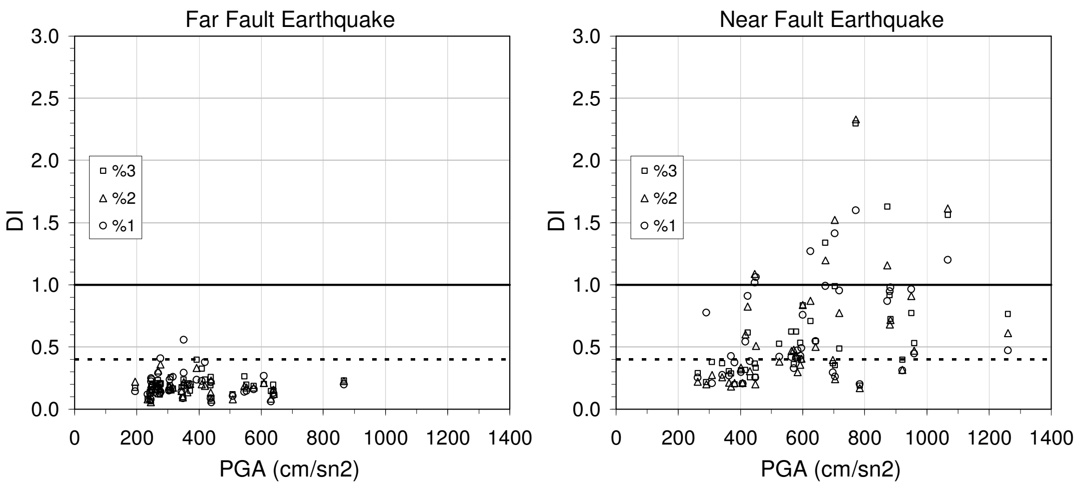

Figure A.19: PGA-DI relationship for columns dimensions of 40x40 cm

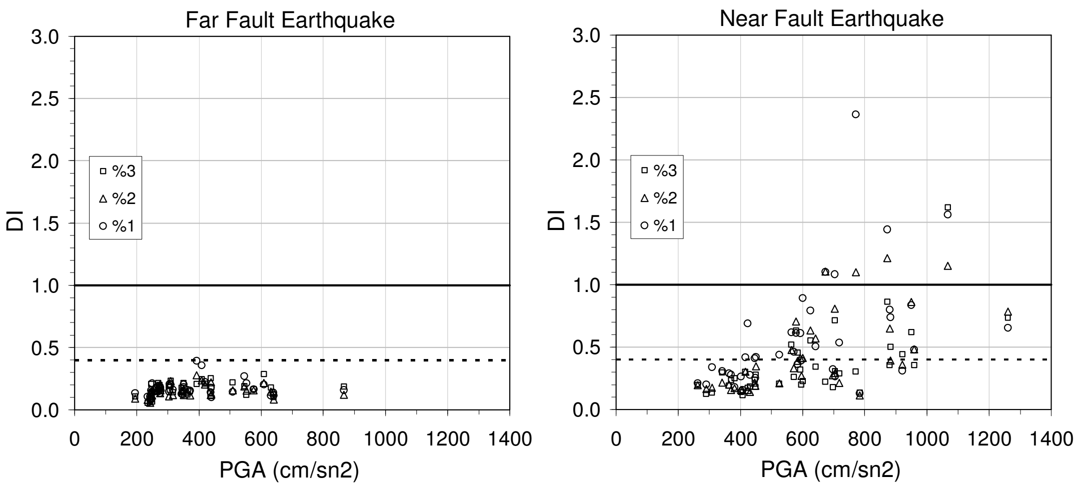

Figure A.20: PGA-DI relationship for columns dimensions of 50x50 cm

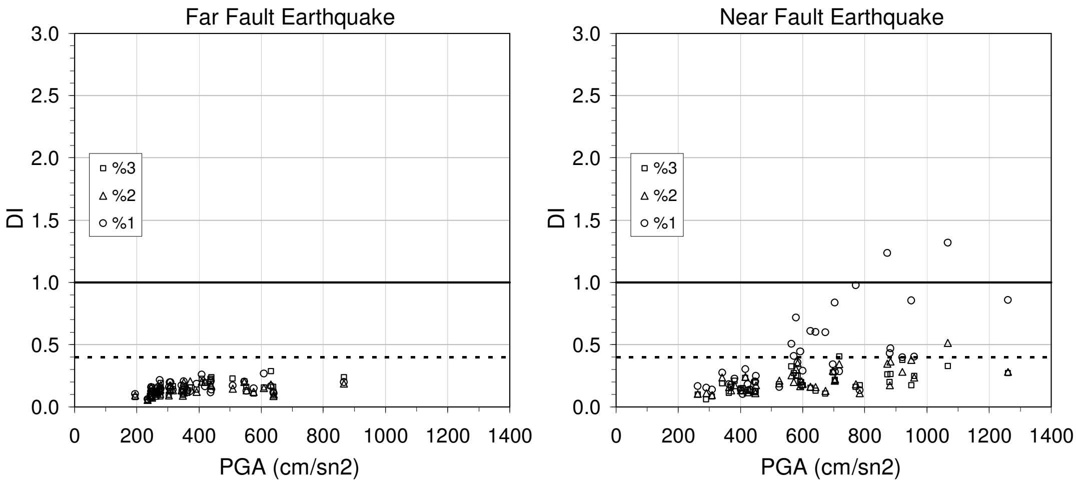

Figure A.21: PGA-DI relationship for columns dimensions of 60x60 cm

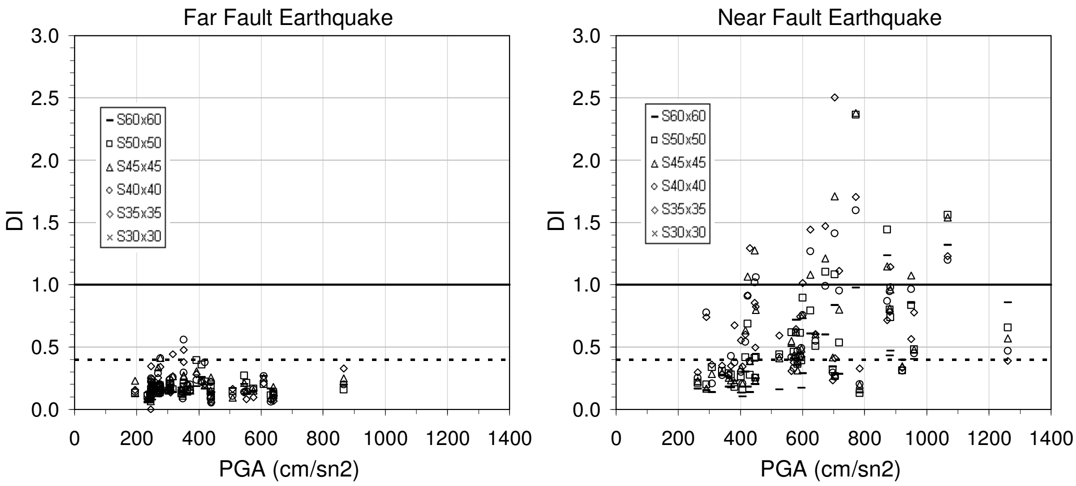

Figure A.22: PGA-DI relationship for columns longitudinal reinforcement ratio of 1 %

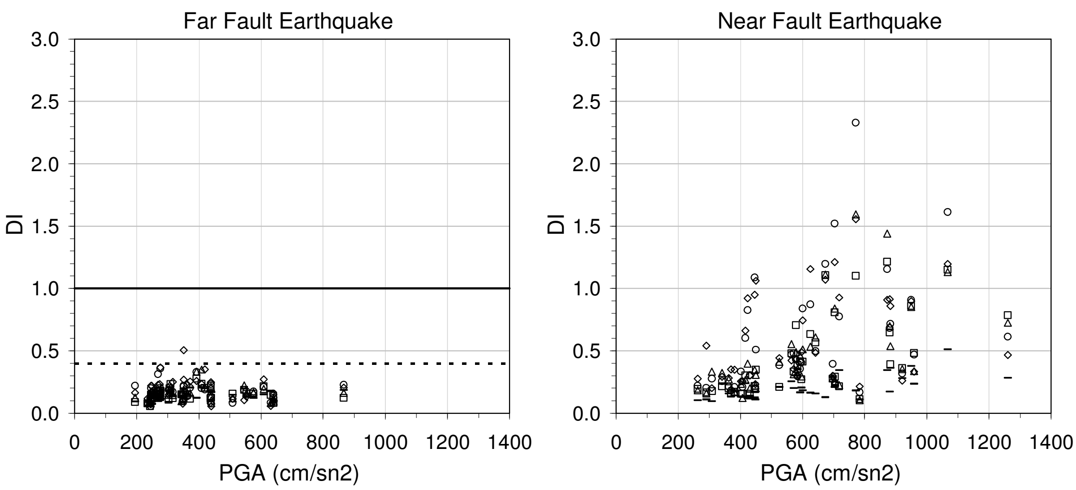

Figure A.23: PGA-DI relationship for columns longitudinal reinforcement ratio of 2 %

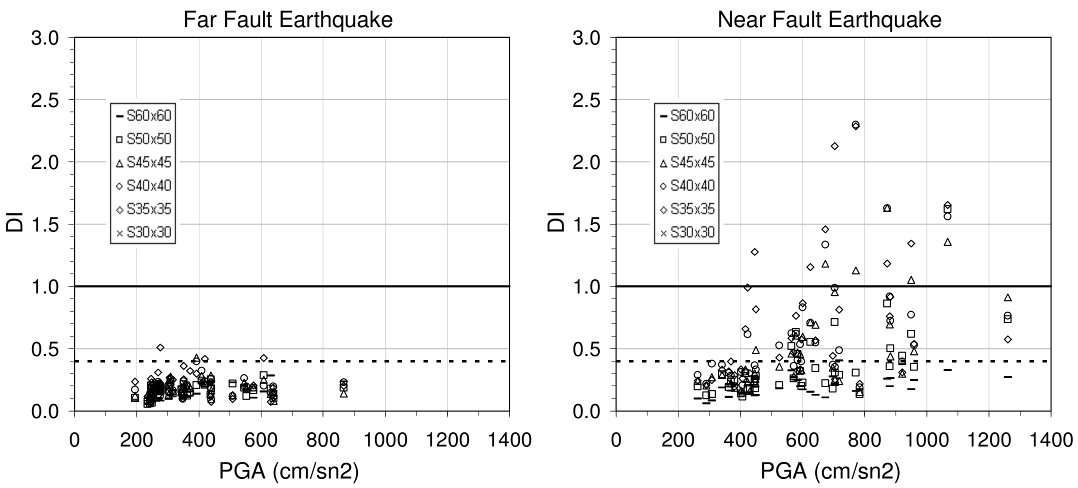

Figure A.24: PGA-DI relationship for columns longitudinal reinforcement ratio of 3 %

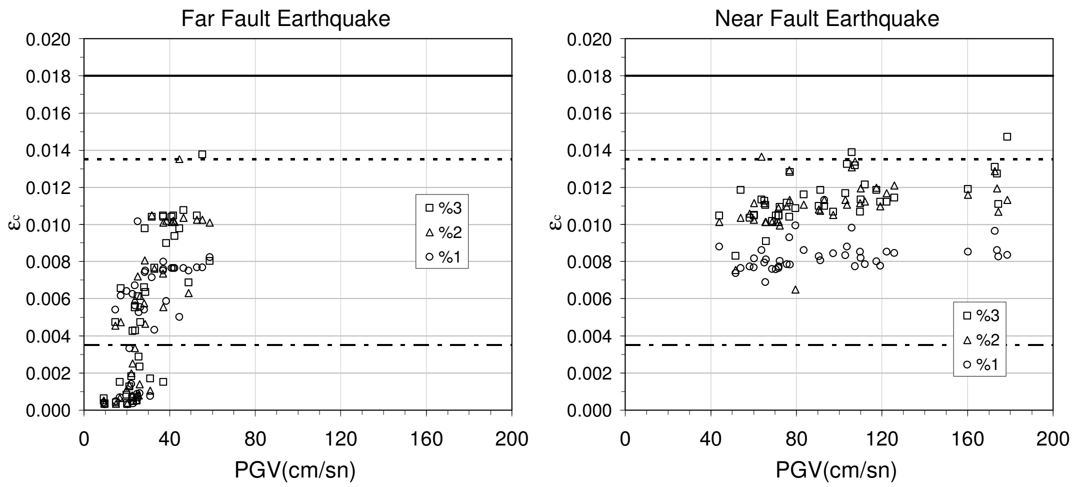

Figure A.25: $(\varepsilon_c)_{max}$ -DI relationship for columns dimensions of 30x30 cm

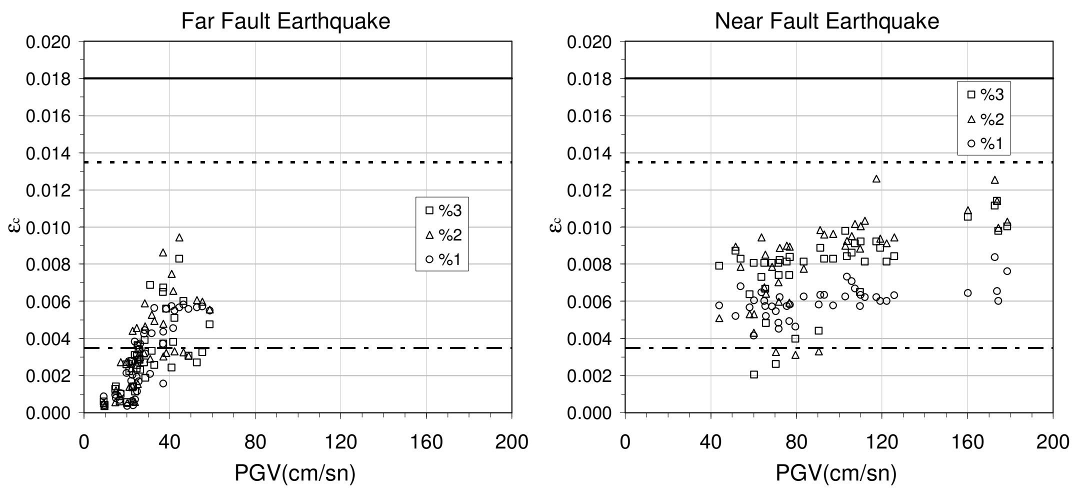

Figure A.26: $(\varepsilon_c)_{max}$-DI relationship for columns dimensions of 40x40 cm

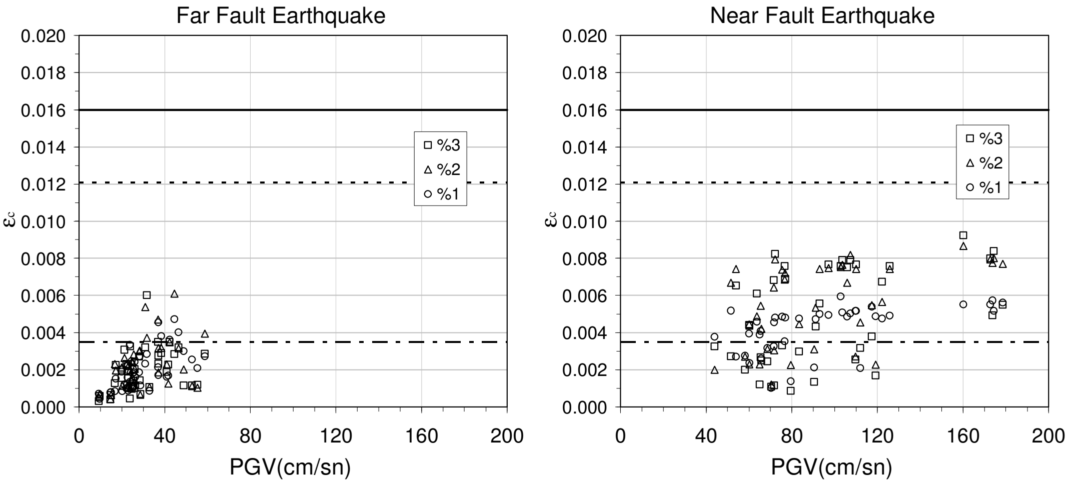

Figure A.27: $(\varepsilon_c)_{max}$-DI relationship for columns dimensions of 50x50 cm

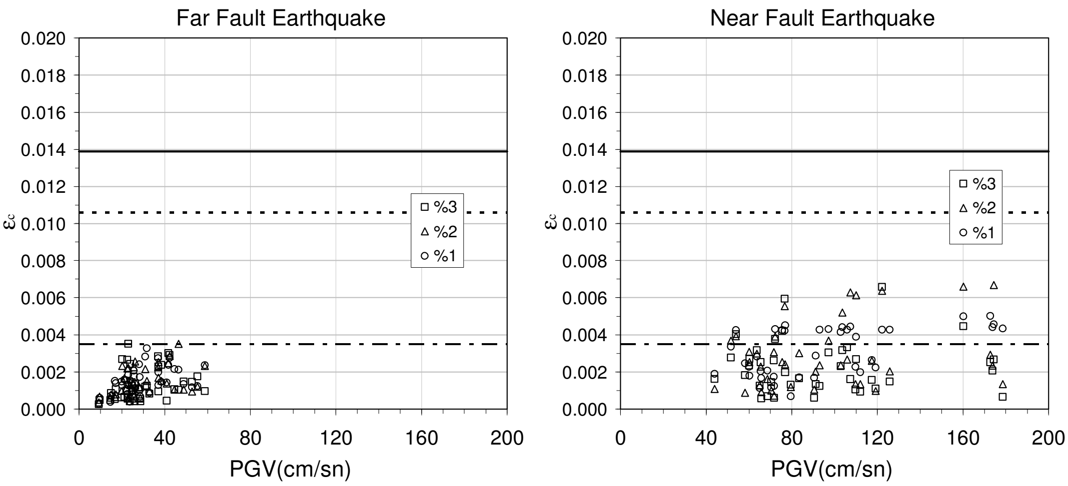

Figure A.28: $(\varepsilon_c)_{max}$-DI relationship for columns dimensions of 60x60 cm

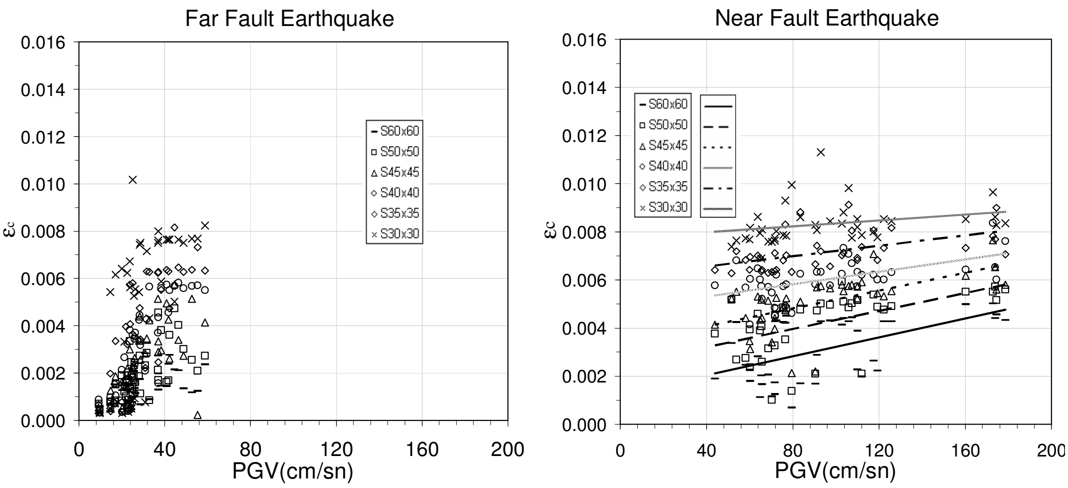

Figure A.29: $(\varepsilon_c)_{max}$-DI relationship for columns longitudinal reinforcement ratio of 1 %

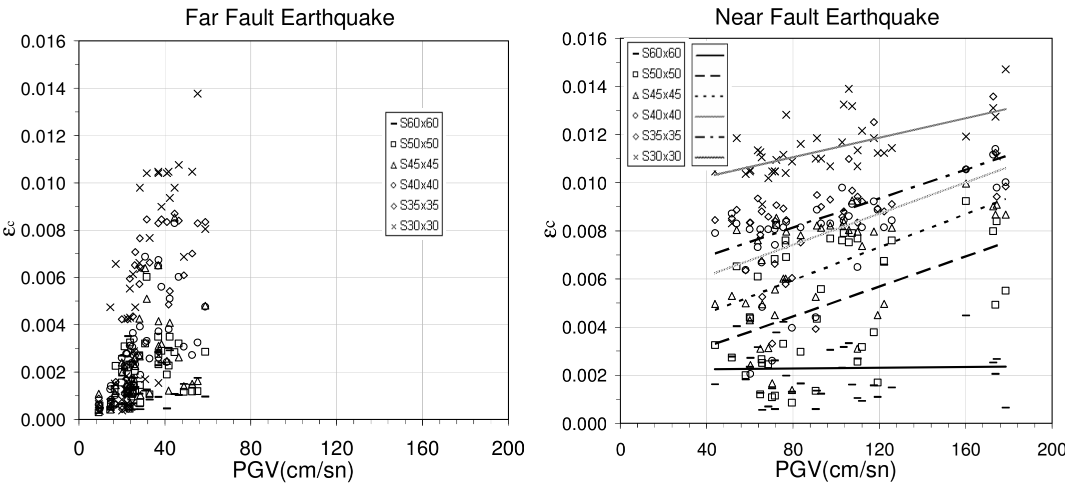

Figure A.30: $(\varepsilon_c)_{maz}$-DI relationship for columns longitudinal reinforcement ratio of 3 %

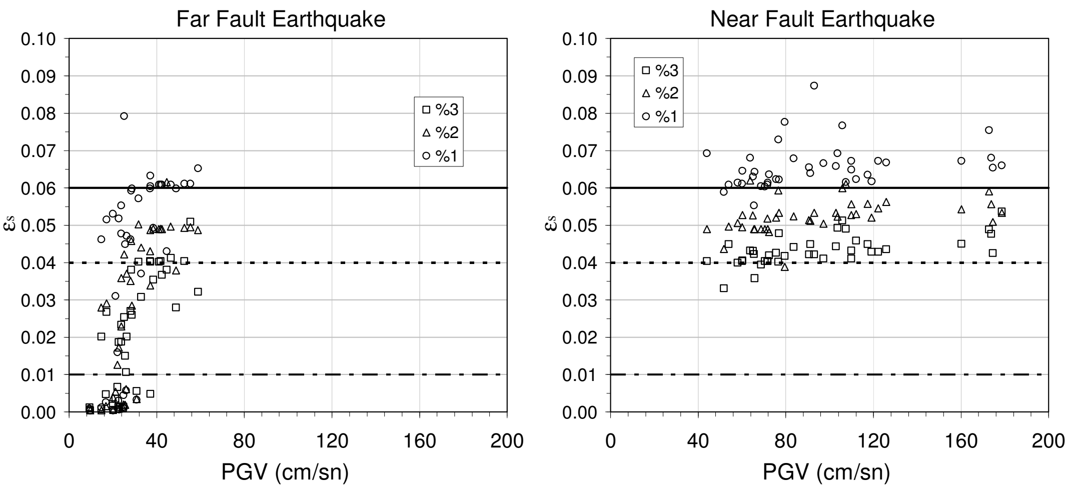

Figure A.31: $(\varepsilon_s)_{max}$-DI relationship for columns dimensions of 30x30 cm

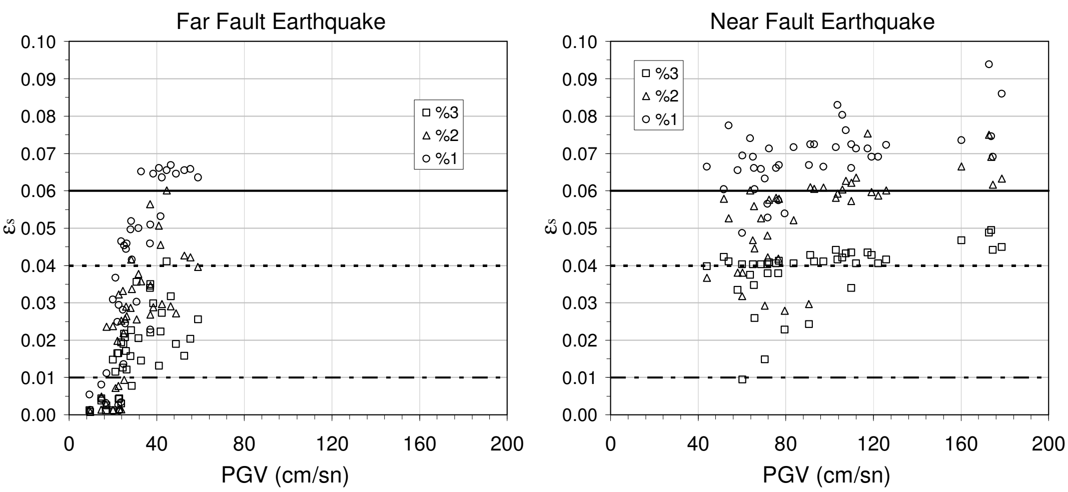

Figure A.32: $(\varepsilon_s)_{max}$-DI relationship for columns dimensions of 40x40 cm

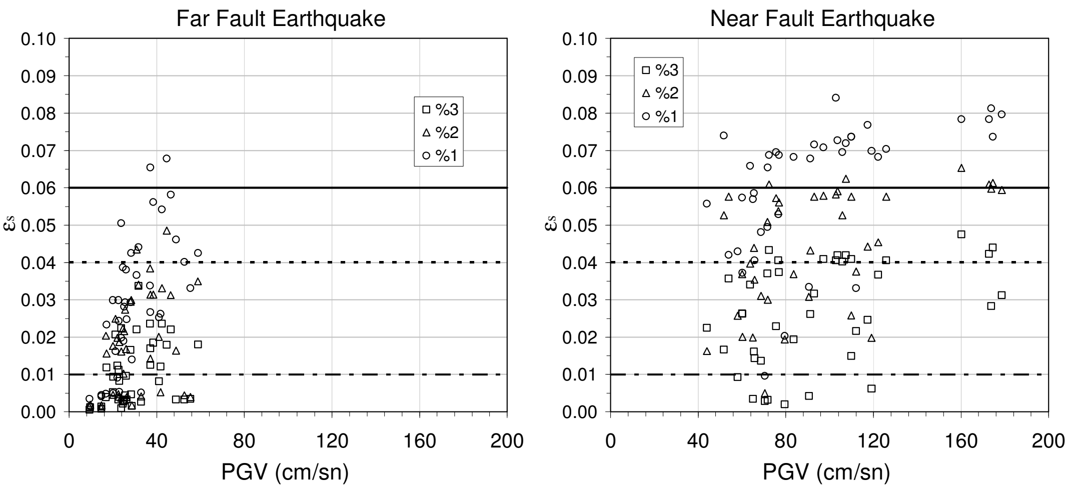

Figure A.33: $(\varepsilon_s)_{max}$-DI relationship for columns dimensions of 50x50 cm

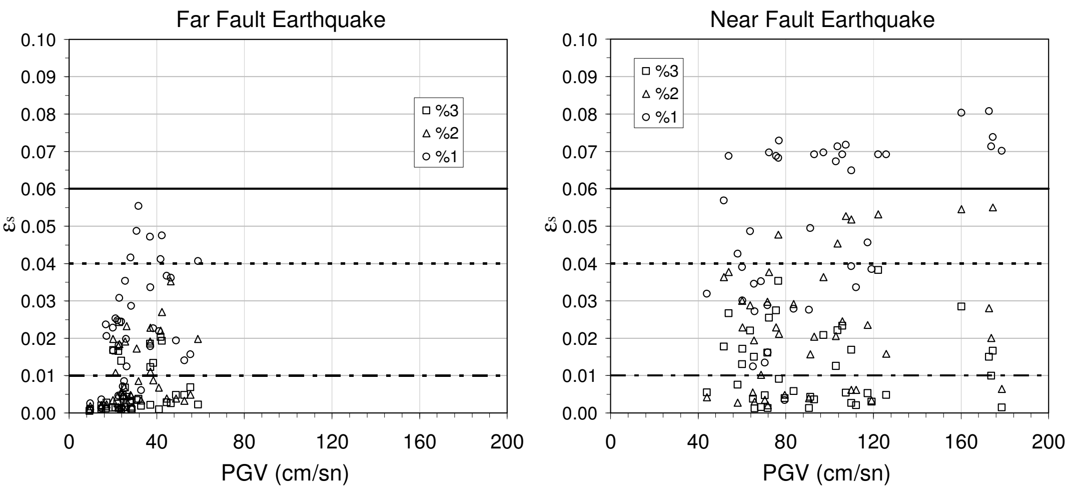

Figure A.34: $(\varepsilon_s)_{max}$-DI relationship for columns dimensions of 60x60 cm

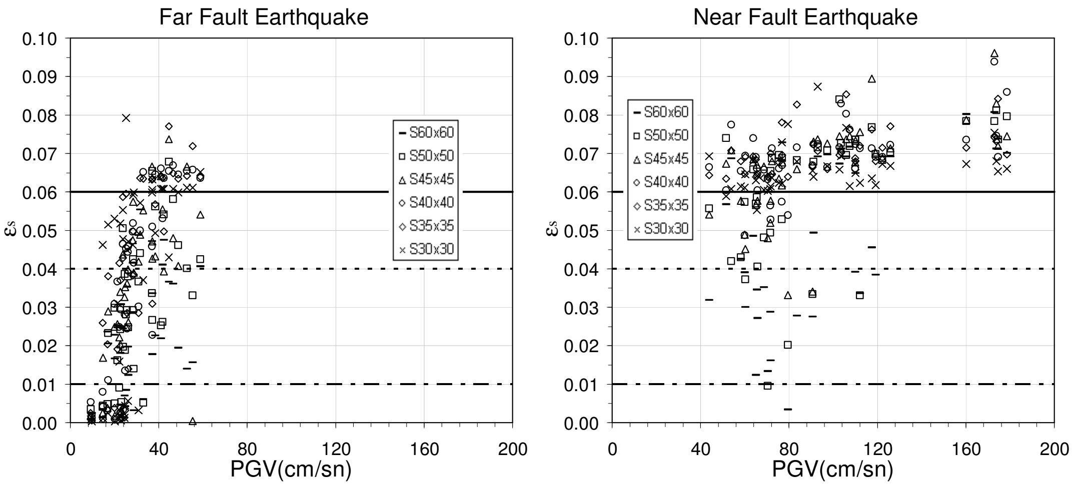

Figure A.35: $(\varepsilon_s)_{max}$-DI relationship for columns longitudinal reinforcement ratio of 1 %

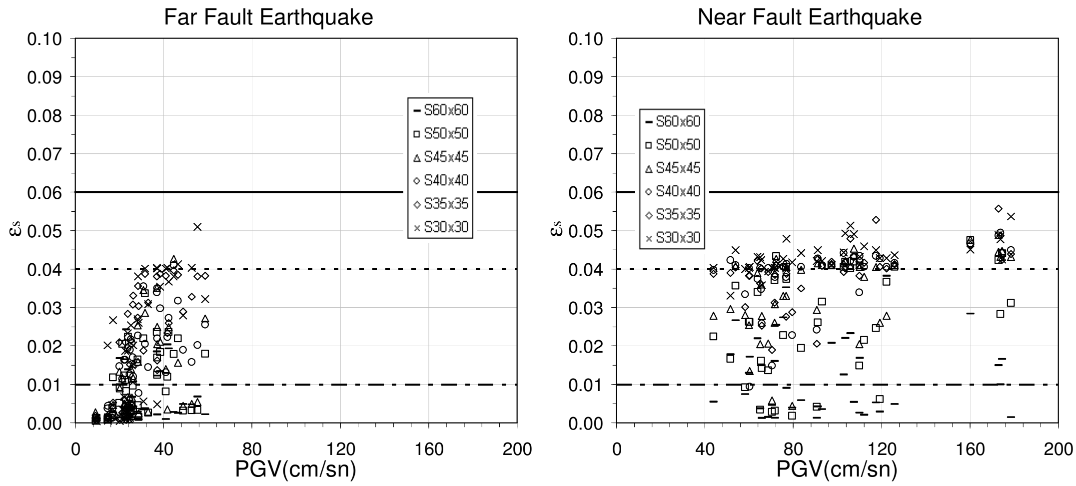

Figure A.36: $(\varepsilon_s)_{max}$-DI relationship for columns longitudinal reinforcement ratio of 3 %

BACKGROUND

Melih SÜRMELİ was born in 1980 in Hatay. He attended Yıldız Technical University Department of Civil Engineering between 1999 and 2004. After graduation from university in 2004, he worked as a design engineer in a private company for nine months and since September 2005, he has been doing his M.Sc. degree in Istanbul Technical University Department of Structural Engineering.